

PAPER • OPEN ACCESS

Neural networks and quantum field theory

To cite this article: James Halverson *et al* 2021 *Mach. Learn.: Sci. Technol.* **2** 035002

View the [article online](#) for updates and enhancements.

You may also like

- [Universal signature of quantum entanglement across cosmological distances](#)
Suddhasattwa Brahma, Arjun Berera and Jaime Calderón-Figueroa
- [Wilsonian effective actions and the IR/UV mixing in noncommutative gauge theories](#)
Valentin V. Khoze and Gabriele Travaglini
- [Functional flows in QED and the modified Ward–Takahashi identity](#)
Yuji Igarashi, Katsumi Itoh and Jan M Pawłowski



PAPER

Neural networks and quantum field theory

OPEN ACCESS

RECEIVED
22 August 2020REVISED
8 February 2021ACCEPTED FOR PUBLICATION
8 March 2021PUBLISHED
27 April 2021

Original Content from
this work may be used
under the terms of the
[Creative Commons
Attribution 4.0 licence](#).

Any further distribution
of this work must
maintain attribution to
the author(s) and the title
of the work, journal
citation and DOI.



James Halverson , Anindita Maiti* and Keegan Stoner

Department of Physics, Northeastern University, Boston, MA 02115, United States of America

* Author to whom any correspondence should be addressed.

E-mail: maiti.a@northeastern.edu**Keywords:** Wilsonian RG flow, infinite width NNGP, finite width NN, Gaussian processes, quantum field theory

Abstract

We propose a theoretical understanding of neural networks in terms of Wilsonian effective field theory. The correspondence relies on the fact that many asymptotic neural networks are drawn from Gaussian processes (GPs), the analog of non-interacting field theories. Moving away from the asymptotic limit yields a non-Gaussian process (NGP) and corresponds to turning on particle interactions, allowing for the computation of correlation functions of neural network outputs with Feynman diagrams. Minimal NGP likelihoods are determined by the most relevant non-Gaussian terms, according to the flow in their coefficients induced by the Wilsonian renormalization group. This yields a direct connection between overparameterization and simplicity of neural network likelihoods. Whether the coefficients are constants or functions may be understood in terms of GP limit symmetries, as expected from 't Hooft's technical naturalness. General theoretical calculations are matched to neural network experiments in the simplest class of models allowing the correspondence. Our formalism is valid for any of the many architectures that becomes a GP in an asymptotic limit, a property preserved under certain types of training.

Contents

1. Introduction	3
1.1. Related work	3
1.2. Our contributions	4
2. Asymptotic neural networks, Gaussian processes, and free field theory	5
2.1. General theory	6
2.2. Neural network correlation functions with Feynman diagrams	7
2.3. Examples: infinite width single-layer networks	9
2.4. Experiments: falloff to GP Feynman diagrams at large width	11
2.5. N -scaling of correlation functions of fully-connected networks	14
3. Neural networks and non-Gaussian processes with effective field theory	17
3.1. Correlation functions in NGPs with interacting Feynman diagrams	19
3.2. Four-point and six-point NGP correlation functions	22
3.3. Neural network coupling constants and GP symmetries	23
3.4. Independence in EFT of single-layer networks	24
3.5. Experiments: correlations in single-layer networks with EFT	26
3.6. Experiments: precision quartic fitting and EFT tests of $G^{(4)}$	29
4. Minimal non-Gaussian process likelihoods with Wilsonian renormalization	31
4.1. Neural network non-Gaussian process flows with β -functions	33
4.2. Renormalization analysis for fully-connected networks	34
4.3. Experiments: flows in single-layer networks	35
5. Conclusions	37
Appendix A. Review of Gaussian integrals	39
Appendix B. 2-pt functions/kernels of example networks	44
References	47

1. Introduction

The relationship between asymptotic neural networks and Gaussian processes (GPs) provides a strong hint towards a theoretical understanding of deep learning. Rather than considering a neural network to be determined by draws from a parameter space distribution, this perspective considers neural networks themselves as draws from a function space distribution. The essential idea is that a family of neural network architectures

$$f_{\theta,N} : \mathbb{R}^{d_{\text{in}}} \rightarrow \mathbb{R}^{d_{\text{out}}} \quad (1)$$

indexed by parameters θ and a discrete hyperparameter N admits a limit $N \rightarrow \infty$ in which networks are drawn from a GP, i.e. a Gaussian distribution on function space,

$$P[f] \sim \exp \left[-\frac{1}{2} \int d^{d_{\text{in}}} x d^{d_{\text{in}}} x' f(x) \Xi(x, x') f(x') \right], \quad (2)$$

where the functional/operator inverse of $\Xi(x, x')$ is the GP kernel. Of course, in practice one usually studies networks with large-but-finite N . These should be drawn from a distribution that receives $1/N$ corrections relative to the Gaussian distribution, i.e. a non-Gaussian process (NGP). Learning is then a data-induced flow of the function space distribution; recent literature and the above argument together suggest that the distribution remains an NGP during training.

The idea that neural networks are drawn from a non-Gaussian (but close-to-Gaussian) distribution on function space is immediately suggestive to physicists: such mathematics provides the backbone of perturbative quantum field theory (QFT), the framework that underlies numerous physical systems, from superconductors to the Standard Model of particle physics. From the perspective of Feynman's path integral, non-interacting ('free') quanta or particles are described by appropriate Gaussian distributions on function (field) space, where details depend on symmetries and particle properties such as Lorentz or rotational invariance and spin. When the fields do not have any vacuum expectation value the corresponding GP has mean zero and the $2n$ -pt correlation functions are entirely determined by the 2-pt statistics. Physically, this corresponds to n particles propagating past one another without interacting. Such quantum field theories are exactly solvable due to their Gaussian nature. Interactions between particles arise precisely due to non-Gaussian corrections to the log likelihood, known as the action in physics.

In this paper¹ we develop a sharp correspondence² between neural networks and QFT. We will introduce a framework known as Wilsonian effective field theory (EFT) for studying neural networks, utilizing it to determine minimal NGP likelihoods associated with neural network architectures, making modifications from the usual physics contexts when necessary. For brevity, we will refer to the general idea as a NN–QFT correspondence.

1.1. Related work

An EFT approach to neural networks is possible whenever a family of architectures admits a GP limit, which is the case for many modern architectures. Though the original NN–GP correspondence [1] was in the context of infinitely wide single-layer fully-connected networks, which admit computable kernels [2], recent work has shown that infinitely wide deep fully-connected networks [3, 4] are drawn from GPs, as are deep convolutional networks in the infinite channel limit [5, 6]. In [7–9], Yang developed a language for understanding which architectures admit GP limits, which was utilized to demonstrate that any standard architecture admits a GP limit, i.e. any architecture that is a composition of multilayer perceptrons, recurrent neural networks, skip connections [10, 11], convolutions [12–16] or graph convolutions [17–22], pooling [15, 16], batch [23] or layer [24] normalization, and/or attention [25, 26]. Furthermore, though these results apply to randomly initialized neural networks, appropriately trained networks are also drawn from GPs [27, 28]. NGPs have been used to model finite neural networks in [29–32], with some key differences from our work. For these reasons, we believe that an EFT approach to neural networks is possible under a wide variety of circumstances.

While working on this project two papers appeared that also utilize Feynman diagrams in neural networks, and we would therefore like to differentiate our work. In [33] diagrams were associated to a different class of Gaussian integrals associated with neural network parameters drawn from a Gaussian distribution; they were used to put bounds on correlation functions in infinite width neural networks.

¹ We use alphabetical authorship as in high energy physics. Maiti and Stoner contributed equally to this work.

² Developing the correspondence will require using language from both communities in a way that will sometimes be obvious to experts in one of the fields. We hope the additional clarity is worth the tedium.

In contrast, our Gaussian (and non-Gaussian) integrals are over the function space associated with the GP or NGP, crucially relying on the central limit theorem [31]. Focuses on preactivation distribution flow associated with perturbative corrections in the width parameter. Both of these interesting papers differ from our approach, which uses Feynman diagrams in our application of Wilsonian EFT to determine NGP likelihoods. It is applicable to any family of architectures admitting a GP limit, and knowledge of the GP limit and EFT together allow for the prediction of NGP correlation functions. Couplings are extracted from experiments and matched to theory predictions for their flow under the renormalization group (RG).

1.2. Our contributions

In this work we alternate between a general development of the theory behind a NN–QFT correspondence and its experimental verification³. We do so in the simplest class of architectures admitting such a description, single-layer fully-connected networks. By construction, the point is precisely to *not* take an infinite width limit $N \rightarrow \infty$, instead treating the neural networks as perturbations of the associated GP, modeled by perturbing the GP to an NGP by adding corrections according to the rules of Wilsonian EFT. A summary of our results:

- **Higher-point GP statistics.** We review how n -pt correlation functions in GPs, $n > 2$, may be computed using non-interacting Feynman diagrams and demonstrate the experimental falloff to GP predictions as $N \rightarrow \infty$ in three classes of single-layer networks.
- **Neural net and NGP likelihoods from Wilsonian EFT.** We develop rules for treating the NGPs associated with finite N networks. Non-Gaussian terms correspond to particle interactions and have coefficients (‘couplings’) corresponding to interaction strengths. We compute the 4-pt and 6-pt functions using interacting Feynman diagrams. In the single-layer networks, 4-pt couplings are extracted from experiments. These couplings are used to make predictions for the 6-pt function and 4-pt function evaluated on test set inputs, which we verify experimentally.
- **Couplings and GP limit symmetries.** Whether the coefficient of a non-Gaussian term in the NGP likelihood is a constant or a function is of practical importance. We demonstrate that this may be understood in terms of ‘t Hooft’s notion (‘technical naturalness’) that the couplings may be small when setting them to zero recovers a symmetry. The coefficient is nearly a constant when the GP limit is translation invariant, i.e. if setting its variance to zero recovers a symmetry.
- **Minimal NGP likelihoods and renormalization group (RG) flow.** Our approach introduces a parameter Λ known as the cutoff, so technically there is an infinite class of NGPs designed to describe one set of experiments. If all are equally effective, the predictions must not depend on Λ , which yields a differential equation known as a β -function governing the couplings at different values of the cutoff. The induced flow in coupling space is known as Wilsonian RG flow, and the couplings are said to ‘run’. We compute the β -functions for 4-pt couplings in some of our examples and experimentally verify their running. As a limit in Λ is taken, the flow renders some coefficients negligible, yielding a minimal NGP likelihood.

These elements, particularly EFT and RG flow, constitute the essentials of an NN–QFT correspondence, as they constitute the essentials of a modern approach to QFT.

For our ML readers: this approach immediately connects overparameterization with neural net likelihood simplicity. That is, neural networks with increasingly large numbers of parameters are drawn from increasingly simple distributions. This was already implicit in the connection between asymptotic neural networks and GPs, and also in the fact that non-Gaussian corrections to GPs should be $1/N$ suppressed. However, the Wilsonian RG adds another layer to the story: at any fixed N there is a family of NGPs indexed by a continuous parameter Λ , and by taking limits in Λ many of the non-Gaussian terms in the NGP likelihood become negligible, leading to simpler NGP likelihoods. This physics-motivated technique introduces a gained simplicity, verified in the results of our NN experiments: to excellent approximation, a *single number* is all that it takes to correct GP correlation functions to NGP (neural network output) correlation functions, despite the fact that in moving away from the GP limit an infinite number of neural network parameters are lost. For other architectures it may be that additional parameters that are the coefficients of non-Gaussian terms in the probability distribution function are needed; for our architectures we also study three-parameter models, but find that one suffices to model the correlation functions to excellent approximation in experiments.

We also recognize that our experimental focus on randomly initialized networks, rather than trained networks, means that we have left an understanding of learning to future work. This is intentional, as our

³ We provide an implementation of our code at <https://github.com/keeganstoner/nn-qft>.

primary goal in this work is to develop EFT techniques for treating the NGPs associated with neural networks. We emphasize that though we have not treated trained networks directly, our techniques apply to trained networks that are close to GPs. Shown in [8, 9, 34], randomly initialized infinite width NNs are GPs, and further, the GP property persists under appropriate training [8, 27, 28, 34, 35]. Such trained networks at finite width should be effectively described using our techniques, which only requires being close to a GP.

For our physicist readers: in applying EFT techniques to the NGPs from which neural networks are drawn, there are a number of important changes from the usual cases in QFT. Some of them include:

- **Tree-level divergences.** In the absence of δ -functions that collapse integrals associated with internal points, divergences may arise in tree-level diagrams. Of course, proper regularization and renormalization renders them a feature, not a bug.
- **Lack of derivatives.** GP kernels are functions on input space, but their inverses, which appear in the GP probability distribution function, in general need not have derivatives (though sometimes cases they could). If not, they are akin to space-dependent mass terms, rather than kinetic terms, which are sometimes considered in cosmology [36]. We plan to include derivatives in future work.
- **Coupling functions.** Most notably, couplings in NGPs are not necessarily constants, and their spatial (input) variance can be understood in terms of technical naturalness.

Physicist readers may also notice that we have followed a school of thought in QFT due to Coleman, which implores the student to first understand the basics of perturbation theory and renormalization in the case of spin-0 particles, since the introduction of higher spin particles does not change the basic conceptual framework. Coleman's approach is even more natural in a NN-QFT correspondence, since the scalar outputs associated with neural networks mean that (as functions) they should be understood as scalar fields, which correspond to spin-0 particles. Of course this could change with further developments in neural networks, but it is appropriate for now. Another element of Coleman's school is that perturbation theory in QFT is 'just Gaussian integrals' (with some additional decorations), which we review in detail in appendix A.

This paper is organized as follows. In section 2 we review GPs and explain how they correspond to free field theories. We demonstrate the higher-point correlation functions may be computed from two-point statistics using non-interacting Feynman diagrams, and experimentally demonstrate the falloff to GP predictions in the $N \rightarrow \infty$ limit. In section 3 we introduce a treatment of the NGPs associated with finite N networks in terms of Wilsonian EFT, including the introduction of interacting Feynman diagrams for the computation of correlation functions. We extract 4-pt couplings and use them to make 6-pt predictions, which are verified experimentally. Technical naturalness is discussed in regards to when and why couplings should be constants versus functions. In section 4 we introduce Wilsonian RG as applied to neural networks, computing some β -functions that govern the running of couplings and verifying them experimentally. We argue that 6-pt couplings are negligible due to being irrelevant, in the Wilsonian sense.

2. Asymptotic neural networks, Gaussian processes, and free field theory

In this section we wish to draw a sharp analogy between GPs, neural networks, and techniques from free field theory. In this analogy we will facilitate computations of correlation functions in the GP limit with Feynman diagrams, representing correlation functions in terms of the kernel $K(x, x')$ that determines the GP. We will then specify to a concrete class of neural networks—single layer feedforward networks in their infinite width limit—that exemplify the general idea, demonstrating that theoretical calculations with Feynman diagrams in the GP and associated combinatorics agree with experiments, up through the 6-pt functions.

The essential idea connecting GPs and free field theory is simple to state. Some classes of neural network architectures admit a limit $N \rightarrow \infty$ where a randomly initialized neural network in that class is equivalent to a draw from a GP, i.e. the neural network outputs evaluated on fixed inputs are described by draws from a multivariate Gaussian distribution. Meanwhile, a field configuration $f(x)$ in a free field theory is also drawn from a multivariate Gaussian distribution, and it is precisely the Gaussian nature of the associated path integral that makes the theory solvable, i.e. all correlation functions of the fields $f(x)$ may be computed exactly. The free field theory is a GP, with the kernel describing the dynamical propagation of field quanta.

Some aspects of this section are stated in the literature, see e.g. [29–31], but we wish to fully develop the formalism in order to facilitate new results obtained in later sections. The essentials of the GP-Free QFT correspondence are presented in table 1.

Table 1. Correspondence between quantities in the GP/asymptotic neural network and free QFT.

GP/asymptotic NN	Free QFT
Input x	External space or momentum space point
Kernel $K(x_1, x_2)$	Feynman propagator
Asymptotic NN $f(x)$	Free field
Log-likelihood	Free action S_{GP}

2.1. General theory

Let us develop the connection between neural networks, GPs, and free field theory. For simplicity we assume that the mean μ of the GP is zero, corresponding to zero vacuum expectation value (VEV) in the field theory, an assumption which we will relax in subsequent work.

Consider a family of neural network architectures with learnable parameters θ and a discrete hyperparameter N ,

$$f_{\theta, N} : \mathbb{R}^{d_{\text{in}}} \rightarrow \mathbb{R}^{d_{\text{out}}}, \quad (3)$$

where at initialization the learnable parameters are drawn as $\theta \sim P(\theta)$. The parameter distribution $P(\theta)$ and the network architecture together induce an implicit distribution on function space from which the neural network is drawn, $P(f)$. We will often drop the explicit subscripts θ, N for brevity.

For many architectures there is a limit $N \rightarrow \infty$ in which the distribution on functions becomes a GP, which means that the neural network outputs $\{f(x_1), \dots, f(x_k)\}$ evaluated on any fixed set of k inputs $\{x_1, \dots, x_k\}$ are drawn from a multivariate Gaussian distribution $\mathcal{N}(\mu, \Xi^{-1})$,

$$\{f(x_1), \dots, f(x_k)\} \sim \mathcal{N}(\mu, \Xi^{-1}), \quad (4)$$

which by assumption in this paper has $\mu = 0$. The inverse covariance matrix Ξ is determined by the kernel function $K(x, x')$ as $(\Xi^{-1})_{ij} = K_{ij} := K(x_i, x_j)$. Since $\mu = 0$, the GP is entirely determined by its covariance, which in turn is entirely determined by the kernel. Correlation functions between n outputs can be expressed as

$$G^{(n)}(x_1, \dots, x_n) = \frac{\int df f_1 \dots f_n e^{-\frac{1}{2} f_i \Xi_{ij} f_j}}{Z}, \quad (5)$$

and are called n -pt functions, where the partition function $Z = \int df e^{-S}$, and $S = -\frac{1}{2} f_i \Xi_{ij} f_j$ is the log-likelihood, or ‘action’ in physics language. Einstein summation is implicit, and $f_i := f(x_i)$ is a vector of outputs on a fixed set of inputs $\{x_i\}$ with dimension $d_{\text{in}} = d$.

Of course, the GP is defined for any $\{x_1, \dots, x_k\}$ for any k , and therefore it is natural to take the continuum limit, in which case the correlation functions become

$$G^{(n)}(x_1, \dots, x_n) = \frac{\int df f(x_1) \dots f(x_n) e^{-S}}{Z}, \quad (6)$$

where the log-likelihood is now

$$S = \frac{1}{2} \int d^{d_{\text{in}}} x d^{d_{\text{in}}} x' f(x) \Xi(x, x') f(x') \quad (7)$$

and $\Xi(x, x') = K^{-1}(x, x')$ is the inverse covariance function, defined by

$$\int d^{d_{\text{in}}} x' K(x, x') \Xi(x', x'') = \delta^{(d_{\text{in}})}(x - x''), \quad (8)$$

where $\delta^{(d_{\text{in}})}(x - x'')$ is the d_{in} -dimensional Dirac delta function. This equation is the continuum analog of the relation $(\Xi^{-1})_{ij} = K_{ij}$ in the discrete case.

We note important special cases, some of which arise below, that will also be the subject of follow-up work. Suppose in (7) we had $\Xi(x, x') = \Xi(x) L_{\sigma}(x, x')$ where $L_{\sigma}(x, x')$ is any family of functions that limits to $L_0(x, x') = \delta^{(d_{\text{in}})}(x - x')$; for instance, a family of normalized Gaussians of variance σ^2 . In that limit, the double-integral collapses and one is left with

$$S = \frac{1}{2} \int d^{d_{\text{in}}} x f(x) \Xi(x) f(x), \quad (9)$$

which defines a *local* GP, denoting that the associated GP log-likelihood only has one integral over the input space. In this case the associated inversion formula is instead $\Xi(x)K(x, x') = \delta^{(d_{\text{in}})}(x - x')$. If a kernel satisfies this identity, it means it is the kernel of a local GP. At finite σ it can be thought of as a scale of non-locality, and one might call such a GP *semi-local* and try to understand the utility of the scale σ in neural networks. Similarly, one could consider a log-likelihood with f constant and no input integrals $S = \frac{1}{2}f\Xi f$, which one might call an *ultra-local* GP, with associated inversion formula $K\Xi = 1$.

Both the discrete and continuum versions of the GP n -pt functions may be computed exactly using standard Gaussian integral techniques reviewed in appendix A. This would not be the case if the action contained beyond-quadratic terms, though a perturbative expansion may be available for suitably small coefficients of beyond-quadratic terms; see section 3.

A direct physics analog of a GP is a free field theory, which describes a quantum field $\phi(x)$ without any interaction terms. The field $\phi(x)$ depends on the d -dimensional coordinates of space⁴ x and the associated field theory is defined by the path integral

$$Z = \int D\phi e^{-S[\phi]} \quad (10)$$

in terms of an action $S[\phi]$, which is quadratic in the case of a free field theory. A famous example is free scalar field theory, which has

$$S[\phi] = \int d^d x \phi(x)(\square + m^2)\phi(x), \quad (11)$$

with $\square := \partial_\mu \partial^\mu$ and m the mass of the bosonic particle associated to ϕ . The functional inverse of $(\square + m^2)$ is known as the propagator, the 2-pt correlation function in the free field theory, and is the analog of the GP kernel. By virtue of being Gaussian, correlation functions in the free theory may be computed exactly.

Following table 1, an input x to the NN corresponds to a point in space or momentum space $\mathbb{R}^{d_{\text{in}}}$ in QFT. Computed in natural units $\hbar = c = 1$ of high energy physics, the neural network kernel, log-likelihood, and output $f(x)$ are the analogs of the free field theory propagator, free action and free field $\phi(x)$, respectively.

A central point of this work is that taking an infinite-width neural network to a large-but-finite width neural network corresponds to moving away from the GP to a NGP, which in field theory corresponds to turning on interactions. We will do this in section 3.

2.2. Neural network correlation functions with Feynman diagrams

Anticipating their utility when we move away from the GP, in this section we derive Feynman rules for the diagrammatic computation of correlation functions in the GP. The ability to represent such computations diagrammatically, in both quantum field theories and GPs, follows directly from basic properties of Gaussian integrals reviewed in appendix A.

The partition function of the GP is

$$Z_{\text{GP}}[J] = \frac{\int df e^{-S_{\text{GP}} - \frac{1}{2} \int d^{d_{\text{in}}} x J(x)f(x) - \frac{1}{2} \int d^{d_{\text{in}}} y J(y)f(y)}}{Z_{\text{GP},0}}, \quad (12)$$

where we have included the terms involving the source $J(x)$, and $Z_{\text{GP},0} := \int df e^{-S_{\text{GP}}}$ is the associated action, or (negative) log-likelihood, is

$$S_{\text{GP}} = \frac{1}{2} \int d^{d_{\text{in}}} x d^{d_{\text{in}}} y f(x)\Xi(x, y)f(y). \quad (13)$$

The n -pt correlation functions are defined by

$$G_{\text{GP}}^{(n)}(x_1, \dots, x_n) = \frac{\int df f(x_1) \dots f(x_n) e^{-S_{\text{GP}}}}{Z_{\text{GP},0}}. \quad (14)$$

We will consistently label GP quantities with a subscript, since in moving away from the GP limit in neural network architectures we will use EFT to determine deviations from the GP quantities using the NGP effective actions $S = S_{\text{GP}} + \Delta S$.

⁴ Spacetime, in the Lorentzian case. We will focus on the Euclidean case throughout. Depending on the structure of the log-probability, momentum space might be a better analog of the input.

Since all of the f -dependent terms in Z_{GP} are quadratic or below, it can be evaluated exactly by completing the square and performing the Gaussian integral, yielding

$$Z_{\text{GP}}[J] = \exp\left(\frac{1}{2} \int d^{d_{\text{in}}} x d^{d_{\text{in}}} y J(x) K(x, y) J(y)\right), \quad (15)$$

where the $Z_{\text{GP},0}$ factor has canceled. The correlation functions may be written as

$$G_{\text{GP}}^{(n)}(x_1, \dots, x_n) = \left[\left(-\frac{\delta}{\delta J(x_1)} \right) \dots \left(-\frac{\delta}{\delta J(x_n)} \right) Z_{\text{GP}} \right] \Big|_{J=0}. \quad (16)$$

The basic pattern of the computation of (16) emerges from the fact that taking these functional J -derivatives either pulls down factors from the exponential or hits previously-pulled-down J -factors, using $\delta J(x)/\delta J(y) = \delta^{d_{\text{in}}}(x - y)$ repeatedly⁵. The δ -functions make the kernels depend on external points, and depending on n there will be many terms, each with $n/2$ kernel factors. Those terms contain the information of which external points appear in kernels together, motivating the definition of the set of ways to connect the points (x_1, \dots, x_n) in pairs,

$$\text{Wick}(x_1, \dots, x_n) = \{P \in \text{Partitions}(x_1, \dots, x_n) \mid |p| = 2 \forall p \in P\}. \quad (17)$$

This is known as the set of Wick contractions, and it has cardinality $|\text{Wick}(x_1, \dots, x_n)| = (n-1)!!$. With this definition, the procedure of computing $G_{\text{GP}}^{(n)}(x_1, \dots, x_n)$ via J -derivatives yields

$$G_{\text{GP}}^{(n)}(x_1, \dots, x_n) = \sum_{p \in \text{Wick}(x_1, \dots, x_n)} K(a_1, b_1) \dots K(a_{n/2}, b_{n/2}) \quad (18)$$

where we write each element $p \in \text{Wick}(x_1, \dots, x_n)$ as $p = (a_1, b_1), \dots, (a_{n/2}, b_{n/2})$. This simple expression may be read

sum over all ways of pairing up elements in $\{x_1, \dots, x_n\}$, and in each term write a kernel factor $K(a_i, b_i)$ for each of the pairs (a_i, b_i) ,

giving a simple rule for writing down the answer for $G_{\text{GP}}^{(n)}(x_1, \dots, x_n)$, for any n , even when the combinatorics of $\text{Wick}(x_1, \dots, x_n)$ become grotesque.

Diagrammatic representations of the GP follow immediately by a simple rule change:

sum over all ways of connecting the points $\{x_1, \dots, x_n\}$ in pairs, and in each term draw a line between the points in the pair (a_i, b_i) .

Both of these simple colloquial expressions yield correct ways to represent (18), one in terms of a sum of kernel factors, and the other in terms of a sum of diagrams. The diagram-to-analytic map between the two is clearly that for each line between a_i and b_i in a diagram⁶, write a kernel factor $K(a_i, b_i)$. For instance, in the case $n = 2$, $\text{Wick}(x_1, x_2) = \{(x_1, x_2)\}$ and we have

$$\begin{aligned} G_{\text{GP}}^{(2)}(x_1, x_2) &= K(x_1, x_2) \\ &= \text{---} \overline{x_1 \quad x_2} \text{---} \end{aligned} \quad (19)$$

Similarly, $\text{Wick}(x_1, x_2, x_3, x_4) = \{(x_1, x_2), (x_3, x_4)\}, \{(x_1, x_3), (x_2, x_4)\}, \{(x_1, x_4), (x_2, x_3)\}$ and we have

$$\begin{aligned} G_{\text{GP}}^{(4)}(x_1, x_2, x_3, x_4) &= K(x_1, x_2)K(x_3, x_4) + K(x_1, x_3)K(x_2, x_4) + K(x_1, x_4)K(x_2, x_3) \\ &= \begin{array}{c} x_1 \quad x_3 \\ | \quad | \\ x_2 \quad x_4 \end{array} + \begin{array}{c} x_1 \quad x_3 \\ \text{---} \text{---} \\ x_2 \quad x_4 \end{array} + \begin{array}{c} x_1 \quad x_3 \\ \diagdown \quad \diagup \\ x_2 \quad x_4 \end{array} \end{aligned} \quad (20)$$

In connecting points in pairs for any odd n , there is always a leftover point, which corresponds to a factor of J in every term in the analytic expression. Since J is set to zero after taking functional J -derivatives in (16), we conclude that $G_{\text{GP}}^{(n)}(x_1, \dots, x_n) = 0$ for any odd n .

⁵ Details can be found in appendix A.

⁶ These are, of course, the Feynman diagrams of physics, and the rules are known as Feynman rules.

In the analogy to free QFT, quantities in the GP map to associated quantities in the QFT, summarized in table 1. Remembering that the GP can sometimes be realized by asymptotic neural networks, the neural network inputs are the points in space in the QFT, and the kernel is the Feynman propagator, which represents the probability or amplitude of propagation of a particle from one point to another. Notably, due to the Gaussian nature of Z_{GP} , all diagrams in the diagrammatic expressions for $G_{\text{GP}}^{(n)}(x_1, \dots, x_n)$ are simple connections of pairs of points in space, flying past one another without interacting. When Z_{GP} is corrected by non-Gaussian terms, ‘interactions’ arise in a way that we will make concrete in section 3. Thus, the GP/asymptotic neural networks correspond to free (non-interacting) field theories, and moving away from the asymptotic limit corresponds to turning on interactions.

2.3. Examples: infinite width single-layer networks

To experimentally realize the theoretical ideas of this paper, such as utilizing EFT and Wilsonian RG flow for understanding neural networks, we must introduce concrete architectures that will be used in experiments and their corresponding GPs. Specifically, we now introduce the three single-layer architectures we study in this paper and also review the correspondence between infinite width single-layer networks and GPs.

Consider a fully-connected neural network with one hidden layer and elementwise nonlinearity σ , defined by $f(x) = W_1(\sigma(W_0x + b_0)) + b_1$, where the weights and biases, W_i and b_i , characterize the affine transformations for each layer. Including the spaces associated with the hidden layers,

$$f_{\theta,N} : \mathbb{R}^{d_{\text{in}}} \xrightarrow{W_0, b_0} \mathbb{R}^N \xrightarrow{\sigma} \mathbb{R}^N \xrightarrow{W_1, b_1} \mathbb{R}^{d_{\text{out}}}. \quad (21)$$

The weight and bias parameters, collectively labeled as θ , are i.i.d. and drawn from a Gaussian distribution. Specifically, the biases are drawn from $\mathcal{N}(\mu_b, \sigma_b^2)$ and the weights in each layer W_0, W_1 are drawn from $\mathcal{N}(\mu_W, \sigma_W^2/d_{\text{in}})$ and $\mathcal{N}(\mu_W, \sigma_W^2/N)$, respectively, so they are normalized with respect to the input dimension of the associated layer. The first linear layer takes the input x to a preactivation z_0

$$z_0^j = \sum_{i=1}^{d_{\text{in}}} W_0^{ij} x^i + b_0^j, \quad (22)$$

which is then acted on by the elementwise nonlinearity σ , giving a postactivation $x_1^j = \sigma(z_0^j)$, that is acted on by the final linear layer, yielding

$$f_{\theta,N}(x) = z_1^k = \sum_{j=1}^N W_1^{jk} x_1^j + b_1^k, \quad (23)$$

the output of the neural network.

By the central limit theorem (CLT), in the infinite width limit the network outputs are drawn from a Gaussian distribution on function space [1]; i.e. the network outputs are drawn from a GP. This arises because the weight part of output layer of the network defined in (23) is the sum of N i.i.d. terms. In the infinite width limit $N \rightarrow \infty$, we get a finite⁷ sum over these independent parameters. Thus by the CLT we have a neural network output that is selected from a Gaussian distribution, i.e. the neural network evaluated on any finite collection of inputs is drawn from a multivariate Gaussian distribution. This is precisely what defines a GP. We present in figure 1 a schematic of a single-layer feedforward neural network, where the arrows represent the linear layers of weights and biases, and the nonlinear activation function is applied elementwise to each node in the hidden layer. Since the outputs are real scalars, the closest QFT analog of the infinite N neural network is a free scalar theory, albeit with a different two-point function (kernel).

Any neural network f with a linear output layer, such as the single-layer networks in our examples, has a structure that affects its study: it is generally of the form

$$f = f_b + f_W, \quad (24)$$

where f are drawn from independent processes⁸. Due to independence, the 2-pt function associated to f is the sum of the 2-pt functions associated to f_b and f_W . Furthermore, the higher-point correlators associated to f decompose into the higher-point correlators associated to f_b and f_W in the natural way. For instance, just as

$$G^{(2)}(x_1, x_2) = G_b^{(2)}(x_1, x_2) + G_W^{(2)}(x_1, x_2), \quad (25)$$

⁷ Since the elements of W are properly normalized.

⁸ For our initializations they are mean-free processes, which is assumed in the derivations but can be relaxed.

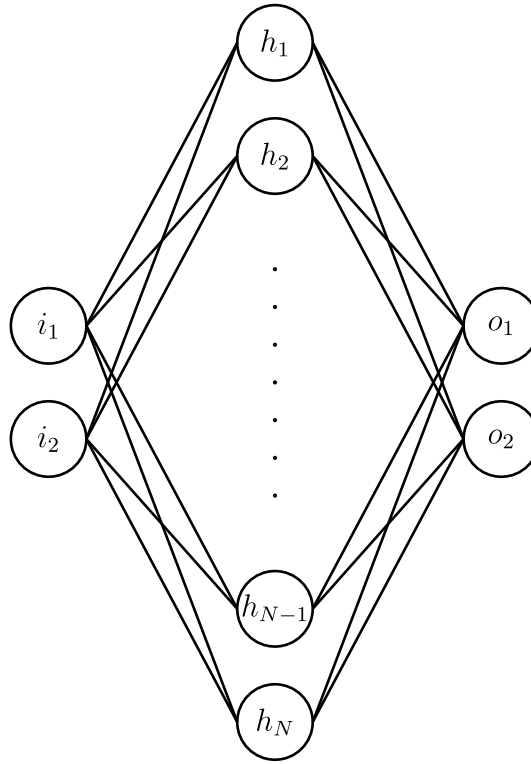


Figure 1. Single-layer fully-connected network of width N , with $d_{\text{in}} = d_{\text{out}} = 2$.

where subscript denotes the correlation functions associated to f_b and f_w , we also have

$$G^{(4)}(x_1, x_2, x_3, x_4) = G_b^{(4)}(x_1, x_2, x_3, x_4) + G_w^{(4)}(x_1, x_2, x_3, x_4) + \sum_{i \neq j \neq k \neq l} G_b^{(2)}(x_i, x_j) G_w^{(2)}(x_k, x_l), \quad (26)$$

and similarly for the higher-point functions. In networks with a linear output layer with Gaussian biases, f_b is a bias term that is drawn from an ultra-local GP at all N (since it does not depend on N), and f_w is the weight-dependent term that becomes a GP as $N \rightarrow \infty$, where the type of GP (non-local, semi-local, local) is model-dependent and depends on the choice of activation function.

One must derive the kernel associated to a given infinite width architecture in order to compute correlation functions in the associated GP. Kernel derivations are done in detail in appendix B via two methods: the first method described in [2] computes the exact 2-pt function for all widths, and a second method in [37] applies only in the GP limit. In the architectures that we study, the methods happen to agree for all widths N , though in general it is only required that the former method recover the result of the latter in the infinite width limit. We also build upon the work of [37] in creating a network with a translation invariant Gaussian kernel.

The networks differ only in their activation functions σ . We now introduce the networks that we study via their activation functions and the associated GP kernels.

2.3.1. Erf-net

The network architecture that we call Erf-net is defined by an error function activation

$$\sigma(z) = \text{Erf}(z) = \frac{2}{\sqrt{\pi}} \int_0^z dt e^{-t^2}. \quad (27)$$

The associated GP kernel is

$$K_{\text{Erf}}(x, x') = \sigma_b^2 + \sigma_w^2 \frac{2}{\pi} \arcsin \left[\frac{2(\sigma_b^2 + \frac{\sigma_w^2}{d_{\text{in}}} x x')}{\sqrt{\left(1 + 2(\sigma_b^2 + \frac{\sigma_w^2}{d_{\text{in}}} x^2)\right) \left(1 + 2(\sigma_b^2 + \frac{\sigma_w^2}{d_{\text{in}}} x'^2)\right)}} \right], \quad (28)$$

which is derived via both methods of [2] and [37] in (B.7).

2.3.2. ReLU-net

The network architecture that we call ReLU-net is defined by ReLU activation function:

$$\sigma(z) = \begin{cases} 0 & z < 0 \\ z & z \geq 0 \end{cases}. \quad (29)$$

The associated GP kernel is

$$K_{\text{ReLU}}(x, x') = \sigma_b^2 + \sigma_W^2 \frac{1}{2\pi} \sqrt{(\sigma_b^2 + \frac{\sigma_W^2}{d_{\text{in}}} x \cdot x)(\sigma_b^2 + \frac{\sigma_W^2}{d_{\text{in}}} x' \cdot x')(\sin \theta + (\pi - \theta) \cos \theta)}, \quad (30)$$

$$\theta = \arccos \left[\frac{\sigma_b^2 + \frac{\sigma_W^2}{d_{\text{in}}} x \cdot x'}{\sqrt{(\sigma_b^2 + \frac{\sigma_W^2}{d_{\text{in}}} x \cdot x)(\sigma_b^2 + \frac{\sigma_W^2}{d_{\text{in}}} x' \cdot x')}} \right],$$

which is derived via both methods of [2] and [37] in (B.14).

2.3.3. Gauss-net

While the two previous examples are well-studied in the literature, such as [2] and [38], in this section we introduce a new activation function in order to obtain a translation invariant GP kernel. This architecture is obtained by adding a normalization layer after the usual exponential activation, according to the process

$$x \rightarrow \exp(Wx + b) \rightarrow \frac{\exp(Wx + b)}{\sqrt{K_{\text{exp}}(x, x)}} \rightarrow f(x), \quad (31)$$

where $K_{\text{exp}}(x, x)$ is the 2-pt function of the intermediate exponential activation layer.

The resulting activation is⁹

$$\sigma(x) = \frac{\exp(Wx + b)}{\sqrt{\exp[2(\sigma_b^2 + \frac{\sigma_W^2}{d_{\text{in}}} x^2)]}}, \quad (32)$$

which unlike usual activations depends on both the preactivation and the input; we have written it entirely in terms of the input by writing $z = Wx + b$. The associated GP kernel

$$K_{\text{Gauss}}(x, x') = \sigma_b^2 + \sigma_W^2 \exp \left[-\frac{\sigma_W^2 |x - x'|^2}{2d_{\text{in}}} \right], \quad (33)$$

is derived via both the methods of [2] and [37] in (B.23). The kernel is particularly simple, a Gaussian¹⁰ in the Euclidean distance between the two inputs. Accordingly, the kernel is invariant under the translation map $x \rightarrow x + c$, $x' \mapsto x' + c$ for any constant vector c . The normalization in σ is crucial for translation invariance.

2.4. Experiments: falloff to GP Feynman diagrams at large width

We now wish to demonstrate that in the infinite width limit the experimental results for the n -pt functions $G^{(n)}$ converge to those of the GP, $G_{\text{GP}}^{(n)}$. For simplicity we will consider the case of a single-dimensional output, $d_{\text{out}} = 1$. Accordingly, we define the deviation in the n -pt function, in terms of experimental n -pt correlation of NN outputs $G^{(n)}$ defined in (39), and theoretical predictions by free field theory $G_{\text{GP}}^{(n)}$, given below

$$\Delta G^{(n)}(x_1, \dots, x_n) = G^{(n)}(x_1, \dots, x_n) - G_{\text{GP}}^{(n)}(x_1, \dots, x_n). \quad (34)$$

For measuring the size of the deviation with respect to the experimental results, it is convenient to define the normalized deviation $m_n(x_1, \dots, x_n) = \Delta G^{(n)} / G_{\text{GP}}^{(n)}(x_1, \dots, x_n)$.

The 2-pt deviation, given below, is the difference between the experimental 2-pt function and the kernel of the corresponding GP.

$$\begin{aligned} \Delta G^{(2)} &= G^{(2)}(x_1, x_2) - G_{\text{GP}}^{(2)}(x_1, x_2) \\ &= \mathbb{E}(f(x_1)f(x_2)) - K(x_1, x_2) \end{aligned}$$

⁹ We thank Greg Yang for discussions of activations that yield translationally invariant kernels.

¹⁰ Hence our choice of the name ‘Gauss-net’.

$$= \frac{1}{n_{\text{nets}}} \sum_{\alpha}^{n_{\text{nets}}} f_{\alpha}(x_1) f_{\alpha}(x_2) - K(x_1, x_2) \quad (35)$$

$f_{\alpha}(x_i)$ denotes the output of the α th network for the input x_i .

The 4-pt and 6-pt deviations are expressed using Wick contractions of products of the kernels evaluated at Wick pairs $p = (x_i, x_j)$. The 4-pt deviation is given by

$$\begin{aligned} \Delta G^{(4)} &= G^{(4)}(x_1, x_2, x_3, x_4) - G_{\text{GP}}^{(4)}(x_1, x_2, x_3, x_4) \\ &= \mathbb{E}(f(x_1) f(x_2) f(x_3) f(x_4)) - \sum_{p \in \text{Wick}(x_1, x_2, x_3, x_4)} K(p_1) K(p_2) \\ &= \frac{1}{n_{\text{nets}}} \sum_{\alpha}^{n_{\text{nets}}} f_{\alpha}(x_1) f_{\alpha}(x_2) f_{\alpha}(x_3) f_{\alpha}(x_4) - \left[K(x_1, x_2) K(x_3, x_4) \right. \\ &\quad \left. + K(x_1, x_3) K(x_2, x_4) + K(x_1, x_4) K(x_2, x_3) \right] \\ &= \frac{1}{n_{\text{nets}}} \sum_{\alpha}^{n_{\text{nets}}} f_{\alpha}(x_1) f_{\alpha}(x_2) f_{\alpha}(x_3) f_{\alpha}(x_4) - \left[\begin{array}{c} x_1 \quad x_3 \\ \vdots \quad \vdots \\ x_2 \quad x_4 \end{array} + \begin{array}{c} x_1 \quad x_3 \\ \text{---} \quad \text{---} \\ x_2 \quad x_4 \end{array} + \begin{array}{c} x_1 \quad x_3 \\ \diagdown \quad \diagup \\ x_2 \quad x_4 \end{array} \right]. \end{aligned} \quad (36)$$

The last line follows from (20).

The 6-pt function is obtained similarly using products of three kernels, where we will use the abbreviation $K(x_i, x_j) =: K_{ij}$ going forward. It is given by

$$\begin{aligned} \Delta G^{(6)} &= G^{(6)}(x_1, x_2, x_3, x_4, x_5, x_6) - \sum_{p \in \text{Wick}(x_1, x_2, x_3, x_4, x_5, x_6)} K(p_1) K(p_2) K(p_3) \\ &= \frac{1}{n_{\text{nets}}} \sum_{\alpha}^{n_{\text{nets}}} f_{\alpha}(x_1) f_{\alpha}(x_2) f_{\alpha}(x_3) f_{\alpha}(x_4) f_{\alpha}(x_5) f_{\alpha}(x_6) \\ &\quad - \left[K_{12} K_{34} K_{56} + K_{12} K_{35} K_{46} + K_{12} K_{36} K_{45} + K_{13} K_{24} K_{56} + K_{13} K_{25} K_{46} + K_{13} K_{26} K_{45} \right. \\ &\quad \left. + K_{14} K_{23} K_{56} + K_{14} K_{25} K_{36} + K_{14} K_{26} K_{35} + K_{15} K_{23} K_{46} + K_{15} K_{24} K_{36} + K_{15} K_{26} K_{34} \right. \\ &\quad \left. + K_{16} K_{23} K_{45} + K_{16} K_{24} K_{35} + K_{16} K_{25} K_{34} \right]. \end{aligned} \quad (37)$$

We remind the reader that in section 2.2 we discussed a simple check of the combinatorics: the Wick contractions for $G_{\text{GP}}^{(n)}$ (n even) involve the number of ways of connecting n points in pairs, which is $(n-1)!! = (n-1)(n-3) \dots 1$. For the $n=6$ case this predicts 15 terms, which we see explicitly in the last equality of (37).

The 2-pt, 4-pt and 6-pt deviations, denoted by $\Delta G^{(n)}$, are calculated experimentally at widths

$$N \in \{2, 3, 4, 5, 10, 20, 50, 100, 500, 1000\} \quad (38)$$

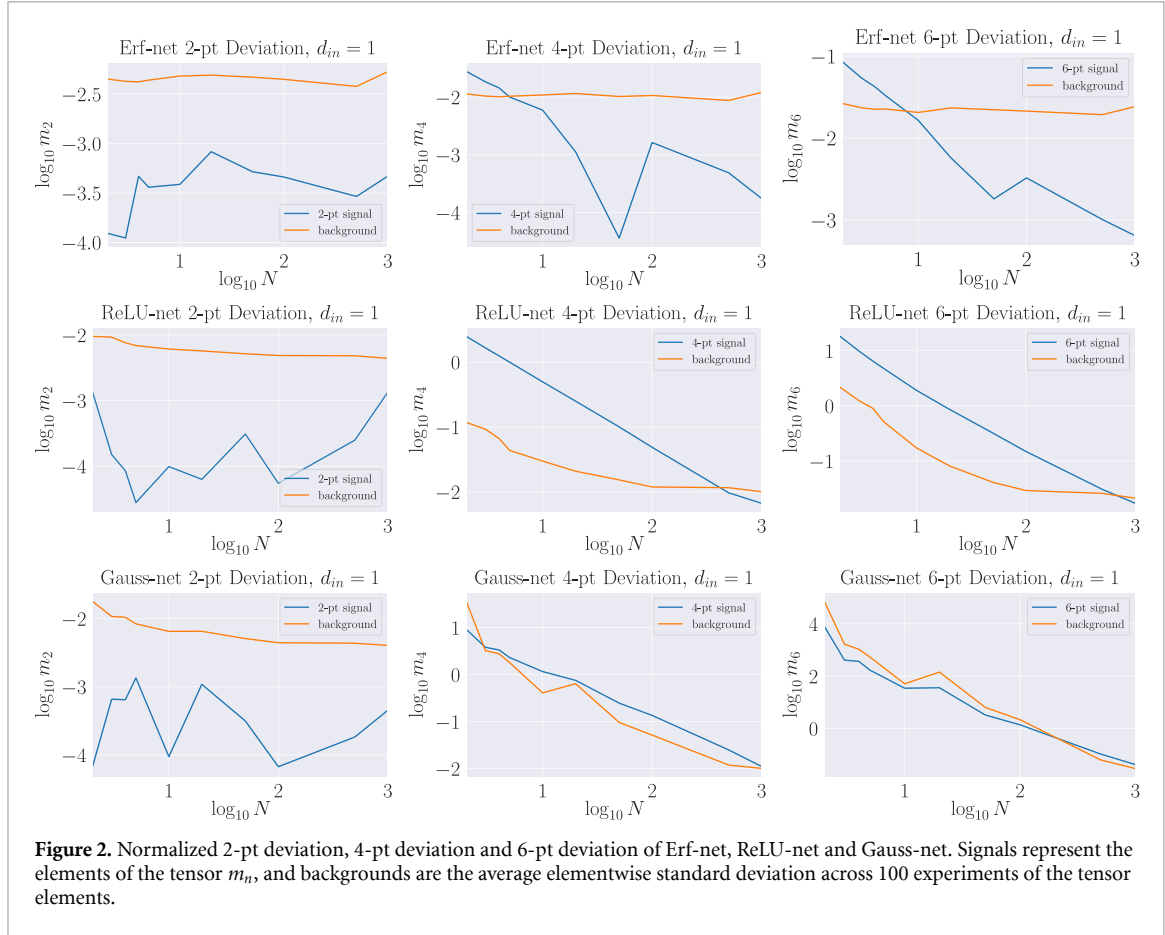
for all three architectures. To do this, for each architecture we calculate the n -pt correlation functions

$$G^{(n)}(x_1, \dots, x_n) = \frac{1}{n_{\text{nets}}} \sum_{\alpha \in \text{nets}}^{n_{\text{nets}}} f_{\alpha}(x_1), \dots, f_{\alpha}(x_n) \quad (39)$$

of outputs $f_{\alpha}(x_i)$ from 100 experimental runs with 10^5 networks each, with weights and biases θ drawn as described in table 2 with $\mu_W = \mu_b = 0$ and $\sigma_b = \sigma_W = 1$ for Erf-net and Gauss-net. Since our experiments have $d_{\text{in}} = 1$, this is $b^i \sim \mathcal{N}(0, 1)$ for $i = 1, 2$ and $W^0 \sim \mathcal{N}(0, 1)$, $W^1 \sim \mathcal{N}(0, 1/N)$. All experiments are done with 100 experiments of 10^5 nets each, for a total of $n_{\text{nets}} = 10^7$. We choose ReLU-net to have a bias of 0 for scaling reasons explained in section 4.3, so $\sigma_b = 0$ for this case. Inputs of ReLU-net are chosen to be all positive so that the kernel is always nonzero; the kernel is zero for opposite-signed inputs in the case $d_{\text{in}} = 1$ and $\sigma_b = 0$. Inputs of Erf-net are chosen to be positive to simplify the functional form in section 3, so that the kernel is always positive. These networks are defined for any $x \in \mathbb{R}^{d_{\text{in}}}$, but the inputs used for experiments were chosen where the finite width NGP is well approximated by local-operator correction terms to the associated log-likelihood. More generally, a neural network may only have some subset of the input space

Table 2. Parameters that define the networks used in GP and non-GP experiments in sections 2.4 and 3.5.

	Inputs $\{x_i\}$	(σ_w^2, σ_b^2)
Gauss-net	$\{-0.01, -0.006, -0.002, +0.002, +0.006, +0.01\}$	(1, 1)
Erf-net	$\{+0.002, +0.004, +0.006, +0.008, +0.010, +0.012\}$	(1, 1)
ReLU-net	$\{+0.2, +0.4, +0.6, +0.8, +1.0, +1.2\}$	(1, 0)



where local correction terms to the GP can give a good description of the NGP at finite width; we will systematically study non-local terms in follow-up work.

To study the falloff to GP predictions $G_{\text{GP}}^{(n)}$ as $N \rightarrow \infty$, the n -pt deviations $\Delta G^{(n)}$ are normalized by the GP prediction to obtain a measure $m_n = \Delta G^{(n)} / G_{\text{GP}}^{(n)}$, with input dependence implicit. These are plotted in figure 2 in comparison to a background defined to be the average elementwise standard deviation (across the 100 experiments) of the experimental m_n , as a function of width N , where for each width the solid blue line is the mean, and error bars are the 95 We expect $\Delta G^{(n)} = G^{(n)} - G_{\text{GP}}^{(n)}$ to show a $1/N$ falloff for all n ; we will prove this in section 2.5. Figure 2 shows that 2-pt deviations $\Delta G^{(2)}$ are below the background level and therefore consistent with zero for all three architectures, indicating that the kernel is an exact measure of the 2-pt correlation function even away from the GP. This is expected, since in appendix B it is shown that the GP kernels associated to the architectures we study are the exact two-point functions at all widths; from here on we therefore use kernel and 2-pt function interchangeably. The 4-pt and 6-pt signals are linearly decreasing (on a log-log scale) with increasing width in the region above the background level, falling below the background level at higher widths. The slope of the line in the region above the background is $\simeq -1$, indicating in our experiments that

$$\Delta G^{(n)} \propto N^{-1} \quad (40)$$

for $n = 4, 6$, up to experimental errors, shown by the flattening of signal well below the background. This explicitly demonstrates the falloff to GP as the width increases.

At large width, therefore, we see that these networks are drawn from GPs, with their statistics entirely determined by Wick contractions of the appropriate kernels, yielding $G_{\text{GP}}^{(n)}$. At small width, the GP prediction

no longer correctly predicts the experimental n -pt function; the neural networks are not drawn from a GP, but instead an NGP. Our goal is to develop a method for capturing non-Gaussian corrections to the log-likelihood.

2.5. N -scaling of correlation functions of fully-connected networks

Having seen that $\Delta G^{(n)} \propto N^{-1}$, we would like to understand this and related results in more theoretical detail. For convenience, we recall that linear output layer acts on the last post-activation as

$$f_{\theta,N}(x) = z_{k,1} = \sum_{j=1}^N W_{k,j,1} x_{j,1} + b_{k,1}, \quad (41)$$

where the post-activation is labeled x_1 since we are considering networks with a single hidden layer. The following results also hold for deep fully-connected networks with l layers, with x_1 replaced by x_l and W_1 by W_l . Henceforth we will use x_l and W_l , for generality, and suppress indices associated with the output and input dimensions, since they do not affect the result (or alternatively take $d_{\text{in}} = d_{\text{out}} = 1$). By x_i^j we denote the last post-activation of the i th input.

We are interested in the N -scaling properties of the correlation functions in these networks. Recall that a neural network with linear output layer is the sum of two functions f_b and f_W drawn from independent processes, $f_b \sim \mathcal{P}_b$ and $f_W \sim \mathcal{P}_W$, and that the bias term f_b does not depend on N . When its entries are drawn from Gaussian, it is an ultra-local GP at all N . Let \mathcal{P} be the process from which $f = f_b + f_W$ is drawn. The correlation functions of \mathcal{P} decompose into sums of products of correlation functions from \mathcal{P}_b and \mathcal{P}_W , and since \mathcal{P}_b does not depend on N and is Gaussian, all N -dependence and non-Gaussianities arise from \mathcal{P}_W .

We first wish to determine the leading N -scaling of the $2k$ -pt correlator $G^{(2k)}(x_1, \dots, x_{2k})$. In our normalizations which following, e.g. [3], the N -dependence of the $k = 1$ case drops out,

$$\begin{aligned} G^{(2)}(x_1, x_2) &= \mathbb{E}[b_1^2] + \sum_{i,j} \mathbb{E}[W_i W_j] \mathbb{E}[x_i^1 x_j^2] \\ &= \mathbb{E}[b_1^2] + \frac{\sigma_W^2}{N} \sum_i \mathbb{E}[x_i^1 x_i^2], \end{aligned} \quad (42)$$

where the factor of N is canceled by the N from the sum. $W_i = W_{l,i}$ and $x_{i,j} = x_{l,i}^j$ are respectively the weight of the l th layer and the post-activation of the l th layer of j th input; we will utilize this notation for rest of this subsection. The leading N -dependence must come from the $k = 2$ case, then, where the relevant term is (with Einstein summation implied)

$$\begin{aligned} G^{(4)}(x_1, x_2, x_3, x_4) &= \mathbb{E}[W_i W_j W_k W_m] \mathbb{E}[x_i^1 x_j^2 x_k^3 x_m^4] + \dots \\ &= \frac{3\sigma_W^4}{N^2} \sum_i \mathbb{E}[x_i^1 x_i^2 x_i^3 x_i^4] + \frac{\sigma_W^4}{N^2} \sum_{i \neq j} \left[\mathbb{E}[x_i^1 x_i^2 x_j^3 x_j^4] \right. \\ &\quad \left. + \mathbb{E}[x_i^1 x_j^2 x_j^3 x_i^4] + \mathbb{E}[x_i^1 x_i^2 x_j^3 x_j^4] + \dots \right], \end{aligned} \quad (43)$$

where the terms that survive in the sum have either two pairs of indices equal or all indices the same. The former correspond to contributions from products of $G_2^{(2)}$ s and come with a factor of $N(N-1)$ that results in a mixed scaling of the $(1 - \frac{1}{N})$, whereas the latter is a contribution to $G^{(4)}$ that is not a product of terms in lower-point functions and comes with a factor of N , leaving a $1/N$ -dependent factor. Thus we expect that we might have $\Delta G^{(4)}$, the deviation from GP results, scales as $1/N$. Being more precise, $\Delta G^{(4)}$ is the same as the *connected* piece of $G^{(4)}$ (see, e.g. QFT textbooks such as [39]),

$$\begin{aligned} &G^{(4)}(x_1, x_2, x_3, x_4) \Big|_{\text{connected}} \\ &= G^{(4)}(x_1, x_2, x_3, x_4) - G^{(2)}(x_1, x_2)G^{(2)}(x_3, x_4) - G^{(2)}(x_1, x_3)G^{(2)}(x_2, x_4) \\ &\quad - G^{(2)}(x_1, x_4)G^{(2)}(x_2, x_3), \\ &= \sum_i \langle W_i^4 \rangle \mathbb{E}[x_i^1 x_i^2 x_i^3 x_i^4] + \sum_{i \neq j} \langle W_i^2 \rangle \langle W_j^2 \rangle \left(\mathbb{E}[x_i^1 x_i^2] \mathbb{E}[x_j^3 x_j^4] + \mathbb{E}[x_i^1 x_i^3] \mathbb{E}[x_j^2 x_j^4] \right. \\ &\quad \left. + \mathbb{E}[x_i^1 x_i^4] \mathbb{E}[x_j^2 x_j^3] \right) - \sum_{i,j} \langle W_i^2 \rangle \langle W_j^2 \rangle \left(\mathbb{E}[x_i^1 x_i^2] \mathbb{E}[x_j^3 x_j^4] + \mathbb{E}[x_i^1 x_i^3] \mathbb{E}[x_j^2 x_j^4] + \mathbb{E}[x_i^1 x_i^4] \mathbb{E}[x_j^2 x_j^3] \right), \end{aligned} \quad (44)$$

$$\begin{aligned}
&= \sum_i \langle W_i^4 \rangle \mathbb{E}[x_i^1 x_i^2 x_i^3 x_i^4] - \sum_i \langle W_i^2 \rangle^2 \left(\mathbb{E}[x_i^1 x_i^2] \mathbb{E}[x_i^3 x_i^4] + \mathbb{E}[x_i^1 x_i^3] \mathbb{E}[x_i^2 x_i^4] + \mathbb{E}[x_i^1 x_i^4] \mathbb{E}[x_i^2 x_i^3] \right), \\
&= \frac{\sigma_W^4}{N^2} \sum_i \left(3 \cdot \mathbb{E}[x_i^1 x_i^2 x_i^3 x_i^4] - \mathbb{E}[x_i^1 x_i^2] \mathbb{E}[x_i^3 x_i^4] - \mathbb{E}[x_i^1 x_i^3] \mathbb{E}[x_i^2 x_i^4] - \mathbb{E}[x_i^1 x_i^4] \mathbb{E}[x_i^2 x_i^3] \right) \propto \frac{1}{N}, \quad (45)
\end{aligned}$$

where $x_i^k = \sigma(z_{i,l-1}^k) = \sigma\left(\sum_{j=1}^{N'} W_{j,l-1}^k x_{i,l-1}^j + b_{l-1}^k\right)$ is the postactivation of the l th layer; N' and $x_{i,l-1}^j$ are respectively the length and postactivation of $(l-2)$ th layer. If $(l-1)$ th layer is the input layer, then $N' = d_{\text{in}}$ and $x_{i,l-1} = x_i$.

Similarly, N -dependence of the 6-pt function arises from

$$G^{(6)}(x_1, x_2, x_3, x_4, x_5, x_6) = \sum_{i,j,k,m,n,o} \mathbb{E}[W_i W_j W_k W_m W_n W_o] \mathbb{E}[x_1^i x_2^j x_3^k x_4^m x_5^n x_6^o]. \quad (46)$$

The terms with all indices the same in pairs but different from one another results in $N(N-1)(N-2)$, leading to an overall scaling of $(1 - \frac{3}{N} + \frac{2}{N^2})$ once the N -dependence of weight variances are taken into account. When four of the indices are the same and the remaining two the same, but different from the four, we have a contribution of $N(N-1)$ that results in a scaling of $(\frac{1}{N} - \frac{1}{N^2})$ after weight variances. We thus see that the leading non-trivial N -dependence is $\propto 1/N$, which can be interpreted as the contribution of the connected part of the 4-pt function to the 6-pt function, via multiplication with a 2-pt function. We have $\Delta G^{(6)} \propto 1/N$, in agreement with experiments.

However, we are also interested in the scaling of the *connected* contributions to the 6-pt function. It is given by

$$\begin{aligned}
&G^{(6)}(x_1, x_2, x_3, x_4, x_5, x_6) \Big|_{\text{connected}} = G^{(6)}(x_1, x_2, x_3, x_4, x_5, x_6) - \sum_{\mathcal{P}(abcdef)} G^{(2)}(x_e, x_f) \\
&\quad \left(G^{(4)}(x_a, x_b, x_c, x_d) G^{(2)}(x_e, x_f) - 2 \cdot G^{(2)}(x_a, x_b) G^{(2)}(x_c, x_d) G^{(2)}(x_e, x_f) \right), \quad (47) \\
&= G^{(6)}(x_1, x_2, x_3, x_4, x_5, x_6) - \sum_{\mathcal{P}(abcdef)} \left(G^{(4)}(x_a, x_b, x_c, x_d) \Big|_{\text{connected}} G^{(2)}(x_e, x_f) \right. \\
&\quad \left. + G^{(2)}(x_a, x_b) G^{(2)}(x_c, x_d) G^{(2)}(x_e, x_f) \right), \\
&= \sum_i \langle W_i^6 \rangle \mathbb{E}[x_i^1 x_i^2 x_i^3 x_i^4 x_i^5 x_i^6] + \sum_{\mathcal{P}(abcdef)} \left(\sum_{i \neq j} \langle W_i^2 \rangle \langle W_j^2 \rangle \mathbb{E}[x_i^a x_i^b x_i^c x_i^d] \mathbb{E}[x_j^e x_j^f] \right. \\
&\quad \left. + \sum_{i \neq j \neq k} \langle W_i^2 \rangle \langle W_j^2 \rangle \langle W_k^2 \rangle \mathbb{E}[x_i^a x_i^b] \mathbb{E}[x_j^c x_j^d] \mathbb{E}[x_k^e x_k^f] - \left[\sum_{i,j} \langle W_i^4 \rangle \langle W_j^2 \rangle \mathbb{E}[x_i^a x_i^b x_i^c x_i^d] \mathbb{E}[x_j^e x_j^f] \right. \right. \\
&\quad \left. \left. - \sum_{i,j} \langle W_i^2 \rangle^2 \langle W_j^2 \rangle \mathbb{E}[x_i^a x_i^b] \mathbb{E}[x_j^c x_j^d] \mathbb{E}[x_j^e x_j^f] + \sum_{i,j,k} \langle W_i^2 \rangle \langle W_j^2 \rangle \langle W_k^2 \rangle \mathbb{E}[x_i^a x_i^b] \mathbb{E}[x_j^c x_j^d] \mathbb{E}[x_k^e x_k^f] \right] \right), \\
&= \sum_i \langle W_i^6 \rangle \mathbb{E}[x_i^1 x_i^2 x_i^3 x_i^4 x_i^5 x_i^6] - \sum_{\mathcal{P}(abcdef)} \sum_i \langle W_i^4 \rangle \langle W_i^2 \rangle \mathbb{E}[x_i^a x_i^b x_i^c x_i^d] \mathbb{E}[x_i^e x_i^f] + \text{terms}, \quad (48)
\end{aligned}$$

and

$$\begin{aligned}
&\text{terms} = \sum_{\mathcal{P}(abcdef)} \left(\sum_{i \neq j \neq k} \langle W_i^2 \rangle \langle W_j^2 \rangle \langle W_k^2 \rangle \mathbb{E}[x_i^a x_i^b] \mathbb{E}[x_j^c x_j^d] \mathbb{E}[x_k^e x_k^f] \right. \\
&\quad \left. + \sum_{i,j} \langle W_i^2 \rangle^2 \langle W_j^2 \rangle \mathbb{E}[x_j^e x_j^f] \left(\mathbb{E}[x_i^a x_i^b] \mathbb{E}[x_i^c x_i^d] + \mathbb{E}[x_i^a x_i^c] \mathbb{E}[x_i^b x_i^d] + \mathbb{E}[x_i^a x_i^d] \mathbb{E}[x_i^b x_i^c] \right) \right. \\
&\quad \left. - \sum_{i,j,k} \langle W_i^2 \rangle \langle W_j^2 \rangle \langle W_k^2 \rangle \mathbb{E}[x_i^a x_i^b] \mathbb{E}[x_j^c x_j^d] \mathbb{E}[x_k^e x_k^f] \right), \quad (49)
\end{aligned}$$

where $\mathcal{P}(abcdef)$ indicates that the sum is over all unique terms made by choices of $\{a, b, c, d, e, f\} \in \{1, 2, 3, 4, 5, 6\}$, where no two elements are the same. Using the expansion,

$$\begin{aligned}
 & \sum_{i,j,k} \langle W_i^2 \rangle \langle W_j^2 \rangle \langle W_k^2 \rangle \mathbb{E}[x_i^a x_i^b] \mathbb{E}[x_j^c x_j^d] \mathbb{E}[x_k^e x_k^f] \\
 &= -2 \cdot \sum_i \langle W_i^2 \rangle^3 \mathbb{E}[x_i^a x_i^b] \mathbb{E}[x_i^c x_i^d] \mathbb{E}[x_i^e x_i^f] \\
 &+ \sum_{i,j} \langle W_i^2 \rangle^2 \langle W_j^2 \rangle \mathbb{E}[x_j^c x_j^d] \left(\mathbb{E}[x_i^a x_i^b] \mathbb{E}[x_i^c x_i^d] + \mathbb{E}[x_i^a x_i^c] \mathbb{E}[x_i^b x_i^d] + \mathbb{E}[x_i^a x_i^d] \mathbb{E}[x_i^b x_i^c] \right) \\
 &- \sum_{i \neq j \neq k} \langle W_i^2 \rangle \langle W_j^2 \rangle \langle W_k^2 \rangle \mathbb{E}[x_i^a x_i^b] \mathbb{E}[x_j^c x_j^d] \mathbb{E}[x_k^e x_k^f], \tag{50}
 \end{aligned}$$

the *connected* part of $G^{(6)}$ is obtained as

$$\begin{aligned}
 & G^{(6)}(x_1, x_2, x_3, x_4, x_5, x_6) \Big|_{\text{connected}} \\
 &= \sum_i \left[\langle W_i^6 \rangle \mathbb{E}[x_i^1 x_i^2 x_i^3 x_i^4 x_i^5 x_i^6] \right. \\
 &- \sum_{\mathcal{P}(abcdef)} \left(\sum_i \langle W_i^4 \rangle \langle W_i^2 \rangle \mathbb{E}[x_i^a x_i^b x_i^c x_i^d] \mathbb{E}[x_i^e x_i^f] - 2 \cdot \sum_i \langle W_i^2 \rangle^3 \mathbb{E}[x_i^a x_i^b] \mathbb{E}[x_i^c x_i^d] \mathbb{E}[x_i^e x_i^f] \right) \Big] \\
 &= \frac{\sigma_W^6}{N^3} \sum_i \left[15 \cdot \mathbb{E}[x_i^1 x_i^2 x_i^3 x_i^4 x_i^5 x_i^6] - 3 \cdot \sum_{\mathcal{P}(abcdef)} \mathbb{E}[x_i^a x_i^b x_i^c x_i^d] \mathbb{E}[x_i^e x_i^f] \right. \\
 &+ 2 \cdot \sum_{\mathcal{P}(abcdef)} \mathbb{E}[x_i^a x_i^b] \mathbb{E}[x_i^c x_i^d] \mathbb{E}[x_i^e x_i^f] \Big]. \tag{51}
 \end{aligned}$$

That is, we have

$$G^{(6)}(x_1, \dots, x_6) \Big|_{\text{connected}} \propto \frac{1}{N^2}, \tag{52}$$

which is $1/N$ -suppressed relative to the connected part of the 4-pt function.

Based on the structure of the two examples we have computed, it is natural to make a conjecture regarding the connected contributions to the $2k$ -pt function. In both cases, when representing the connected correlator in terms of a sum of full correlators, with some terms involving lower correlators, we saw that the only terms that did not cancel were the ones with all indices the same. It is natural to expect this to be general, in which case we have

$$G^{(2k)}(x_1, \dots, x_{2k}) \Big|_{\text{connected}} = \left[G^{(2k)}(x_1, \dots, x_{2k}) - S(x_1, \dots, x_{2k}) \right] \Big|_{\text{internal indices same}}, \tag{53}$$

where the terms in brackets are the general result from consideration of the connected generating functional $W[J]$, which yields an expression for the connected correlator as the full correlator minus sums of products of lower point functions, the latter represented by $S(x_1, \dots, x_{2k})$. The restriction to all internal indices is specific to the linear output layer we have utilized. For instance, in the connected 4-pt function

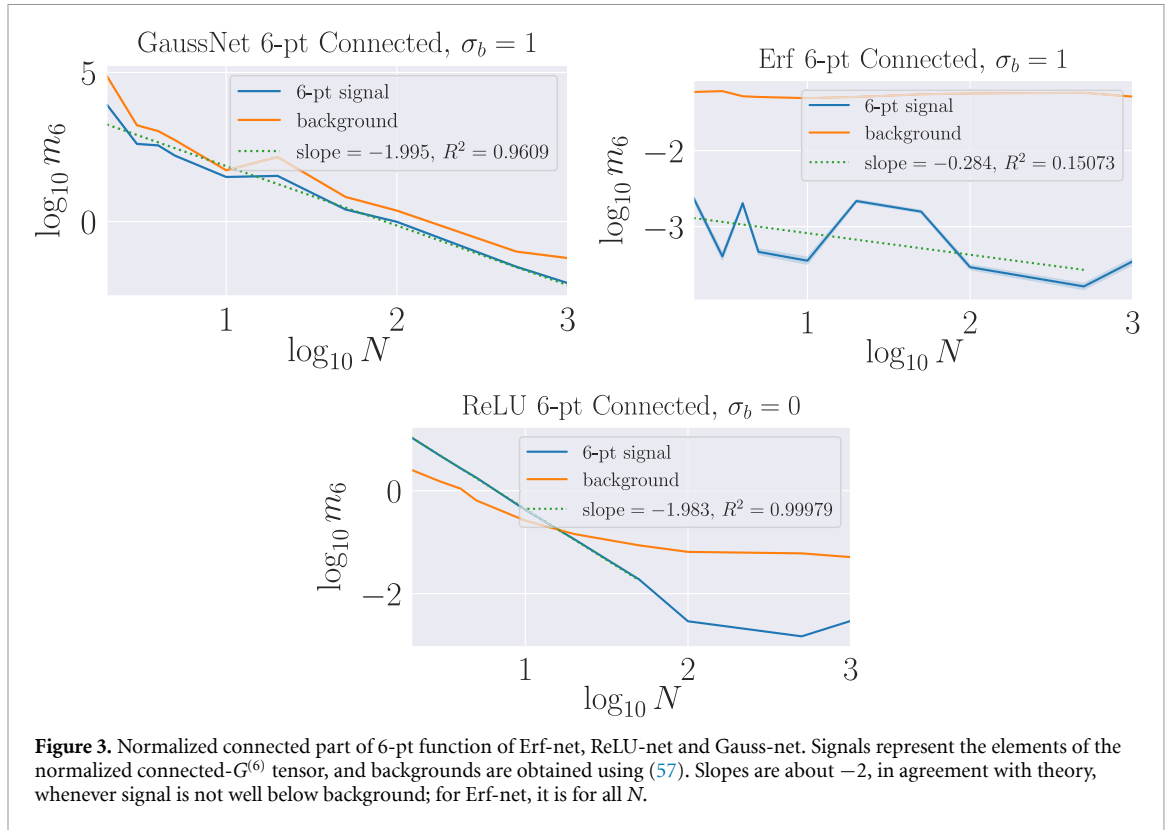
$$S(x_1, \dots, x_4) = G^{(2)}(x_1, x_2) G^{(2)}(x_3, x_4) + G^{(2)}(x_1, x_3) G^{(2)}(x_2, x_4) + G^{(2)}(x_1, x_4) G^{(2)}(x_2, x_3), \tag{54}$$

and the associated restriction in the case of linear output layer is

$$\begin{aligned}
 & \left[G^{(2)}(x_1, x_2) G^{(2)}(x_3, x_4) + G^{(2)}(x_1, x_3) G^{(2)}(x_2, x_4) + G^{(2)}(x_1, x_4) G^{(2)}(x_2, x_3) \right] \Big|_{\text{internal indices same}} \\
 &= \sum_i \langle W_i^2 \rangle^2 \left(\mathbb{E}[x_i^1 x_i^2] \mathbb{E}[x_i^3 x_i^4] + \mathbb{E}[x_i^1 x_i^3] \mathbb{E}[x_i^2 x_i^4] + \mathbb{E}[x_i^1 x_i^4] \mathbb{E}[x_i^2 x_i^3] \right), \tag{55}
 \end{aligned}$$

appears directly in the result for the connected 4-pt function. For our weight distributions, the conjecture implies

$$G^{(2k)}(x_1, \dots, x_{2k}) \Big|_{\text{connected}} \propto \frac{1}{N^{k-1}}, \tag{56}$$



which explicitly holds for the two cases we computed, $k = 1$ and $k = 2$.

Foreshadowing our NGP treatment, our explicit computations have an important implication: the simplest way to have the connected 4-pt and 6-pt correlators scale this way is to have the 4-pt and 6-point couplings scale as $1/N$ and $1/N^2$, respectively, since they generate tree-level contributions to the associated connected correlators.

The background levels in figure 3 is determined by the average of element-wise standard deviations of 100 experiments for each of the n -pt functions at each width, and by further propagating the error to obtain the error in the connected 6-pt function,

$$\left. \delta G^{(6)} \right|_{\text{connected}} = \sqrt{(\delta G^{(6)})^2 + (G^{(2)} \delta G^{(4)})^2}. \quad (57)$$

No error for $G^{(2)}$ is included because we use the exact theory expression. Erf-net connected- $G^{(6)}$ is well below background at all widths, and does not show the expected $1/N^2$ dependence. ReLU-net shows expected $1/N^2$ falloff until it is well below the background level. Gauss-net also shows expected $1/N^2$ dependence. Thus, up to statistical errors $\left. G^{(6)} \right|_{\text{connected}}$ shows $1/N^2$ dependence.

3. Neural networks and non-Gaussian processes with effective field theory

In this section we propose using an approach to QFT known as Wilsonian EFT to understand and analyze neural networks away from their GP limits. From an ML point of view, it can be thought of as a useful way to determine minimal log-likelihoods of NGPs by determining the most relevant non-Gaussian corrections to the GP.

The essential idea is that the GP action S_{GP} does not suffice to determine correlation functions $G^{(n)}$ away from the GP limit, as demonstrated experimentally in section 2.4, but the principles of EFT allows for the determination of corrections ΔS to the GP log-likelihood, yielding an effective log-likelihood for the NGP¹¹ associated to the finite-width neural networks,

$$S = S_{\text{GP}} + \Delta S. \quad (58)$$

¹¹ Henceforth, the NGP effective action.

The organizing principles of EFT are symmetries and scales, which together allow for the determination of an appropriate ΔS that may have its parameters fixed by experiments. It may then be used to make effective (correct) predictions for other experiments.

For the ML reader, let us briefly tour these ideas in physics, where effective field theories correctly describe a vast array of systems, from superfluids and superconductors in condensed matter physics to beta decay and elementary particle interactions¹² in high energy physics. As a concrete example, consider beta decay, a process by which a neutron decays into a proton, electron, and anti-neutrino,

$$n \rightarrow p + e^- + \bar{\nu}_e. \quad (59)$$

From the perspective of the Standard Model, we have a deep knowledge of this process: the neutrons and protons are made up of quarks and the decay process is mediated by an intermediate W-boson. However, this detailed knowledge did not keep Fermi from arriving at an EFT description of the process in 1933 [40], long before quarks and W-bosons were even theorized, let alone discovered over 35 years later. Though symmetries permeate both Fermi's theory and the Standard Model, the crucial insight is one of energy scale: Fermi's interaction that effectively describes beta decay is obtained from the Standard Model by going to lower and lower scattering energies, at which point the contribution from the intermediate W-boson is negligible and an effective four-fermion interaction suffices to describe the process.

In this spirit, we propose understanding neural networks away from GP limits in terms of EFT. Specifically, EFT allows for the determination of an NGP effective action, with its parameters fixed by experiments, which is then used to make verifiable predictions. To that end, the correspondence in table 3 identifies the NN input $x \in \mathbb{R}^{d_{\text{in}}}$ with a point in space or momentum space in field theory, the NN kernel with free or exact propagator in QFT, depending on the NNGP in infinite width limit. The NN output $f(x)$ and log-likelihood now corresponds to the interacting field and the EFT action respectively.

Rather than organizing according to length or momentum scale, the NN-QFT correspondence that we are developing replaces fields as a function of space with neural networks as a function of input, suggesting organization of the problem according to input scale. The interpretation of this in ML depends on the problem, but an example of 'input scale' in images would be brightness.

As in physics, we utilize the quadratic terms to determine classical scaling dimensions, which here are given by the probability of an infinite-width neural net (GP draw) f

$$P[f] = e^{-S_{\text{GP}}[f]} = \exp \left[-\frac{1}{2} \int d^{d_{\text{in}}} x d^{d_{\text{in}}} y f(x) \Xi(x, y) f(y) \right]. \quad (60)$$

Specifically, S_{GP} must be dimensionless; it scales as x^0 , and we write $[S_{\text{GP}}] = 0$. Since $d^{d_{\text{in}}} x$ scales as $x^{d_{\text{in}}}$ it has input dimensions of d_{in} , $[d^{d_{\text{in}}} x] = d_{\text{in}}$, and similarly $[d^{d_{\text{in}}} y] = d_{\text{in}}$. $[S] = 0$ then determines a relation between dimensions of f and Ξ , $[S] = 2d_{\text{in}} + 2[f] + [\Xi] = 0$, which determines the classical scaling dimension of the neural network f ,

$$[f] = -\frac{2d_{\text{in}} + [\Xi]}{2}. \quad (61)$$

This in turn may be used to determine the dimensions of the coefficients of operators that might appear in ΔS . For instance, consider operators

$$\mathcal{O}_k := g_k f(x)^k \quad (62)$$

appearing in ΔS as $\int d^{d_{\text{in}}} x \mathcal{O}_k$. Then $[\Delta S] = 0$ requires $d_{\text{in}} + k[f] + [g_k] = 0$ and we have

$$[g_k] = -d_{\text{in}} + \frac{k(2d_{\text{in}} + [\Xi])}{2}. \quad (63)$$

By (8) and the fact¹³ that $[\delta^{(d_{\text{in}})}(x)] = -d_{\text{in}}$ we have $d_{\text{in}} + [\Xi] + [K] = -d_{\text{in}}$, and therefore can rewrite $[g_k]$ in terms of the scaling dimension of the kernel

$$[g_k] = -d_{\text{in}} - \frac{k[K]}{2}. \quad (64)$$

¹² The Standard Model of particle physics is an effective field theory, and for some measurements it yields perhaps the highest precision agreement between theory and experiment in all of science.

¹³ This follows from the natural d -dimensional extension of the identity $\delta(ax) = \delta(x)/|a|$.

Table 3. Correspondence between quantities in the NGP/finite-width neural network and QFT. See text for discussion on whether the kernel is the free or exact propagator.

NGP/finite NN	Interacting QFT
Input x	External space or momentum space point
Kernel $K(x_1, x_2)$	Free or exact propagator
Network output $f(x)$	Interacting field
Non-Gaussianities	Interactions
Non-Gaussian coefficients	Coupling strengths
Log probability	Effective action S

Unlike in many physical cases, for $[K] \geq 0$ the couplings g_k have dimensions of the same sign $\forall k$. In section 4 we will use arguments from Wilson's picture of the RG to argue that operators \mathcal{O}_k can be safely ignored for sufficiently large k .

How does one construct the effective action of an NGP associated to a neural network architecture that admits a known GP limit? Wilsonian EFT dictates the following rules:

- Determine the symmetries (or desired symmetries) respected by the system of interest.
- Fix an upper bound k on the dimension of any operator appearing in ΔS .
- Define ΔS to contain all operators of dimension $\leq k$ that respect the symmetries.

Since the GP limit is known, the NGP is defined by $S = S_{\text{GP}} + \Delta S$. As we will see in a moment, this allows for the determination of correlation functions. By experimentally measuring them, one may fix coefficients of terms in ΔS and make subsequent predictions.

The desired symmetries may be determined by architecture considerations or, e.g. by demanding that the NGP respects the same symmetries as its GP limit, in which case the NGP symmetries are the symmetries of the GP kernel $K(x_1, x_2)$. The choice of a relevant value of k is sometimes dictated by the system of study. For instance, Fermi knew that his theory must have only spin-1/2 particles¹⁴ and that four of them must interact to describe beta decay. In QFT this requires a term schematically of the form $\psi\psi\psi\psi$, where ψ is a field associated with a spin-1/2 particle. Since $[\psi] = 3/2$ in four dimensions, Fermi's theory needed $k \geq 6$. In the examples we study in this paper, we will see that it is crucial it have $k \geq 4$.

3.1. Correlation functions in NGPs with interacting Feynman diagrams

Having introduced EFT rules that allow for the determination of ΔS , we must introduce a method for computing NGP correlation functions. Before doing this explicitly in the cases of interest, we must briefly introduce the basics of cutoffs and perturbation theory.

First, perturbation theory: consider an NGP associated with a finite-width neural network architecture, with associated effective action $S = S_{\text{GP}} + \Delta S$. The GP correlation functions $G_{\text{GP}}^{(n)}$ were exactly computable precisely because the action S_{GP} was Gaussian, so non-Gaussian corrections in ΔS prevent the NGP n -pt correlation functions

$$G^{(n)}(x_1, \dots, x_n) = \frac{\int df f(x_1) \dots f(x_n) e^{-S}}{Z_0}, \quad \text{where } Z_0 = \int df e^{-S}, \quad (65)$$

from being computed exactly. However, if the coefficients of operators in ΔS are appropriately small, approximating the n -pt functions using perturbation theory is possible. In QFT, this corresponds to the existence of non-trivial interactions, where the interaction strength being small yields a correction to the leading process. As an example, consider corrections to the n -pt function arising from $\Delta S = \int d^{\text{in}} x g_k f(x)^k$, with $k > 2$. Multiplying the numerator and denominator by $1/Z_{\text{GP},0}$ and expanding under the assumption of small g_k , we have

$$G^{(n)}(x_1, \dots, x_n) = \frac{\int df f(x_1) \dots f(x_n) \left[1 - \int d^{\text{in}} x g_k f(x)^k + O(g_k^2) \right] e^{-S_{\text{GP}}/Z_{\text{GP},0}}}{\int df \left[1 - \int d^{\text{in}} x g_k f(x)^k + O(g_k^2) \right] e^{-S_{\text{GP}}/Z_{\text{GP},0}}}. \quad (66)$$

Truncating at a desired order in g_k (here just the leading correction), one obtains an approximation for the n -pt function where the numerator and denominator may both be computed via Wick's theorem, and both

¹⁴ Since the W-boson mediator had not been observed yet.

may be represented diagrammatically¹⁵. The $O(g_k^0)$ contribution in the numerator is precisely the GP n -pt function $G_{\text{GP}}^{(n)}$. The $O(g_k^1)$ term in the numerator may be computed via Wick's theorem, with one of the associated diagrams being a tree-level (no-loops) diagram by which the n external points $\{x_1, \dots, x_n\}$ connect to the point x that is integrated over; the latter is known as the interaction vertex, and is referred to as an internal point. These calculations and vacuum bubble cancellation is reviewed in appendix A.

We now introduce cutoffs. Computing NGP correlation functions via perturbation theory can lead to integrals over input space that naively yield divergences. A simple way to treat the divergence is to cut them off by the replacement

$$S \rightarrow S_\Lambda, \quad (67)$$

where S_Λ differs from S only in the fact that all integrals over input space are bounded from below by $-\Lambda$ and above by Λ , where Λ is positive and known as the cutoff. In QFT it is usually integrals over momenta (of the virtual particles created and annihilated during particle interactions) that are cut off, with the justification that theories have finite regimes of validity; e.g. theories describing scattering done at one momentum scale should not be valid up to arbitrarily high momenta. Accordingly, low energy experiments with momenta $|p| \ll \Lambda$ should be insensitive to the choice of Λ . This requirement imposes that the coefficients of operators in S must obey a differential equation known as the Wilsonian renormalization group equations (RGEs). We will discuss this at length in section 4.3, and demonstrate that, the NGP associated to finite-width ReLU-net satisfies appropriate Wilsonian RGE.

Our discussion of perturbation theory focused on a particular term in ΔS , however, it is of course possible to have many terms in ΔS , each with its own coefficient to expand in, if it is small. This gives a general prescription for approximating correlation functions in neural network NGPs, which may be written as Feynman diagrams via the development of appropriate Feynman rules.

Of course, we are interested in doing neural net experiments that validate theoretical predictions, and so we again focus on the finite width single-layer networks introduced in section 2.3. We have a single output, $d_{\text{out}} = 1$, and therefore one might consider non-Gaussian terms of the form


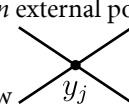
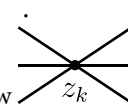
$$\Delta S = \int d^{\text{dim}} x [gf(x)^3 + \lambda f(x)^4 + \alpha f(x)^5 + \kappa f(x)^6 + \dots]. \quad (68)$$

However, all odd-point functions in our experiments must be zero, since the means of the weights and biases are zero. This motivates $g = \alpha = 0$, since when expanded to linear order those terms yield non-trivial contributions to the 3-pt and 5-pt functions, respectively. An intuitive way to see this is that in our randomly initialized neural nets f and $-f$ should be on equal footing, and thus S must have an $f \rightarrow -f$ symmetry (i.e. be invariant under this transformation) that would be broken by either $g \neq 0$ or $\alpha \neq 0$. Furthermore, in section 4 we will explain why for sufficiently large Λ , κ must be negligible, or *irrelevant* in the sense of Wilsonian RG; however, we will consider both until section 4. By these considerations, the effective action we will utilize for the remainder of the paper is

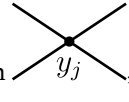
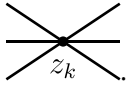
$$S = S_{\text{GP}} + \int d^{\text{dim}} x [\lambda f(x)^4 + \kappa f(x)^6]. \quad (69)$$

In our experiments we will also see that κ is negligible, and therefore a single quartic correction will be sufficient to explain our finite-width neural net experiments.

With this effective action for the NGP, one may compute correlation functions in perturbation theory. Equivalently, one may represent the correlation functions diagrammatically by the following Feynman rules. They may be stated in different ways according to the goals at hand. Here we state them in a way relevant for computing the $O(\lambda^l \kappa^m)$ correction to $G^{(n)}(x_1, \dots, x_n)$, where the ‘interaction vertices’ are y_j ($j = 1, \dots, l$) and z_k ($k = 1, \dots, m$).

- (a) For each of the n external points x_i , draw .
- (b) For each y_j , draw . For each z_k , draw .

¹⁵ Some (all) diagrams in the numerator (denominator) contain vacuum bubbles. A vacuum bubble is a diagram that is not connected to any external points. They may arise as disconnected components of more complicated diagrams, as in the numerator. However, the vacuum bubbles that arise in the denominator precisely cancel those arising in the numerator, so that the final expression for $G^{(n)}$ does not contain any diagrams with vacuum bubbles.

- (c) Determine all ways to pair up the loose ends associated to x_i 's, y_j 's, and z_k 's. This will yield some number of topologically distinct diagrams. Draw them with solid lines.
- (d) Write a sum over the diagrams with an appropriate combinatoric factor out front, which is the number of ways to form that diagram. Each diagram corresponds to an analytic term in the sum.
- (e) For each diagram, write $-\int d^{d_{\text{in}}} y_j \lambda$ for each , and $-\int d^{d_{\text{in}}} z_k \kappa$ for each .
- (f) Write $K(u, v)$ for each $u \quad v$.
- (g) Throw away any terms containing vacuum bubbles; see footnote 15.

As a non-trivial check, after step (b) there are $6m$ z_k loose ends, $4l$ y_j loose ends, and n x_i loose ends, and there are $(n + 4l + 6m - 1)!!$ ways of connecting these in pairs, which must be the sum of the coefficients of the topologically distinct diagrams, including vacuum bubbles.

We *strongly emphasize* that the cases relevant for our experiments require an important modification to what we have presented thus far, which is correct when $S = S_{\text{GP}} + \Delta S$, and ΔS is comprised of only non-Gaussian corrections, i.e. S_{GP} is the only Gaussian part of the action. In that case the two-point function is

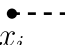
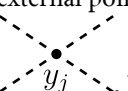
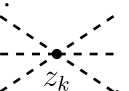

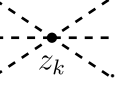
$$G^{(2)}(x_1, x_2) = K(x_1, x_2) + \lambda - \text{and } \kappa - \text{corrections.} \quad (70)$$

In particular, $K(x_1, x_2)$ is the analog of the free-theory propagator in QFT, and it is only the leading piece in the 2-pt function, which receives corrections from interactions.

In the architectures used in our experiments, however, we remind the reader that the GP kernel is the exact 2-pt function for the NGP as well

$$G^{(2)}(x_1, x_2) = K(x_1, x_2), \quad (71)$$

as experimentally demonstrated in section 2.4 and theoretically derived in appendix B. In particular this means that $S \neq S_{\text{GP}} + \Delta S$, but instead $S = S_G + \Delta S$ for some other Gaussian action S_G , defined to be the action such that (71) holds. One can in principle compute S_G , but a simpler modification that we employ is to modify the Feynman rules for computing the $O(\lambda^l \kappa^m)$ correction to $G^{(n)}(x_1, \dots, x_n)$. The complete new Feynman rules in this case are

- (a) For each of the n external points x_i , draw .
- (b) For each y_j , draw . For each z_k , draw .
- (c) Determine all ways to pair up the loose ends associated to x_i 's, y_j 's, and z_k 's. This will yield some number of topologically distinct diagrams. Draw them with dashed lines.
- (d) Write a sum over the diagrams with an appropriate combinatoric factor out front, which is the number of ways to form that diagram. Each diagram corresponds to an analytic term in the sum.
- (d1) Throw away any diagram that has a component with a λ - or κ correction to the 2-pt function.
- (e) For each diagram, write $-\int d^{d_{\text{in}}} y_j \lambda$ for each , and $-\int d^{d_{\text{in}}} z_k \kappa$ for each .
- (f) Write $K(u, v)$ for each $u \quad v$.
- (g) Throw away any terms containing vacuum bubbles.

Despite having presented the complete list, note that the only changes are the dashed lines in steps (b) and (f), and the new step (d1).

Diagrams thrown out at that step should not be included in this case because in writing $K(x_1, x_2)$ for $x_1 \quad x_2$ in step (g), the λ - and κ - corrections to the 2-pt function are already included, since the exact two-point function is the GP kernel. An example of such a diagram is of the form

$$\begin{array}{c} \bullet \quad \bullet \\ \vdots \quad \vdots \\ \bullet \quad \bullet \end{array} \quad \text{in } G^{(4)}(x_1, x_2, x_3, x_4) \quad (72)$$

which is implicitly included in the term of the form

$$\begin{array}{c} \bullet \cdots \cdots \bullet \\ \bullet \cdots \cdots \bullet \end{array} \quad \text{in } G^{(4)}(x_1, x_2, x_3, x_4) \quad (73)$$

when the exact 2-pt function is used. It is easy to identify similar diagrams that must be thrown away as they arise. Of course, this type of modification arises for any NGP in which (71) holds. The $(n + 4l + 6m - 1)!!$ combinatorics may still be used as a non-trivial check prior to discarding diagrams in steps (d1) and (g). Finally, if we draw $\bullet \text{---} \bullet$ in a case where (71) holds, it means the propagator/kernel of S_G .

3.2. Four-point and six-point NGP correlation functions

We now turn to the computation of the 4-pt and 6-pt functions, since they will be studied in our experiments. We emphasize, however, that the calculations here are valid for the stated orders in λ and κ for broader classes of NGPs associated with neural network architectures.

Since in our experiments the NGP two-point function $G^{(2)}$ is exactly the kernel in the GP limit, i.e. (71) holds, we are in the case where $S = S_G + \Delta S$. Accordingly we use the second set of Feynman rules in which $\bullet \text{---} \bullet$ represents the propagator of S_G and $\bullet \cdots \bullet$ represents the exact two-point function. We may represent the two-point function in perturbation theory as

$$\begin{aligned} G^{(2)}(x_1, x_2) &= \bullet \text{---} \bullet - \lambda \left[12 \begin{array}{c} \bullet \text{---} \bullet \\ \text{---} \bullet \end{array} \right] - \kappa \left[90 \begin{array}{c} \bullet \text{---} \bullet \\ \text{---} \bullet \end{array} \right] \\ &= \bullet \cdots \bullet \\ &= K(x_1, x_2), \end{aligned} \quad (74)$$

where the second diagrammatic equation represents the analytic expression via the second set of Feynman rules, critically relying on step (d1).

The 4-pt and 6-pt functions may be computed similarly. To simplify the Feynman diagrams we add the additional rule that we do not label external points, which is to be interpreted as summing over all combinations of external points. The 4-pt function is

$$\begin{aligned} G^{(4)}(x_1, x_2, x_3, x_4) &= 3 \begin{array}{c} \bullet \text{---} \bullet \\ \bullet \text{---} \bullet \end{array} - \lambda \left[72 \begin{array}{c} \bullet \text{---} \bullet \\ \text{---} \bullet \end{array} + 24 \begin{array}{c} \bullet \text{---} \bullet \\ \text{---} \bullet \end{array} \right] \\ &- \kappa \left[540 \begin{array}{c} \bullet \text{---} \bullet \\ \text{---} \bullet \end{array} + 360 \begin{array}{c} \bullet \text{---} \bullet \\ \text{---} \bullet \end{array} \right] \\ &= 3 \begin{array}{c} \bullet \cdots \bullet \\ \bullet \cdots \bullet \end{array} - 24 \lambda \begin{array}{c} \bullet \cdots \bullet \\ \text{---} \bullet \end{array} - 360 \kappa \begin{array}{c} \bullet \cdots \bullet \\ \text{---} \bullet \end{array} \\ &= K(x_1, x_2)K(x_3, x_4) + K(x_1, x_3)K(x_2, x_4) + K(x_1, x_4)K(x_2, x_3) \\ &- 24 \int d^{d_{\text{in}}} y \lambda K(x_1, y)K(x_2, y)K(x_3, y)K(x_4, y) \\ &- 360 \int d^{d_{\text{in}}} z \kappa K(x_1, z)K(x_2, z)K(x_3, z)K(x_4, z)K(z, z) \end{aligned} \quad (75)$$

and the 6-pt function is

$$\begin{aligned}
 G^{(6)}(x_1, x_2, x_3, x_4, x_5, x_6) &= 15 \left[\text{diagram 1} \right] - \lambda \left[540 \left[\text{diagram 2} \right] + 360 \left[\text{diagram 3} \right] \right] \\
 &- \kappa \left[720 \left[\text{diagram 4} \right] + 5400 \left[\text{diagram 5} \right] + 4050 \left[\text{diagram 6} \right] \right] \\
 &= 15 \left[\text{diagram 7} \right] - 360 \lambda \left[\text{diagram 8} \right] - \kappa \left[720 \left[\text{diagram 9} \right] + 5400 \left[\text{diagram 10} \right] \right] \\
 &= \left[K_{12}K_{34}K_{56} + K_{12}K_{35}K_{46} + K_{12}K_{36}K_{45} + K_{13}K_{24}K_{56} + K_{13}K_{25}K_{46} + K_{13}K_{26}K_{45} + K_{14}K_{23}K_{56} \right. \\
 &+ K_{14}K_{25}K_{36} + K_{14}K_{26}K_{35} + K_{15}K_{23}K_{46} + K_{15}K_{24}K_{36} + K_{15}K_{26}K_{34} + K_{16}K_{23}K_{45} + K_{16}K_{24}K_{35} \\
 &+ K_{16}K_{25}K_{34} \left. \right] - 24 \int d^{d_{\text{in}}} y \lambda \left[K_{1y}K_{2y}K_{3y}K_{4y}K_{56} + K_{1y}K_{2y}K_{3y}K_{5y}K_{46} + K_{1y}K_{2y}K_{4y}K_{5y}K_{36} \right. \\
 &+ K_{1y}K_{3y}K_{4y}K_{5y}K_{26} + K_{2y}K_{3y}K_{4y}K_{5y}K_{16} + K_{1y}K_{2y}K_{3y}K_{6y}K_{45} + K_{1y}K_{2y}K_{4y}K_{6y}K_{35} \\
 &+ K_{1y}K_{3y}K_{4y}K_{6y}K_{25} + K_{2y}K_{3y}K_{4y}K_{6y}K_{15} + K_{1y}K_{2y}K_{5y}K_{6y}K_{34} + K_{1y}K_{3y}K_{5y}K_{6y}K_{24} \\
 &+ K_{2y}K_{3y}K_{5y}K_{6y}K_{14} + K_{1y}K_{4y}K_{5y}K_{6y}K_{23} + K_{2y}K_{4y}K_{5y}K_{6y}K_{13} + K_{3y}K_{4y}K_{5y}K_{6y}K_{12} \left. \right] \\
 &- 720 \int d^{d_{\text{in}}} z \kappa \left[K_{1z}K_{2z}K_{3z}K_{4z}K_{5z}K_{6z} - 360 \int d^{d_{\text{in}}} z \kappa \left[K_{zz}K_{1z}K_{2z}K_{3z}K_{4z}K_{56} \right. \right. \\
 &+ K_{zz}K_{1z}K_{2z}K_{3z}K_{5z}K_{46} + K_{zz}K_{1z}K_{2z}K_{4z}K_{5z}K_{36} + K_{zz}K_{1z}K_{3z}K_{4z}K_{5z}K_{26} \\
 &+ K_{zz}K_{2z}K_{3z}K_{4z}K_{5z}K_{16} + K_{zz}K_{1z}K_{2z}K_{3z}K_{6z}K_{45} + K_{zz}K_{1z}K_{2z}K_{4z}K_{6z}K_{35} \\
 &+ K_{zz}K_{1z}K_{3z}K_{4z}K_{6z}K_{25} + K_{zz}K_{2z}K_{3z}K_{4z}K_{6z}K_{15} + K_{zz}K_{1z}K_{2z}K_{5z}K_{6z}K_{34} \\
 &+ K_{zz}K_{1z}K_{3z}K_{5z}K_{6z}K_{24} + K_{zz}K_{2z}K_{3z}K_{5z}K_{6z}K_{14} + K_{zz}K_{1z}K_{4z}K_{5z}K_{6z}K_{23} \\
 &+ K_{zz}K_{2z}K_{4z}K_{5z}K_{6z}K_{13} + K_{zz}K_{3z}K_{4z}K_{5z}K_{6z}K_{12} \left. \right] \left. \right], \tag{76}
 \end{aligned}$$

where again the analytic expression corresponds to the second set of Feynman diagrams according to the Feynman rules. Note the simplicity of the second diagrammatic representation relative to its corresponding analytic expression.

3.3. Neural network coupling constants and GP symmetries

We have argued that non-Gaussian corrections are crucial in neural networks and they correspond to turning on interactions from the QFT point of view. Such corrections arise as terms in ΔS , each with a coefficient encoding the interaction strength, such as λ or κ in (69).

For convenience we have thus far ignored important questions about any interaction coefficient appearing in ΔS : are they constants? In QFT language such quantities are called coupling constants, but this is simply an artifact of the translation invariant QFTs that physicists most often study. For instance, in the Standard Model of particle physics a parameter analogous to λ quantifies the self-interaction of the Higgs boson, and all such coupling constants have historically proven to be invariant under spatial translations on Earth; they are independent of whether the scattering experiment is done at CERN in Switzerland or Fermilab in Illinois. This follows from the translation invariance of the entire Standard Model action, which therefore also predicts that the same couplings would be measured in proton scattering experiments near Alpha Centauri. That is, couplings are constants in spacetime.

But in NGPs associated with neural network architectures, do we expect¹⁶ the coefficients such as λ and κ to truly be constants? What role should translation invariance play in such considerations? To this end we employ a powerful principle due to 't Hooft:

Technical naturalness: a coupling g appearing in ΔS may be small relative to Λ if a symmetry is restored when g is set to zero.

¹⁶ In our Feynman rules, we have left the coefficients λ and κ inside the integrals in anticipation of this question.

A concept underlying technical naturalness is that g itself may receive large corrections in varying the cutoff¹⁷ Λ , i.e. in varying $\Lambda \rightarrow \Lambda'$,

$$g \rightarrow g + \Delta g \text{ with } \frac{\Delta g}{g} \gg 1. \quad (77)$$

However, in some cases it is possible to show that $\Delta g = 0$ if S has a symmetry. If g itself breaks the symmetry, but the symmetry is restored when $g \rightarrow 0$, then as $g \rightarrow 0$ we must have $\Delta g \rightarrow 0$ as well. In some concrete cases, this is enforced by $\Delta g = g \alpha$ where α is some function mild enough that $\Delta g \rightarrow 0$ as $g \rightarrow 0$. If g is small, this ensures that corrections to it are also small, so that g is small for all values of the cutoff. In such a case, g is said to be *technically natural*. A simple example is the electron mass m_e in quantum electrodynamics: m_e is small relative to the electroweak scale and corrections to the mass are $\Delta m_e \propto m_e$, ensuring that it remains small as the cutoff is varied. As $m_e \rightarrow 0$, a symmetry of electrons called the ‘chiral symmetry’ is restored. The small electron mass m_e is technically natural.

Technical naturalness is directly applicable to our discussion of coupling constants versus coupling functions in NGPs associated with neural networks. For instance, is λ a constant or a function of the input space? To examine this question in light of technical naturalness, consider a simple case where λ is the only non-Gaussian coefficient and is decomposed as

$$\lambda(x) = \bar{\lambda} + \delta\lambda(x), \quad (78)$$

with a constant piece $\bar{\lambda}$ plus some non-constant piece $\delta\lambda(x)$. The variance of λ is determined by $\delta\lambda$, which in general is not invariant under translations $T: x \rightarrow x + c$. When $\delta\lambda = 0$, λ is a constant, and when it is small, λ is effectively a constant. But should $\delta\lambda$ be small? This is where technical naturalness is useful. It states that

$$\frac{\delta\lambda}{\lambda} \ll 1 \quad (79)$$

is reasonable to expect if there is a symmetry in the $\delta\lambda \rightarrow 0$ limit. Since $\delta\lambda$ breaks T , a relevant question is whether T is restored when $\delta\lambda \rightarrow 0$. This occurs when S_{GP} , and specifically its kernel $K(x, y)$, is T -invariant. In examples with multiple couplings, the relevant question is whether T is restored when all couplings go to zero, i.e. again whether or not $K(x, y)$ is T -invariant.

Technical naturalness therefore leads to the following concrete conjecture:

Conjecture: couplings in NGPs associated to neural network architectures are constants (or nearly constants) if the kernel $K(x, y)$ associated with their GP limit is translationally invariant.

This is a conjecture rather than a theorem because technical naturalness is not proven in general, but is instead a guiding principle in physics. In our experiments, however, the conjecture can be tested: while the kernels associated with Erf-net and ReLU-net are not T -invariant, the Gauss-net kernel is T -invariant. We will verify the conjecture in these examples by demonstrating that couplings are effectively constants in Gauss-net.

3.4. Independence in EFT of single-layer networks

Recall that a neural network with linear output layer, such as our examples, is a process \mathcal{P} from which $f = f_b + f_w$ is drawn; f_b and f_w are drawn from independent processes $f_b \sim \mathcal{P}_b$ and $f_w \sim \mathcal{P}_w$. Processes \mathcal{P}_b are independent of width N and always Gaussian, provided the biases are Gaussian; whereas \mathcal{P}_w admits non-Gaussianities and N -dependence. Independence means that the distribution is a product, and therefore the log-likelihood of the GP can be expressed as

$$S_{GP} = S_{GP}^b + S_{GP}^w = \int d^{d_{in}} x d^{d_{in}} y \left[f_b(x) \Xi_b(x, y) f_b(y) + f_w(x) \Xi_w(x, y) f_w(y) \right], \quad (80)$$

where

$$\int d^{d_{in}} x' K(x, x')_{W/b} \Xi(x', x'')_{W/b} = \delta^{(d_{in})}(x - x''), \quad (81)$$

W/b denotes that the equation applies to both the weight and bias pieces, and the neural network kernel is given by $K(x, y) = K_b(x, y) + K_w(x, y)$. Classical scaling dimensions of independent outputs f_w and f_b become

¹⁷ That is, due to Wilsonian renormalization group flow, as we will exemplify in section 4.

$$[f_{W/b}] = -\frac{2d_{\text{in}} + [\Xi_{W/b}]}{2}, \quad (82)$$

which may also be expressed in terms of $[K_{W/b}]$.

Due to the independence of f_b and f_W in our examples, the non-Gaussian correction to the log-likelihood of NGP is $\Delta S = \Delta S_b + \Delta S_W$, where the first (second) term only depends on f_b (f_W). Since in our examples the bias entries are Gaussian, $\Delta S_b = 0$. Therefore, $S = S_{\text{GP}} + \Delta S_W$, and a local ΔS_W is given by

$$\Delta S_W = \int d^{d_{\text{in}}} x [g f_W(x)^3 + \lambda f_W(x)^4 + \alpha f_W(x)^5 + \kappa f_W(x)^6 + \dots]. \quad (83)$$

We will consider a simple non-locality in section 3.6, and see that for the inputs we study the local approximation works well. Classical scaling dimensions of general operators $\mathcal{O}_k := g_k f_W(x)^k$ is given by

$$[g_k] = -d_{\text{in}} + \frac{k(2d_{\text{in}} + [\Xi_W])}{2} = -d_{\text{in}} - \frac{k[K_W]}{2}. \quad (84)$$

If $[K_W] \geq 0$, operators \mathcal{O}_k can be sufficiently ignored for large k , as all g_k have scaling dimensions with same sign. Considering corrections to the n -pt function from $\Delta S_W = \int d^{d_{\text{in}}} x g_k f_W(x)^k$ with $k > 2$, we have

$$G^{(n)}(x_1, \dots, x_n) = \frac{\int df f(x_1) \dots f(x_n) [1 - \int d^{d_{\text{in}}} x g_k f_W(x)^k + O(g_k^2)] e^{-S_{\text{GP}}/Z_{\text{GP},0}}}{\int df [1 - \int d^{d_{\text{in}}} x g_k f_W(x)^k + O(g_k^2)] e^{-S_{\text{GP}}/Z_{\text{GP},0}}}, \quad (85)$$

which may be computed to any given order using Feynman diagrams.

The effective action utilized for our examples is

$$S = S_{\text{GP}} + \int d^{d_{\text{in}}} x [\lambda f_W(x)^4 + \kappa f_W(x)^6]. \quad (86)$$

The Feynman rules remain unchanged, except now any propagator attached to internal vertices are those

associated to f_W , e.g. $u \quad v$ corresponding to $K_W(u, v)$. With this, the 2-pt remains unaltered; whereas 4-pt and 6-pt functions are respectively given by

$$\begin{aligned} G^{(4)}(x_1, x_2, x_3, x_4) &= 3 \text{ (diagram: two parallel horizontal lines)} - \lambda \left[72 \text{ (diagram: two horizontal lines with a loop labeled } y \text{ between them)} + 24 \text{ (diagram: two crossing lines)} \right] \\ &- \kappa \left[540 \text{ (diagram: two horizontal lines with a bubble labeled } z \text{ between them)} + 360 \text{ (diagram: two crossing lines with a bubble labeled } z \text{ in the center)} \right] \\ &= 3 \text{ (diagram: two parallel dashed horizontal lines)} - 24 \lambda \text{ (diagram: two crossing dashed lines labeled } y \text{)} - 360 \kappa \text{ (diagram: two crossing dashed lines with a bubble labeled } z \text{)} \\ &= K(x_1, x_2)K(x_3, x_4) + K(x_1, x_3)K(x_2, x_4) + K(x_1, x_4)K(x_2, x_3) \\ &- 24 \int d^{d_{\text{in}}} y \lambda K_W(x_1, y)K_W(x_2, y)K_W(x_3, y)K_W(x_4, y) \\ &- 360 \int d^{d_{\text{in}}} z \kappa K_W(x_1, z)K_W(x_2, z)K_W(x_3, z)K_W(x_4, z)K_W(z, z) \end{aligned} \quad (87)$$

$$\begin{aligned}
G^{(6)}(x_1, x_2, x_3, x_4, x_5, x_6) &= 15 \left[\text{Diagram 1} \right] - \lambda \left[540 \text{Diagram 2} + 360 \text{Diagram 3} \right] \\
&- \kappa \left[720 \text{Diagram 4} + 5400 \text{Diagram 5} + 4050 \text{Diagram 6} \right] \\
&= 15 \left[\text{Diagram 7} \right] - 360 \lambda \left[\text{Diagram 8} \right] - \kappa \left[720 \text{Diagram 9} + 5400 \text{Diagram 10} \right] \\
&= \left[K_{12}K_{34}K_{56} + K_{12}K_{35}K_{46} + K_{12}K_{36}K_{45} + K_{13}K_{24}K_{56} + K_{13}K_{25}K_{46} + K_{13}K_{26}K_{45} + K_{14}K_{23}K_{56} \right. \\
&+ K_{14}K_{25}K_{36} + K_{14}K_{26}K_{35} + K_{15}K_{23}K_{46} + K_{15}K_{24}K_{36} + K_{15}K_{26}K_{34} + K_{16}K_{23}K_{45} + K_{16}K_{24}K_{35} \\
&+ K_{16}K_{25}K_{34} \left. \right] - 24 \int d^{\text{din}} y \lambda \left[K_{W,1y}K_{W,2y}K_{W,3y}K_{W,4y}K_{56} + K_{W,1y}K_{W,2y}K_{W,3y}K_{W,5y}K_{46} \right. \\
&+ K_{W,1y}K_{W,2y}K_{W,4y}K_{W,5y}K_{36} + K_{W,1y}K_{W,3y}K_{W,4y}K_{W,5y}K_{26} + K_{W,2y}K_{W,3y}K_{W,4y}K_{W,5y}K_{16} \\
&+ K_{W,1y}K_{W,2y}K_{W,3y}K_{W,6y}K_{45} + K_{W,1y}K_{W,2y}K_{W,4y}K_{W,6y}K_{35} + K_{W,1y}K_{W,3y}K_{W,4y}K_{W,6y}K_{25} \\
&+ K_{W,2y}K_{W,3y}K_{W,4y}K_{W,6y}K_{15} + K_{W,1y}K_{W,2y}K_{W,5y}K_{W,6y}K_{34} + K_{W,1y}K_{W,3y}K_{W,5y}K_{W,6y}K_{24} \\
&+ K_{W,2y}K_{W,3y}K_{W,5y}K_{W,6y}K_{14} + K_{W,1y}K_{W,4y}K_{W,5y}K_{W,6y}K_{23} + K_{W,2y}K_{W,4y}K_{W,5y}K_{W,6y}K_{13} \\
&+ K_{W,3y}K_{W,4y}K_{W,5y}K_{W,6y}K_{12} \left. \right] - 720 \int d^{\text{din}} z \kappa \left[K_{W,1z}K_{W,2z}K_{W,3z}K_{W,4z}K_{W,5z}K_{6z} \right. \\
&- 360 \int d^{\text{din}} z \kappa \left[K_{W,zz}K_{W,1z}K_{W,2z}K_{W,3z}K_{W,4z}K_{56} + K_{W,zz}K_{W,1z}K_{W,2z}K_{W,3z}K_{W,5z}K_{46} \right. \\
&+ K_{W,zz}K_{W,1z}K_{W,2z}K_{W,4z}K_{W,5z}K_{36} + K_{W,zz}K_{W,1z}K_{W,3z}K_{W,4z}K_{W,5z}K_{26} + K_{W,zz}K_{W,2z}K_{W,3z}K_{W,4z}K_{W,5z}K_{16} \\
&+ K_{W,zz}K_{W,1z}K_{W,2z}K_{W,3z}K_{W,6z}K_{45} + K_{W,zz}K_{W,1z}K_{W,2z}K_{W,4z}K_{W,6z}K_{35} + K_{W,zz}K_{W,1z}K_{W,3z}K_{W,4z}K_{W,6z}K_{25} \\
&+ K_{W,zz}K_{W,2z}K_{W,3z}K_{W,4z}K_{W,6z}K_{15} + K_{W,zz}K_{W,1z}K_{W,2z}K_{W,5z}K_{W,6z}K_{34} + K_{W,zz}K_{W,1z}K_{W,3z}K_{W,5z}K_{W,6z}K_{24} \\
&+ K_{W,zz}K_{W,2z}K_{W,3z}K_{W,5z}K_{W,6z}K_{14} + K_{W,zz}K_{W,1z}K_{W,4z}K_{W,5z}K_{W,6z}K_{23} + K_{W,zz}K_{W,2z}K_{W,4z}K_{W,5z}K_{W,6z}K_{13} \\
&+ K_{W,zz}K_{W,3z}K_{W,4z}K_{W,5z}K_{W,6z}K_{12} \left. \right], \tag{88}
\end{aligned}$$

We have expanded to leading order in λ and κ . Since the connected 4-pt and 6-pt functions scale as $1/N$ and $1/N^2$, respectively, (see section 2.5), we infer the same scaling for λ and κ , allowing us to ignore κ at leading order in $1/N$ in our experiments. The statement of technical naturalness gets trivially modified to an associated statement for K_W .

3.5. Experiments: correlations in single-layer networks with EFT

Having explained how to utilize EFT to analyze neural network architectures and their associated NGPs, in this section we verify the ideas experimentally. The logic is simple, as EF techniques are supposed to accomplish three things:

- Give a candidate ΔS_W for the NGP.
- Fix coefficients of operators in ΔS_W with experiments.
- Once fixed, make predictions for other experiments and verify them.

In this section, we will use experimental measurements of $G^{(4)}$ at fixed width to determine λ , and then use the determined λ to make predictions for $G^{(6)}$ at the same width and verify it against experiments. We choose widths 5, 20, and 1000 for Erf-net, ReLU-net, and Gauss-net experiments respectively, to ensure that the networks of our interest receive non-trivial corrections to the GP, as demonstrated experimentally in section 2.

The coupling λ may be extracted from experimental measurements of $G^{(4)}$. When κ is negligible¹⁸ and λ is a constant, (75) gives

$$\lambda = \frac{K(x_1, x_2)K(x_3, x_4) + K(x_1, x_3)K(x_2, x_4) + K(x_1, x_4)K(x_2, x_3) - G^{(4)}(x_1, x_2, x_3, x_4)}{24 \int d^{\text{din}} y K_W(x_1, y)K_W(x_2, y)K_W(x_3, y)K_W(x_4, y)}. \tag{89}$$

Therefore, by measuring $G^{(4)}(x_1, x_2, x_3, x_4)$ in experiments and performing the theoretical computations for the rest of the expression, λ may be experimentally measured.

¹⁸ We will verify this in the large cutoff limit experimentally, and theoretically in section 4.3.

Slight complications arise when, more generally, the coupling is a function

$$\lambda(y) = \bar{\lambda} + \delta\lambda(y) \quad (90)$$

with $\bar{\lambda}$ a constant. In that case (75) gives

$$\bar{\lambda} = \frac{K_{12}K_{34} + K_{13}K_{24} + K_{14}K_{23} - G^{(4)}(x_1, x_2, x_3, x_4)}{24 \int d^{d_{\text{in}}} y \Delta_{1234y}} - \frac{\int d^{d_{\text{in}}} y \delta\lambda(y) \Delta_{1234y}}{\int d^{d_{\text{in}}} y \Delta_{1234y}} \quad (91)$$

where $K_{W,ij}$ abbreviates $K_W(x_i, x_j)$ and $\Delta_{1234y} = K_{W,1y}K_{W,2y}K_{W,3y}K_{W,4y}$. If $\delta\lambda$ is small then the first term

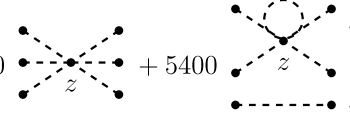
$$\lambda_m(x_1, x_2, x_3, x_4) := \frac{K_{12}K_{34} + K_{13}K_{24} + K_{14}K_{23} - G^{(4)}(x_1, x_2, x_3, x_4)}{24 \int d^{d_{\text{in}}} y \Delta_{1234y}} \quad (92)$$

dominates, which may be measured experimentally by measuring $G^{(4)}$ and then using the known theoretical expressions of the GP kernels to compute λ_m , which becomes a rank four tensor on a fixed set of inputs. Since $\bar{\lambda}$ is a constant and (91) holds, variance in λ_m correlates with variance in $\delta\lambda$, and when the variance is small

$$\lambda \simeq \bar{\lambda} \simeq \text{mean}(\lambda_m(x_1, x_2, x_3, x_4)). \quad (93)$$

The approximation is exact in the limit of constant λ , i.e. $\delta\lambda \rightarrow 0$. Therefore, by measuring λ_m we approximately measure λ as $\text{mean}(\lambda_m(x_1, x_2, x_3, x_4))$ ¹⁹, which we refer to as the measured value of λ .

Given the measured value of λ , we would like to use it to make theoretical predictions for $G^{(6)}$ that may be experimentally verified. To this end, we define the 6-pt deviation

$$\begin{aligned} \delta'(x_1, \dots, x_6) &:= G^{(6)}(x_1, \dots, x_6) - \sum_{15 \text{ combinations}} \left[K(x_i, x_j) K(x_k, x_l) K(x_m, x_n) \right. \\ &\quad \left. - 24 \int d^{d_{\text{in}}} y \lambda K_W(x_i, y) K_W(x_j, y) K_W(x_k, y) K_W(x_l, y) K(x_m, x_n) \right] \\ &= -\kappa \left[720 \text{ (diagram 1)} + 5400 \text{ (diagram 2)} \right] \end{aligned} \quad (94)$$


where the last equality follows from (76). To obtain a sense of the size of the deviation we normalize it with respect to the experimental 6-pt function of the NGP,

$$\delta(x_1, \dots, x_6) := \frac{\delta'(x_1, \dots, x_6)}{G^{(6)}(x_1, \dots, x_6)} \quad (95)$$

For perturbation theory to hold, $|\delta(x_1, \dots, x_6)| \ll 1$ is required. Since κ is negligible in the limit of large cutoff Λ and it is suppressed by $1/N$ relative to λ , we expect $|\delta(x_1, \dots, x_6)|$ to converge to 0 in the large- N and large- Λ limits. For each NN architecture, $|\delta(x_1, \dots, x_6)|$ is given by the difference between the orange line and 1.0 in figures 4–6.

3.5.1. Gauss-net

In figure 4 we show the results of Gauss-net experiments, which were carried out with the same set of parameters introduced in section 2.3. All experiments in this section were performed with $n_{\text{nets}} = 10^7$. The fixed-cutoff experiments are done at

$$\Lambda \rightarrow \infty, \quad N \in \{2, 3, 4, 5, 10, 20, 50, 100, 500, 1000\}. \quad (96)$$

The $G^{(6)}$ prediction experiments using λ_m are done at width $N = 1000$ and $\Lambda \rightarrow \infty$, since the Gauss-net kernel goes to zero at large x and therefore its EFT integrals converge.

¹⁹ The rank four tensor $\lambda_m(x_1, x_2, x_3, x_4)$ is symmetric and the mean is taken over its unique (upper triangular) elements.

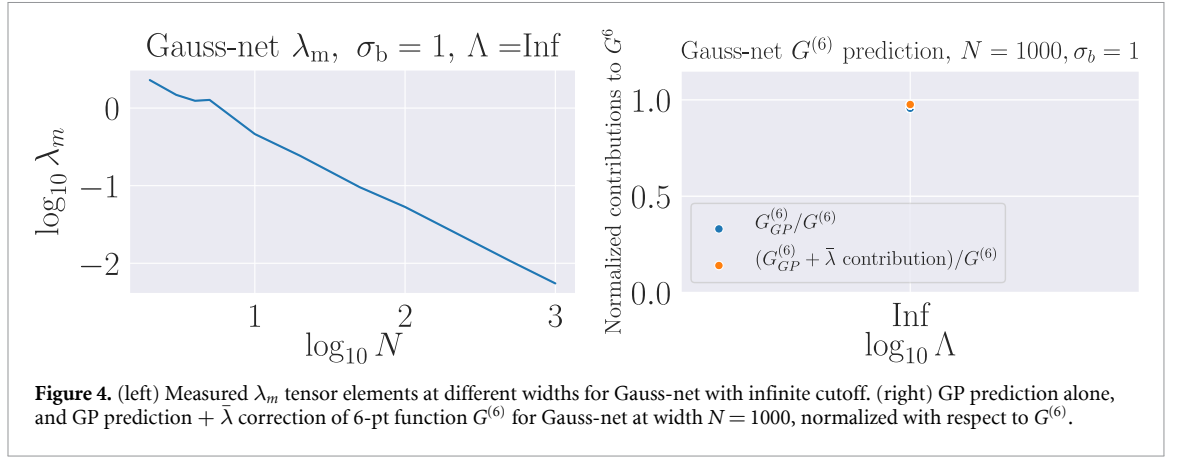


Figure 4. (left) Measured λ_m tensor elements at different widths for Gauss-net with infinite cutoff. (right) GP prediction alone, and GP prediction + $\bar{\lambda}$ correction of 6-pt function $G^{(6)}$ for Gauss-net at width $N = 1000$, normalized with respect to $G^{(6)}$.

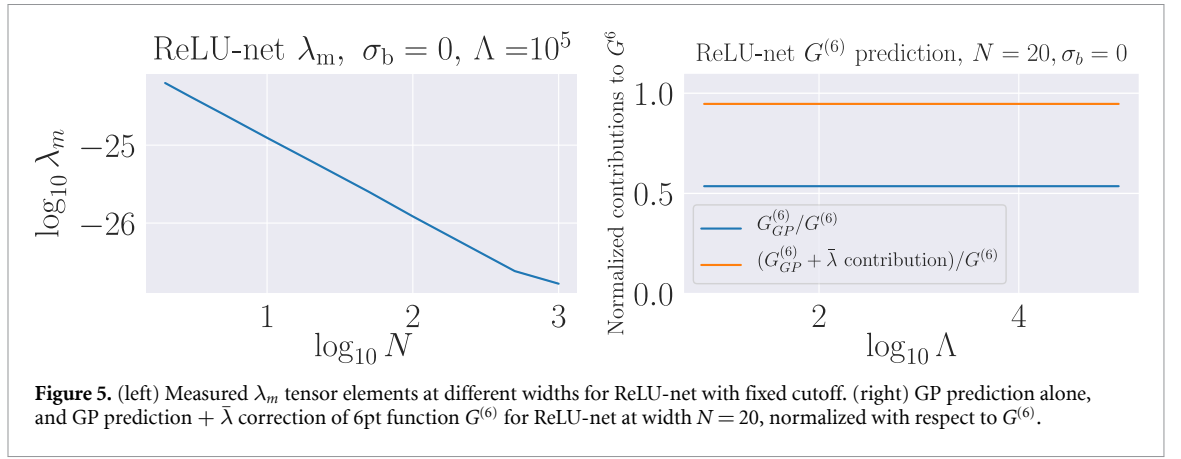


Figure 5. (left) Measured λ_m tensor elements at different widths for ReLU-net with fixed cutoff. (right) GP prediction alone, and GP prediction + $\bar{\lambda}$ correction of 6-pt function $G^{(6)}$ for ReLU-net at width $N = 20$, normalized with respect to $G^{(6)}$.

In the left plot we present measurements for the rank-4 tensor λ_m at fixed cutoff. Despite being a rank-4 tensor, we see that there is very little variance across the elements, indicating that λ_m is effectively constant; we will discuss this in a moment. In the right plot we present the GP contribution to $G^{(6)}$, normalized by $G^{(6)}$ so that a correct theoretical prediction would be 1; we see $G_{GP}^{(6)}$ falls short of this. However, we also demonstrate excellent match to experiment when the perturbative correction in λ is added, implying that δ is effectively zero; the EFT has correctly predicted the experimental measurements of the 6-pt function.

As discussed in section 3.3, by technical naturalness a parameter is allowed to be small when setting it to zero restores a symmetry. We observe from the (lack of) variance in the left plot in figure 4 that $\delta\lambda/\bar{\lambda}$ is indeed small, i.e. λ is effectively a constant. This is expected because λ is technically natural for Gauss-net: translation invariance is recovered when $\delta\lambda$ vanishes, as the Gauss-net GP kernel is translation invariant. In fact, this was by design. We started with a translation-invariant kernel since we desire an example with coupling constants rather than coupling functions, which we expected would be enforced by technical naturalness.

3.5.2. ReLU-net

Further, we read off λ_m tensor and its components from ReLU-net in figure 5. The fixed-cutoff experiments were done with $\Lambda = 10^5$, and the fixed-width λ_m experiments and $G^{(6)}$ predictions are done at width and cutoffs

$$N = 20, \quad \Lambda \in \{7, 10, 15, 20, 30, 40, 50, 70, 100, 200, 500, 1000, 2000, 5000, 7000, 10000, 20000, 40000, 60000, 80000, 100000\}. \quad (97)$$

Similar results can be shown at other widths.

The widths were chosen so the 4-pt and 6-pt functions were NGPs and above the background level, as seen in figure 2. As with Gauss-net, we show in the left plot all elements of the rank-4 tensor λ_m at various widths and fixed cutoff $\Lambda = 10^5$. Using the measured λ , we show the results of the corresponding $G^{(6)}$ prediction in the right plot. We see similarly that the GP prediction $G_{GP}^{(6)}$ does not account for the 6-pt function $G^{(6)}$, and the λ contribution gives a significant additive correction.

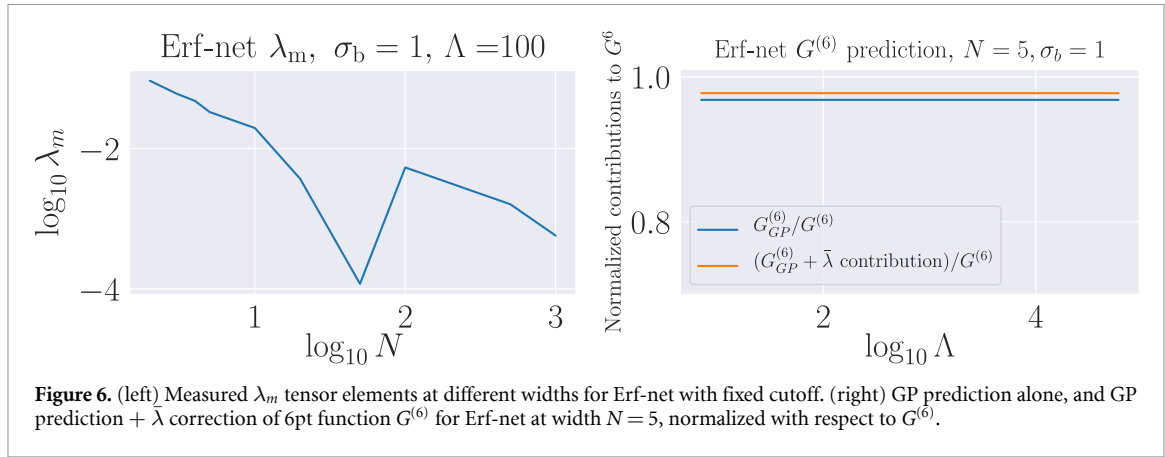


Figure 6. (left) Measured λ_m tensor elements at different widths for Erf-net with fixed cutoff. (right) GP prediction alone, and GP prediction + $\bar{\lambda}$ correction of 6pt function $G^{(6)}$ for Erf-net at width $N = 5$, normalized with respect to $G^{(6)}$.

3.5.3. Erf-net

We obtain λ_m tensor and its independent components from experimental results for the third and last architecture Erf-net in figure 6. As with ReLU-net, the fixed-cutoff experiments were done at $\Lambda = 10^5$, and the fixed-width experiments were performed at width $N = 5$.

As with the previous two networks, we show all elements of the tensor λ_m in the left plot at the given widths, the quartic coupling appears effectively constant due to smallness of variations across its tensor elements. The right plot shows the GP prediction $G_{GP}^{(6)}$ being corrected by the $\bar{\lambda}$ term, and together they give a good approximation of the 6-pt function $G^{(6)}$.

3.6. Experiments: precision quartic fitting and EFT tests of $G^{(4)}$

We now provide another test of EFT techniques via a test-train split for $\Delta G^{(4)}$ predictions. Specifically, since $\Delta G^{(4)}$ is a continuous function of inputs, we may fit EFT parameters for a finite set of inputs and then test whether they make accurate predictions for unseen inputs. We may do this using only the quartic couplings because they are leading in $1/N$, as demonstrated in section 2.5. In the process, it introduces another method for measuring couplings.

In section 3.5 we considered the 6-pt functions receiving leading corrections due to the term

$$\Delta S_W = \int d^{d_{\text{in}}} x \lambda f_W(x)^4, \quad (98)$$

with $\lambda = \lambda_0$, a constant. In general however, one might consider λ being a local and/or non-local function of x , and test out the best functional form of λ for a given architecture. We design three such models

$$M_1 : \Delta S_W^1 = \int d^{d_{\text{in}}} x \lambda_0 f_W(x)^4, \quad (99)$$

$$M_2 : \Delta S_W^2 = \int d^{d_{\text{in}}} x (\lambda_0 + \lambda_2 x^2) f_W(x)^4, \quad (100)$$

$$M_3 : \Delta S_W^3 = \int d^{d_{\text{in}}} x (\lambda_0 + \lambda_2 x^2) f_W(x)^4 + \int d^{d_{\text{in}}} x d^{d_{\text{in}}} y \lambda_{\text{NL}} f_W(x)^2 f_W(y)^2. \quad (101)$$

Since this fit was done using the 4-pt function, an input consists of a 4-tuple of external points (x_1, x_2, x_3, x_4) . The 10^7 experiments were run twice, using two disjoint sets of external points called the test set and train set, described in table 4. First, we train the model. For each of the three model types, we compute $\Delta G^{(4)}$ averaged over 10^7 experiments, and also piecewise contributions from the EFT (proportional to the couplings), for all combinations of the external points in the train set. This gives a rank four tensor $\Delta G_{\text{exp}}^{(4)}$ and EFT corrections $\Delta G_{\text{EFT}}^{(4)}$. At leading order in the λ -couplings the EFT corrections are a sum of three terms, each proportional to a coupling, giving

$$\Delta G_{\text{EFT}}^{(4)} = \lambda_0 T_0(x_1, \dots, x_4) + \lambda_2 T_2(x_1, \dots, x_4) + \lambda_{\text{NL}} T_{\text{NL}}(x_1, \dots, x_4). \quad (102)$$

Via perturbation theory, we have

Table 4. Inputs for test-sets and train-sets.

$\{x_i^{\text{Gauss-net}}\} = \{-0.01, -0.006, -0.002, +0.002, +0.006, +0.01\}$ $\{x_i^{\text{ReLU-net}}\} = \{+0.2, +0.4, +0.6, +0.8, +1.0, +1.2\}$ $\{x_i^{\text{Erf-net}}\} = \{+0.002, +0.004, +0.006, +0.008, +0.010, +0.012\}$		
	Train set inputs x_i	Test set inputs x_i
Gauss-net	$\frac{\sqrt{2}}{2} x_i^{\text{Gauss-net}}$	$x_i^{\text{Gauss-net}}$
ReLU-net	$\frac{\sqrt{2}}{2} x_i^{\text{ReLU-net}}$	$x_i^{\text{ReLU-net}}$
Erf-net	$\frac{\sqrt{2}}{2} x_i^{\text{Erf-net}}$	$x_i^{\text{Erf-net}}$

Table 5. Optimized values of λ_0 , λ_2 , λ_{NL} and resulting MAPE and MSE loss upon application to test-sets.

	$(\lambda_0, \lambda_2, \lambda_{\text{NL}})$	Test (MAPE, MSE)
Gauss M_0	(0.0, 0.0, 0.0)	(100, 0.019)
Gauss M_1	(0.0046, 0.0, 0.0)	(0.0145, 6.8×10^{-10})
Gauss M_2	(0.0043, 0.0011, 0.0)	(0.0144, 6.7×10^{-10})
Gauss M_3	(0.00062, 0.00016, 0.0015)	(0.0156, 7.5×10^{-10})
ReLU M_0	(0.0, 0.0, 0.0)	(100, 0.003)
ReLU M_1	(6.2×10^{-11} , 0.0, 0.0)	(0.0035, 7.6×10^{-12})
ReLU M_2	(1.2×10^{-18} , 8.7×10^{-15} , 0.0)	(0.0013, 1.5×10^{-12})
ReLU M_3	(1.2×10^{-18} , 8.7×10^{-15} , 6.8×10^{-17})	(0.0012, 1.2×10^{-12})
Erf M_0	(0.0, 0.0, 0.0)	(100, 0.006)
Erf M_1	(0.039, 0.0, 0.0)	(0.030, 8.3×10^{-10})
Erf M_2	(0.040, -0.00043, 0.0)	(0.0042, 1.9×10^{-11})
Erf M_3	(0.0019, -0.0054, 0.0063)	(0.037, 1.1×10^{-9})

$$\begin{aligned}
T_0(x_1, \dots, x_4) &= 24 \int d^{d_{\text{in}}} x K_W(x_1, x) K_W(x_2, x) K_W(x_3, x) K_W(x_4, x) \\
T_2(x_1, \dots, x_4) &= 24 \int d^{d_{\text{in}}} x x^2 K_W(x_1, x) K_W(x_2, x) K_W(x_3, x) K_W(x_4, x) \\
T_{\text{NL}}(x_1, \dots, x_4) &= 8 \int d^{d_{\text{in}}} x d^{d_{\text{in}}} y \left[K_W(x_1, x) K_W(x_2, x) K_W(x_3, y) K_W(x_4, y) \right. \\
&\quad + K_W(x_1, x) K_W(x_2, y) K_W(x_3, x) K_W(x_4, y) + \\
&\quad \left. + K_W(x_1, x) K_W(x_2, y) K_W(x_3, y) K_W(x_4, x) \right]. \tag{103}
\end{aligned}$$

These tensors can then be compared elementwise and the values of λ can be found such that they minimize a cost function over all tensor elements. This will yield an EFT whose functional form best approximates the true functional form of the $\Delta G_{\text{exp}}^{(4)}$. We find the optimal parameter fits by using PyTorch to minimize the mean squared error between experimental measures of $\Delta G^{(4)}$ and corresponding EFT predictions $\Delta G_{\text{EFT}}^{(4)}$ for each model M_1 , M_2 , and M_3 using stochastic gradient descent. We test the effectiveness of the measured λ_0 , λ_2 and λ_{NL} by making predictions for the test set, computing the MSE loss and MAPE between $\Delta G^{(4)}$ and the EFT model contribution. MAPE is the mean absolute percent error, defined as

$$\text{MAPE} = \frac{1}{p} \sum_{i=1}^p \frac{A_i - F_i}{A_i}. \tag{104}$$

A_i , F_i and p are respectively the experimental $\Delta G^{(4)}(x_1, x_2, x_3, x_4)$, corresponding EFT prediction and total number of tensor elements in 4-pt function.

We present the results in table 5. M_0 denotes a control model defined by $(\lambda_0, \lambda_2, \lambda_{\text{NL}}) = (0, 0, 0)$, which we present to show the MSE loss before optimizing. The results show that adding a new local term to the model, i.e. going from M_1 to M_2 , significantly improves the accuracy of the EFT at predicting $\Delta G^{(4)}$ in all three architectures. This can be seen by comparing the MAPE and MSE results, both measurements of error, which decrease when moving to model M_2 from model M_1 . The nonlocal model M_3 only improves test set fitting in ReLU-net. Since the model M_3 consists of only one of many possible nonlocal quartic EFT terms, we claim this type of term only improves the local ReLU-net EFT away from the train set. This suggests that some of the functional dependence of $\Delta G^{(4)}$ for ReLU-net is captured by the nonlocal term in M_3 . Despite

still being reasonably good models, the other two architectures become less accurate when this term is added, which can be seen by the increased MAPE and MSE errors of model M_3 compared with M_1 and M_2 in Gauss-net and Erf-net. We claim this is because $\Delta G^{(4)}$ for these networks have a nonlocality that is not well described by the final term in M_3 ; their functional dependence is more complicated than the models we have tested here. Deeper analysis of any given network architecture can be done to find a more predictive local or nonlocal EFT term. We will do this in future work.

4. Minimal non-Gaussian process likelihoods with Wilsonian renormalization

In section 3 we demonstrated that we can use a Wilsonian EFT approach to neural networks to make experimentally verifiable predictions for correlation functions of the associated NGPs. This procedure can be carried out for any fixed cutoff Λ that yields a perturbative NGP. In doing so we claimed that we could ignore higher-than-quartic terms in the NGP effective action, and promised to justify the assumption. We do so now, and will also explain and experimentally demonstrate the relationship between the EFTs at different values of Λ .

The correct physics framework for these ideas is the Wilsonian RG. This seminal idea in QFT has led to some of the deepest results in both condensed matter and high energy physics, including multiple Nobel prizes, and is the subject of extensive discussions and presentation in any modern QFT textbook. We will present a streamlined perspective on it that is relevant for understanding applications in neural networks.

Our explanation of the RG applied to neural network NGPs will be grounded in experiments²⁰, which applies in particular to the sort of neural network experiments that we have carried out. Consider any experiment that draws an ensemble of neural networks f_α and computes their outputs on a fixed set of inputs

$$\mathcal{S}_{\text{in}} = \{x_1, \dots, x_{N_{\text{in}}}\}. \quad (105)$$

Given these measured outputs, the experimental correlation functions are measured via

$$G^{(n)}(x_1, \dots, x_n) = \frac{1}{n_{\text{nets}}} \sum_{\alpha \in \text{nets}}^{n_{\text{nets}}} f_\alpha(x_1) \dots f_\alpha(x_n), \quad (106)$$

which contain essential information about the distribution of neural networks induced by the chosen architecture and parameter distribution, as well as data if they have been trained. These results are concrete experimental facts, and the goal of theory is to explain them.

To that end, noting that wide varieties [37] of both trained and untrained networks admit a limit in which they are drawn from GPs, we propose constructing theories of the neural networks away from the GP limit by perturbing it to an NGP, encoded in

$$\Delta S = \int_{-\infty}^{\infty} d^{d_{\text{in}}} x \sum_{l \leq k} g_{\mathcal{O}_l} \mathcal{O}_l, \quad (107)$$

where the sum is over all operators \mathcal{O}_l of scaling dimension $l \leq k$ for some fixed k and the operators are themselves functions of neural network outputs; they are monomials in our cases. This yields an action for the NGP, S_{NGP} , with distribution

$$P[f] = e^{-S_{\text{NGP}}[f]}. \quad (108)$$

Using standard techniques reviewed in appendix A and carried out in section 3, correlation functions $G^{(n)}(x_1, \dots, x_n)$ may be computed perturbatively in the coefficients $g_{\mathcal{O}_l}$ and matched to experiments, where the GP kernel plays a crucial role, although GP predictions for n -pt functions are modified by various ‘interaction’ terms of strength $g_{\mathcal{O}_l}$.

However, in carrying out such computations one regularly encounters divergences arising from integrals over the space of inputs to f , which are neural network inputs in our framework, and usually position or momentum space in QFT. Needless to say, these divergences prevent the theoretical correlation functions from matching the finite ones measured in experiments. In QFT these are infinities that were ‘swept under the rug’ in complaints from the 1960s, but this viewpoint is archaic and incorrect from a modern perspective, since the issue is solved by a proper understanding of renormalization, particularly the one developed by Wilson.

²⁰ A wonderful physics-version of this discussion is in Part III.1 of [41].

Since the divergences arise from the boundaries of the ΔS integral being $\pm\infty$ ²¹, it is natural to attempt to get rid of them by cutting them off, as was physically motivated in section 3.1. That is, replace (107) by

$$\Delta S_\Lambda = \int_{-\Lambda}^{\Lambda} d^{d_{\text{in}}} x \sum_{l \leq k} g_{\mathcal{O}_l}(\Lambda) \mathcal{O}_l. \quad (109)$$

In the QFT analogy, this refers to the finite width NNs receiving corrections to the GP in terms of interactions involving generation and annihilation of ‘virtual particles/excitations’ that spans the input space between $\{-\Lambda, \Lambda\}$. In case of real-life neural networks, an example of cutoff scale and its insignificance to actual NN correlation functions can be understood through an MNIST with greyscale handwritten digits. Let the input space be $\mathbb{R}^{28 \times 28}$, with the real numbers corresponding to each of 28×28 pixels being $-\infty$, 0 and ∞ respectively at pure black, pure grey and pure white colors; i.e. the real number represents brightness. Images in the dataset that are grey correspond to experimental inputs close to zero. Computing NGP correlation functions via perturbation theory, integrating from pure black to pure white colors, may introduce divergences; a way to regulate this is by limiting the integration variable within some threshold black and white colors, leading to $\Delta S \rightarrow \Delta S_\Lambda$. This threshold corresponds to a maximum brightness and maximum darkness scale, which in a Wilsonian sense is unimportant as a slight change in very high threshold amount of black and white colors cannot meaningfully affect correlation functions associated with grey images, i.e. inputs near zero. Thus, high scale brightness and darkness thresholds in MNIST are analogous to high scale cutoffs in EFT.

Doing this for some fixed value of Λ such that $|x_i| \ll \Lambda$ for all $x_i \in \mathcal{S}_{\text{in}}$, one may use the experimental results for $G^{(n)}(x_1, \dots, x_m)$ to extract the values of $g_{\mathcal{O}_l}(\Lambda)$ at that value of Λ , which may then be used to make other predictions that may be experimentally verified; this is what we did in section 3.5. In general, since the operators are truncated at dimension $l \leq k$ there are a finite number of $g_{\mathcal{O}_l}(\Lambda)$, yet an infinite number of n -pt functions receive corrections from them, i.e. we have a finite number of quantities are making an infinite number of predictions.

We now arrive at the essence of the Wilsonian RG. In passing from (107) to (109), we passed from one ΔS to a one-parameter family ΔS_Λ with parameter Λ . Yet there is one set of experimental n -pt functions and a continuous infinity of theories associated with ΔS_Λ , each of which by the above process may make correct predictions for the experiments. It is clear, therefore, that

$$\frac{dG^{(n)}(x_1, \dots, x_n)}{d\Lambda} = 0. \quad (110)$$

Applying this to the theoretically computed n -pt functions yields differential equations that describe how the couplings $g_{\mathcal{O}_l}(\Lambda)$ vary as Λ is varied. This is to be expected: if we have an EFT making correct predictions at some value of Λ with $x_i \ll \Lambda$, we should be able to do the same thing for infinitesimally shifted cutoff $\Lambda + \delta\Lambda$, which will lead to slightly different couplings $g_{\mathcal{O}_l}(\Lambda + \delta\Lambda)$. The differential equations are referred to as RGEs, which include the β -function associated to the coupling, defined as

$$\beta(g_{\mathcal{O}_l}) := \frac{dg_{\mathcal{O}_l}}{d\log\Lambda}, \quad (111)$$

which may be extracted from (110). The RGEs give rise to a flow in the couplings induced by varying Λ , known as RG flow.

Now consider an RG flow in the space of couplings that begins at a point in coupling space where they are all non-trivial. Given this initial condition, the β -functions determine a trajectory through coupling space and the opposite directions along the trajectory correspond to raising and lowering Λ . Couplings that decrease, increase, or stay the same along one direction of the flow are said to be *irrelevant*, *relevant*, and *marginal*, respectively; their corresponding operators inherit the same names. The names are clear: go far enough along an RG flow and the irrelevant couplings go to zero, they may be ignored. Upon switching the direction of the flow, the names are reversed, though in physics one often considers unidirectional flows to low energies (long distances) since at higher energies the flows may be altered by the existence of a yet-undiscovered particle.

Consider the effective action (69) in light of this discussion of irrelevant, relevant, and marginal operators. It contains 4-pt and 6-pt couplings only, λ and κ . From (64), the couplings associated have input-space dimensions

$$[\lambda] = [g_4] = -d_{\text{in}} - 2[K], \quad [\kappa] = [g_6] = -d_{\text{in}} - 3[K], \quad (112)$$

²¹ This is not an issue with Gauss-net since its kernel tends toward 0 in a way where all EFT integrals are finite, as will be discussed later.

respectively, where $[K]$ denotes the scaling dimension of the NN kernel in the GP limit. For $[K] \geq 0$, both λ and κ are irrelevant (in the large Λ limit) due to having negative dimensions. If $[K] = 0$, they decrease at the same rate since they would both scale with the same dimension $-[d_{\text{in}}]$. When $[K] > 0$, κ decreases more quickly than λ as the cutoff increases, since $[\kappa] < [\lambda]$; and in the limit of large cutoff, the n -pt functions receive negligible corrections from κ , in comparison to corrections due to λ , and one may effectively ignore κ .

We emphasize that the dimension of the couplings depends explicitly on d_{in} . This is analogous to a well-known effect from QFT, where the dimension of spacetime affects the RG flow; similarly, d_{in} affects the flow in neural networks. We will see this explicitly in the example of ReLU-net, where $[\lambda] = -d_{\text{in}} - 4$, which will appear explicitly in slopes of appropriate RG experimental plots, as well as theoretical analysis. Throughout this work $d_{\text{out}} = 1$, so we will leave associated experiments to future work, but in analogy to QFT it is clear that changing the number of scalar fields—changing d_{out} —can affect the RG flow. For instance, in QFT the location of the Wilson-Fisher fixed point depends on the number of scalar fields N .

Given that λ is irrelevant, one may wonder why it cannot also be ignored. The proper prescription is that the leading operators necessary to account for a given phenomenon must be included. If we ignored *all* couplings g_k since they are irrelevant, we would be back in the GP limit and unable to account for the finite width experiments. To explain the experiments, one must keep the most relevant coupling; $g_3 = 0$ since the 3-pt function is zero, and therefore $\lambda = g_4$ is the leading coupling, despite being termed irrelevant.

As an example of this phenomenon in physics, consider an EFT of the blue sky, which describes the scattering of light off of neutral spin-0 particles in the atmosphere. The lowest dimension operator that can describe this scattering process is

$$\frac{c}{\Lambda^2} \phi^* \phi F_{\mu\nu} F^{\mu\nu}, \quad (113)$$

where the ϕ field and its conjugate represent the spin-0 particles and F is the gauge-invariant field strength tensor of electromagnetism associated with the photon. We have used the particle physics convention of writing the coupling as a dimensionless c with the cutoff explicitly introduced. This operator is irrelevant, but since it is the lowest dimension operator that gives rise to gauge-invariant scattering of light off of neutral atoms, it must be included in the EFT. In fact, it reproduces the Rayleigh cross-section that explains why blue light scatters more strongly than red light.

4.1. Neural network non-Gaussian process flows with β -functions

Having introduced the central ideas of the RG, we now address more concretely how these β -functions may be extracted from cutoff-dependent correlation functions, organizing the calculations according to model (architecture) independent and dependent pieces. This split arises naturally for some architectures. For instance, some terms in the kernels are shared amongst all single layer fully-connected networks, while others depend on the specific architecture, as determined by the activation function.

The kernels associated to a class of neural network architectures can be expressed in terms of a model independent (within the architecture class) term α and a model dependent term ς .

$$K(x, x') = \alpha + \varsigma(x, x'), \quad (114)$$

where we assumed that the first and second terms are input independent and dependent, respectively, since it is true in the networks we study and more generally to deep fully-connected networks; it is straightforward to study the case where the first-term is input-dependent, as well. For instance, the kernels in section 2.3 allow for explicit comparison.

Substituting this form of the kernel into the 4-pt function in (75) lets us rewrite the $G^{(4)}(x_1, x_2, x_3, x_4)$ in terms of model independent terms $\gamma_{4,i}$ and model dependent terms $\varrho_{4,i}$, for simplicity analyzing the case where λ and κ are approximately constants. The subscripts 4 and i refer to the order of the correlation function and $O(i)$ corrections to the GP expression respectively.

$$G^{(4)}(x_1, x_2, x_3, x_4) = \gamma_{4,0} + \varrho_{4,0} - \lambda \int_{-\Lambda}^{\Lambda} d^{d_{\text{in}}} x (\gamma_{4,\lambda} + \varrho_{4,\lambda}) - \kappa \int_{-\Lambda}^{\Lambda} d^{d_{\text{in}}} x (\gamma_{4,\kappa} + \varrho_{4,\kappa}). \quad (115)$$

Similarly (114) can be substituted into the 6-pt function given in (76) to express it in terms of model independent terms $\gamma_{6,i}$ and model dependent terms $\varrho_{6,i}$, as the following

$$G^{(6)}(x_1, x_2, x_3, x_4, x_5, x_6) = \gamma_{6,0} + \varrho_{6,0} - \lambda \int_{-\Lambda}^{\Lambda} d^{d_{\text{in}}} x (\gamma_{6,\lambda} + \varrho_{6,\lambda}) - \kappa \int_{-\Lambda}^{\Lambda} d^{d_{\text{in}}} x (\gamma_{6,\kappa} + \varrho_{6,\kappa}). \quad (116)$$

Irrespective of the NN structure, the terms $\gamma_{n,0}$ and $\varrho_{n,0}$ are independent of the integration variable x , as they are tree level corrections to the n -pt functions, and independent of any interaction vertices in respective Feynman diagrams.

The RG equations can be obtained by taking derivatives of the 4-pt and 6-pt function with respect to log of the cutoff scale Λ ,

$$\begin{aligned} \frac{\partial G^{(4)}(x_1, x_2, x_3, x_4)}{\partial \log \Lambda} = 0 = & \frac{\partial \lambda}{\partial \log \Lambda} \int_{-\Lambda}^{\Lambda} d^{d_{\text{in}}} x (\gamma_{4,\lambda} + \varrho_{4,\lambda}) + \lambda \frac{\partial (\int_{-\Lambda}^{\Lambda} d^{d_{\text{in}}} x (\gamma_{4,\lambda} + \varrho_{4,\lambda}))}{\partial \log \Lambda} \\ & + \frac{\partial \kappa}{\partial \log \Lambda} \int_{-\Lambda}^{\Lambda} d^{d_{\text{in}}} x (\gamma_{4,\kappa} + \varrho_{4,\kappa}) + \kappa \frac{\partial (\int_{-\Lambda}^{\Lambda} d^{d_{\text{in}}} x (\gamma_{4,\kappa} + \varrho_{4,\kappa}))}{\partial \log \Lambda}, \end{aligned} \quad (117)$$

$$\begin{aligned} \frac{\partial G^{(6)}(x_1, x_2, x_3, x_4, x_5, x_6)}{\partial \log \Lambda} = 0 = & \frac{\partial \lambda}{\partial \log \Lambda} \int_{-\Lambda}^{\Lambda} d^{d_{\text{in}}} x (\gamma_{6,\lambda} + \varrho_{6,\lambda}) + \lambda \frac{\partial (\int_{-\Lambda}^{\Lambda} d^{d_{\text{in}}} x (\gamma_{6,\lambda} + \varrho_{6,\lambda}))}{\partial \log \Lambda} \\ & + \frac{\partial \kappa}{\partial \log \Lambda} \int_{-\Lambda}^{\Lambda} d^{d_{\text{in}}} x (\gamma_{6,\kappa} + \varrho_{6,\kappa}) + \kappa \frac{\partial (\int_{-\Lambda}^{\Lambda} d^{d_{\text{in}}} x (\gamma_{6,\kappa} + \varrho_{6,\kappa}))}{\partial \log \Lambda}. \end{aligned} \quad (118)$$

In the limit of large Λ , κ is negligible, and the last terms in (117) and (118) vanish. In that case, (117) and (118) can be simplified to the following

$$\begin{aligned} & \frac{\partial \lambda}{\partial \log \Lambda} \int_{-\Lambda}^{\Lambda} d^{d_{\text{in}}} x \left[\frac{\int_{-\Lambda}^{\Lambda} d^{d_{\text{in}}} x (\gamma_{6,\lambda} + \varrho_{6,\lambda})}{\int_{-\Lambda}^{\Lambda} d^{d_{\text{in}}} x (\gamma_{6,\kappa} + \varrho_{6,\kappa})} - \frac{\int_{-\Lambda}^{\Lambda} d^{d_{\text{in}}} x (\gamma_{4,\lambda} + \varrho_{4,\lambda})}{\int_{-\Lambda}^{\Lambda} d^{d_{\text{in}}} x (\gamma_{4,\kappa} + \varrho_{4,\kappa})} \right] \\ & + \lambda \left[\frac{1}{\int_{-\Lambda}^{\Lambda} d^{d_{\text{in}}} x (\gamma_{6,\kappa} + \varrho_{6,\kappa})} \frac{\partial (\int_{-\Lambda}^{\Lambda} d^{d_{\text{in}}} x (\gamma_{6,\lambda} + \varrho_{6,\lambda}))}{\partial \log \Lambda} \right. \\ & \quad \left. - \frac{1}{\int_{-\Lambda}^{\Lambda} d^{d_{\text{in}}} x (\gamma_{4,\kappa} + \varrho_{4,\kappa})} \frac{\partial (\int_{-\Lambda}^{\Lambda} d^{d_{\text{in}}} x (\gamma_{4,\lambda} + \varrho_{4,\lambda}))}{\partial \log \Lambda} \right] = 0. \end{aligned}$$

Solving the above gives us the RG equation of λ , $\beta(\lambda)$.

4.2. Renormalization analysis for fully-connected networks

In this section we specify the renormalization analysis of the previous section to the case of a network with linear output layer and Gaussian biases, which include fully-connected networks and specifically the single-layer networks of our experiments.

Doing so is important for clarity because, as emphasized in section 3.4, the architectures we study are drawn from processes \mathcal{P} of functions of the form $f = f_b + f_W$, where f_b and f_W are drawn from independent processes $f_b \sim \mathcal{P}_b$ and $f_W \sim \mathcal{P}_W$, with \mathcal{P}_b Gaussian. The associated log-likelihood correction is therefore $\Delta S = \Delta S_W = \int_{-\infty}^{\infty} d^{d_{\text{in}}} x \sum_{l \leq k} g_{\mathcal{O}_l} \mathcal{O}_l$, which contributes to the distribution $P_W = e^{-S_{\text{NGP}}[f_W]}$; that is, all the non-Gaussianities involve only f_W , not f_b . Divergences may arise in perturbation theory from the boundaries of ΔS_W being $\pm\infty$, but can be removed using a cutoff scale Λ , yielding

$$\Delta S_{W,\Lambda} = \int_{-\Lambda}^{\Lambda} d^{d_{\text{in}}} x \sum_{l \leq k} g_{\mathcal{O}_l} \mathcal{O}_l, \quad (119)$$

which serves as the basis for perturbation theory and renormalization for any fixed Λ .

Input-space dimensions of 4-pt and 6-pt couplings λ and κ in (69) are now

$$[\lambda] = [g_4] = -d_{\text{in}} - 2[K_W], \quad [\kappa] = [g_6] = -d_{\text{in}} - 3[K_W], \quad (120)$$

respectively, where $[K_W]$ denotes scaling dimension of the kernel associated with \mathcal{P}_W in GP limit. Since K_W is the only part of the kernel that may give rise to divergences when computing correlation functions perturbatively, as only f_W appears in ΔS_W , we focus on the NGP flows in terms of K_W . For a general class of neural network architectures

$$K_W(x, x') = \varsigma(x, x'), \quad (121)$$

which will be utilized in concrete analyses.

A crucial difference from equations (115) and (116) is that these examples do not have model-independent terms from output biases in the interaction contributions to the correlation functions.

Specifically, we can rewrite $G^{(4)}(x_1, x_2, x_3, x_4)$ in terms of a model-independent term $\gamma_{4,0}$ (that does not arise from interactions) and model dependent terms $\varrho_{4,i}$. For simplicity we analyze the case where λ and κ are approximately constants. The subscripts 4 and i refer to the order of the correlation function and $O(i)$ corrections to the GP expression respectively.

$$G^{(4)}(x_1, x_2, x_3, x_4) = \gamma_{4,0} + \varrho_{4,0} - \lambda \int_{-\Lambda}^{\Lambda} d^{d_{\text{in}}} x \varrho_{4,\lambda} - \kappa \int_{-\Lambda}^{\Lambda} d^{d_{\text{in}}} x \varrho_{4,\kappa}. \quad (122)$$

Similarly the 6-pt function can be expressed in terms of a model independent term $\gamma_{6,0}$ (that does not arise from interactions) and model dependent terms $\varrho_{6,i}$, as the following

$$G^{(6)}(x_1, x_2, x_3, x_4, x_5, x_6) = \gamma_{6,0} + \varrho_{6,0} - \lambda \int_{-\Lambda}^{\Lambda} d^{d_{\text{in}}} x \varrho_{6,\lambda} - \kappa \int_{-\Lambda}^{\Lambda} d^{d_{\text{in}}} x \varrho_{6,\kappa}. \quad (123)$$

Irrespective of the NN structure, the terms $\gamma_{n,0}$ and $\varrho_{n,0}$ are independent of the integration variable x , as they are tree level corrections to the n -pt functions, and independent of any interaction vertices in respective Feynman diagrams.

The RG equations can be obtained by taking derivatives of above 4-pt and 6-pt function with respect to log of the cutoff scale Λ ,

$$\begin{aligned} \frac{\partial G^{(4)}(x_1, x_2, x_3, x_4)}{\partial \log \Lambda} = 0 &= \frac{\partial \lambda}{\partial \log \Lambda} \int_{-\Lambda}^{\Lambda} d^{d_{\text{in}}} x \varrho_{4,\lambda} + \lambda \frac{\partial (\int_{-\Lambda}^{\Lambda} d^{d_{\text{in}}} x \varrho_{4,\lambda})}{\partial \log \Lambda} \\ &+ \frac{\partial \kappa}{\partial \log \Lambda} \int_{-\Lambda}^{\Lambda} d^{d_{\text{in}}} x \varrho_{4,\kappa} + \kappa \frac{\partial (\int_{-\Lambda}^{\Lambda} d^{d_{\text{in}}} x \varrho_{4,\kappa})}{\partial \log \Lambda}, \end{aligned} \quad (124)$$

$$\begin{aligned} \frac{\partial G^{(6)}(x_1, x_2, x_3, x_4, x_5, x_6)}{\partial \log \Lambda} = 0 &= \frac{\partial \lambda}{\partial \log \Lambda} \int_{-\Lambda}^{\Lambda} d^{d_{\text{in}}} x \varrho_{6,\lambda} + \lambda \frac{\partial (\int_{-\Lambda}^{\Lambda} d^{d_{\text{in}}} x \varrho_{6,\lambda})}{\partial \log \Lambda} \\ &+ \frac{\partial \kappa}{\partial \log \Lambda} \int_{-\Lambda}^{\Lambda} d^{d_{\text{in}}} x \varrho_{6,\kappa} + \kappa \frac{\partial (\int_{-\Lambda}^{\Lambda} d^{d_{\text{in}}} x \varrho_{6,\kappa})}{\partial \log \Lambda}. \end{aligned} \quad (125)$$

In the limit of large N , and potentially of large Λ , we may ignore κ and equations (124) and (125) can be simplified to

$$\begin{aligned} \frac{\partial \lambda}{\partial \log \Lambda} \int_{-\Lambda}^{\Lambda} d^{d_{\text{in}}} x \left[\frac{\int_{-\Lambda}^{\Lambda} d^{d_{\text{in}}} x \varrho_{6,\lambda}}{\int_{-\Lambda}^{\Lambda} d^{d_{\text{in}}} x \varrho_{6,\kappa}} - \frac{\int_{-\Lambda}^{\Lambda} d^{d_{\text{in}}} x \varrho_{4,\lambda}}{\int_{-\Lambda}^{\Lambda} d^{d_{\text{in}}} x \varrho_{4,\kappa}} \right] &+ \lambda \left[\frac{1}{\int_{-\Lambda}^{\Lambda} d^{d_{\text{in}}} x \varrho_{6,\kappa}} \frac{\partial (\int_{-\Lambda}^{\Lambda} d^{d_{\text{in}}} x \varrho_{6,\lambda})}{\partial \log \Lambda} \right. \\ &\left. - \frac{1}{\int_{-\Lambda}^{\Lambda} d^{d_{\text{in}}} x \varrho_{4,\kappa}} \frac{\partial (\int_{-\Lambda}^{\Lambda} d^{d_{\text{in}}} x \varrho_{4,\lambda})}{\partial \log \Lambda} \right] = 0. \end{aligned}$$

Solving the above gives us the RG equation of $\lambda, \beta(\lambda)$ in our examples.

4.3. Experiments: flows in single-layer networks

In this subsection we analyze the flow in the coupling λ according to the techniques introduced in section 4.2.

4.3.1. Gauss-net

Recall that the Gauss-net kernel is given by

$$K_{\text{Gauss}}(x, x') = \sigma_b^2 + \sigma_W^2 \exp \left[-\frac{\sigma_W^2 |x - x'|^2}{2d_{\text{in}}} \right]. \quad (126)$$

Note that $|K_W(x, x')| < 1 \forall x \neq x'$; and $|K_W(x, x')| = 1$ when $x = x'$. At large x and fixed x' (which arises, for instance, when x is an integration variable and x' an external input) K_W exponentially dies off to zero, leading to convergent interaction integrals.

At small input x' , a careful analysis using Taylor expansion shows that in the regimes we are studying, i.e. small x , $[K_W] = \epsilon < 0$. The scaling of the couplings can be obtained from (120), giving $[\lambda] = -d_{\text{in}} - 2\epsilon$ and $[\kappa] = -d_{\text{in}} - 3\epsilon$. This suggests that λ scales to zero slightly faster than κ , but we see in our 6-pt experiments that the λ contributions nevertheless dominate over the κ contributions. Therefore at sufficiently large cutoff, κ becomes negligible, giving another reason to ignore it beyond the parametric control in $1/N$. Thus,

Table 6. Inputs $\{x_i\}$ for ReLU-net RG experiments in section 4.3 when $d_{\text{in}} = 2, 3$.

	$d_{\text{in}} = 2$	$d_{\text{in}} = 3$
ReLU-net	$\{(0.5000, 0.5000),$ $(0.5000, 1.0000),$ $(1.0000, 0.5000),$ $(1.0000, 1.0000)\}$	$\{(0.2000, 0.2000, 0.2000),$ $(1.0000, 1.0000, 0.2000),$ $(0.2000, 1.0000, 1.0000),$ $(1.0000, 0.2000, 1.0000)\}$

in the limit of large cutoff scales, where κ becomes negligible, the variations in 4-pt functions of Gauss-net with respect to $\log(\Lambda)$ can be used to obtain the RG equation of λ for Gauss-net.

Due to the fast convergence of K_W to 0, corrections to n -pt functions of Gauss-net from ΔS_W are all finite, and do not require renormalization. Put differently, the integrals do not diverge in the limit $\Lambda \rightarrow \infty$. Though not necessary, it is still possible to introduce a cutoff and study the flow of couplings, e.g. $\beta(\lambda)$ by various choice of cutoffs Λ , it is just not particularly interesting because for sufficiently large Λ , the couplings no longer change.

4.3.2. ReLU-net

Next we obtain the RG equation for ReLU-net architecture in the limit where κ becomes negligible.

Recall that the ReLU kernel is given by

$$K_{\text{ReLU}}(x, x') = \sigma_b^2 + \sigma_W^2 \cdot \frac{1}{2\pi} \sqrt{(\sigma_b^2 + \frac{\sigma_W^2}{d_{\text{in}}} x \cdot x)(\sigma_b^2 + \frac{\sigma_W^2}{d_{\text{in}}} x' \cdot x')} (\sin \theta + (\pi - \theta) \cos \theta),$$

$$\theta = \arccos \left[\frac{\sigma_b^2 + \frac{\sigma_W^2}{d_{\text{in}}} x \cdot x'}{\sqrt{(\sigma_b^2 + \frac{\sigma_W^2}{d_{\text{in}}} x \cdot x)(\sigma_b^2 + \frac{\sigma_W^2}{d_{\text{in}}} x' \cdot x')}} \right].$$

Comparing this with (121),

$$K_W(x, x') = \varsigma(x, x') = \sigma_W^2 \cdot \frac{1}{2\pi} \sqrt{(\sigma_b^2 + \frac{\sigma_W^2}{d_{\text{in}}} x \cdot x)(\sigma_b^2 + \frac{\sigma_W^2}{d_{\text{in}}} x' \cdot x')} (\sin \theta + (\pi - \theta) \cos \theta)$$

$$= h_1(x, x') h_2(\theta), \quad (127)$$

$$\text{where } h_1(x, x') = \sqrt{(\sigma_b^2 + \frac{\sigma_W^2}{d_{\text{in}}} x \cdot x)(\sigma_b^2 + \frac{\sigma_W^2}{d_{\text{in}}} x' \cdot x')},$$

$$h_2(\theta) = (\sin \theta + (\pi - \theta) \cos \theta).$$

K_W has been further separated into a bounded θ -dependent component h_2 and an unbounded component h_1 .

Here, we adjusted the inputs to those in table 6 to make our deviations measures sensible. The 4-pt function receives a large contribution from the λ -corrections when $x > \frac{\sigma_b \sqrt{d_{\text{in}}}}{\sigma_W}$ and x' is one of the inputs in our experiments; in this limit, which is relevant for our experiments since $\sigma_b = 0$, $h_1(x, x')$ can be approximated as the following

$$h_1(x, x') = \frac{\sigma_W^2}{d_{\text{in}}} |x| |x'|, \quad (128)$$

then the 4-pt function becomes

$$G^{(4)}(x_1, x_2, x_3, x_4) = \Lambda\text{-independent term} - \lambda \int_{-\Lambda}^{\Lambda} d^{d_{\text{in}}} x 24 \frac{\sigma_W^8}{d_{\text{in}}^4} |x|^4 |x_1| |x_2| |x_3| |x_4| \prod_{i=1}^4 h_2(\theta_i),$$

where each θ_i denotes the angle between external vertex x_i and internal vertex x . The integral is carried out by rotating the input-space to the spherical coordinates, where the $|x|$ and angular integrals may be carried out separately, since the θ_i do not depend on the magnitude of x or x_i . Each of θ_i remains bounded in $[0, 2\pi]$ as x is integrated across $(-\infty, \infty)$, and therefore, is not affected by the x -scaling. Thus each of $h_2(\theta_i)$ are bounded functions, and unaffected by the x -scaling; leading to the scaling dimension $\left[\prod_{i=1}^4 h_2(\theta_i) \right] = 0$.

Combining this with (128), and the choice of $\sigma_b^2 = 0$ in both first and final linear layers, the scaling dimension of ReLU kernel is given by $[K(x, x')] = 2$ and $[K_W(x, x')] = 2$, when $x > \frac{\sigma_b \sqrt{d_{\text{in}}}}{\sigma_W}$ and x' is one of the inputs in our experiments. Following (120), the 4-pt and 6-pt couplings scale as $[\lambda] = -d_{\text{in}} - 4$ and

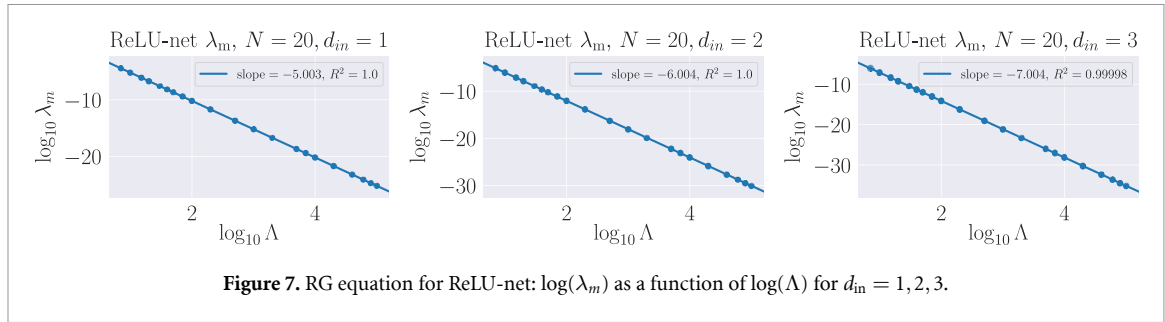


Figure 7. RG equation for ReLU-net: $\log(\lambda_m)$ as a function of $\log(\Lambda)$ for $d_{in} = 1, 2, 3$.

$[\kappa] = -d_{in} - 6$ respectively. This implies that κ becomes increasingly more negligible with respect to λ as Λ becomes larger; κ is also negligible at large N due to being $1/N$ suppressed relative to λ . In particular, this implies that the RG equation for λ can be entirely obtained in terms of $\mathcal{O}(\lambda)$ corrections to the 4-pt function; i.e. the κ corrections may be ignored.

Evaluating the full 4-pt function at $\mathcal{O}(\lambda)$ in large cutoff limit, we obtain

$$G^{(4)}(x_1, x_2, x_3, x_4) = \Lambda\text{-independent term} - \lambda j_1 \Lambda^{d_{in}+4}, \quad (129)$$

where j_1 is obtained by redefining the products of external vertices with other constants; trivial check shows that it is independent of Λ , and therefore we need not compute it, because it will drop out of $\beta(\lambda)$. Taking derivatives, we can obtain the RG equation as the following

$$\frac{\partial \lambda}{\partial \log \Lambda} \Lambda^{d_{in}+4} + (d_{in} + 4) \lambda \Lambda^{d_{in}+4} = 0, \quad (130)$$

which yields

$$\beta(\lambda) := \frac{\partial \lambda}{\partial \log(\Lambda)} = -(d_{in} + 4) \lambda. \quad (131)$$

After integration we get

$$\log \lambda = -(d_{in} + 4) \log \Lambda + p_1, \quad (132)$$

where p_1 is the constant of integration.

We verify above RG equation against the log-log variations of experimental value(s) of λ_m at different cutoff scales Λ . Equation (92) is used to obtain the rank-4 tensor λ_m at different choice of cutoff scales, given in (97). All independent tensor elements of λ_m are plotted below against respective Λ , in a log-log format, at different values of d_{in} .

The best fit lines in figure 7 are in excellent agreement with the theoretical prediction at (132); indeed, the slopes are $\sim -(d_{in} + 4)$ to excellent approximation. We emphasize the explicit dependence on d_{in} . Here λ appears to be a constant, but there is a small amount of variance on the same order displayed in figure 5 that is not visible due to the scale of the y -axis.

5. Conclusions

In this paper we have developed a correspondence between neural networks and QFT, providing a theoretical understanding for a function-space approach to neural networks.

The central idea is to treat neural network architectures $f_{\theta, N}$ that become GPs in the $N \rightarrow \infty$ limit using techniques from Wilsonian EFT. Specifically, at finite N the distribution on function space from which the neural networks are drawn is no longer Gaussian; the GP distribution is corrected to an associated NGP distribution that may be treated using EFT. The corrections have coefficients known as couplings, in physics, that encode interaction strengths.

Overall, we focused our developments on the two central ideas in EFT, applied in the context of neural networks:

- **EFT is effective.** A finite number of measured couplings yield many verifiable predictions.
- **EFT yields minimal NGP likelihoods.** Couplings vary with cutoff according to differential equations that govern flow on coupling space. Along the flow, some couplings become negligible, yielding a likelihood where all but the most important pieces can be safely ignored.

These were verified in concrete experiments in the simplest class of models admitting a GP limit: single layer fully-connected networks. We strongly emphasize, however, that our techniques are applicable to any architecture admitting a GP limit. Since we provided a concrete summary of our results in the introduction, we omit such a summary here.

Instead, we would like to conclude mentioning important areas for progress that we have not addressed, and then making some general comments and providing outlook.

Our work has developed a treatment of NN distributions in terms of QFT, focusing on the near-Gaussianity of the distributions at large-but-finite N . By focusing on the most essential elements of the correspondence, we have left a number of interesting and important directions for future work. One would be to understand when a local operator approach to NGP distributions, as we took in some of our models, suffices. Another is to understand the flow of the NGP distribution during training, perhaps from a neural tangent kernel [28] point of view. Finally, it would be interesting to understand how other types of fields—e.g. fermionic fields or the vector fields of electromagnetism—might arise in neural networks, where scalar fields are most natural.

Physicist readers may not be familiar with thinking of neural networks from a function space point of view, despite the fact that they think this way in QFT. However, many have trained a randomly initialized neural network, and then repeated it a number (say, M) of times to verify stability of the results. In doing so one is drawing M untrained neural networks from the prior induced by the parameter distributions and network architecture, and training the networks turns them into draws from some other distribution, the trained distribution. From this perspective, the process of supervised learning is simply learning the one-point function of the trained distribution; given an ensemble of trained nets, one should generate predictions from the ensemble expectation value of the outputs, the one-point function. Due to the prevalence of GP limits for many different architectures, in both randomly initialized and appropriately trained networks, the desired distributions on function space are nearly Gaussian, and therefore amenable to QFT techniques.

In the ML literature, it was (borrowing the inspirational language) ‘dreamed’ in [31] that flows in distributions of preactivations are akin to RG flows; we would like to comment on this in light of our work. We did not emphasize it so as to not introduce too many ideas, but our techniques apply not only to GPs associated with network outputs, but also those that may arise at intermediate layers. For instance, in deep fully-connected networks the central limit theorem may be applied [3] not just to the network outputs, but also the preactivations of the hidden layer, leading to an EFT description of the NGP associated with each layer’s preactivation. However, the details of the NGP effective action associated to each layer depends on both the previous layers’ activation functions and the width of that layer; i.e. the number of preactivations, which is the dimension of the GP distribution or number of quantum fields in the correspondence. This gives rise to structural differences in the effective actions that go beyond a simple flow in the couplings, so in general the relationship between preactivations flows and RG flows is (again borrowing language) a ‘spiritual resemblance,’ not an exact correspondence. Choosing all hidden layers to have the same non-linear activation function and width may make the analogy more direct.

Continuing down this direction, at a given layer of width N one could write the NGP effective action (log-likelihood) such that the N preactivations depend on the preactivations of a previous layer of width M , rather than the d_{in} inputs to the overall network. In this case it would naively appear that the EFT for the N preactivations would be in M -dimensional space, rather than d_{in} -dimensional space. These would be two EFT descriptions of the same preactivation NGP, but in different dimensions. What seems like a puzzle here (the arbitrariness of the dimensions) is likely resolved by a careful consideration of dimensionality, namely the first preactivation distribution having d_{in} -dimensional support in the M -dimensional space.

Equipped with a sharp NN–QFT correspondence, it is natural to try to import other ideas from QFT into the study of neural networks from a function space perspective. Perhaps those, together with the ideas implemented in this paper, can lead to a richer theoretical understanding of the many empirical successes in deep learning over the last decade.

Data availability statement

All data that support the findings of this study are included within the article (and any supplementary files).

Acknowledgments

We thank Michael Douglas and Greg Yang for suggestions on a draft of this manuscript and Microsoft Research for supporting the ‘Physics \cap ML’ meeting in 2019 that partially inspired this work. We thank Liam

Fitzpatrick, Sergei Gukov, Kiel Howe, and Matt Schwartz for helpful conversations. J H is supported by NSF CAREER Grant PHY-1848089.

Appendix A. Review of Gaussian integrals

A.1. Single and multivariable cases

All Gaussian integrals can be evaluated exactly as

$$\int_{-\infty}^{+\infty} dx \exp\left(-\frac{1}{2}ax^2\right) = \left(\frac{2\pi}{a}\right)^{\frac{1}{2}}. \quad (\text{A.1})$$

The associated $2n$ -pt function is the expectation value of the single variable operator x^{2n} ; it can be obtained by repeatedly differentiating the above by $-2(d/da)$ to give

$$\langle x^{2n} \rangle = \frac{\int_{-\infty}^{+\infty} dx \exp\left(-\frac{1}{2}ax^2\right) x^{2n}}{\int_{-\infty}^{+\infty} dx \exp\left(-\frac{1}{2}ax^2\right)} = \frac{1}{a^n} (2n-1)!! . \quad (\text{A.2})$$

The $(2n-1)!!$ factor in (A.2) can be thought of as the number of ways to connect $2n$ points in pairs, which is a version of what is known as Wick contraction in the physics literature. Using this, $\langle x^{2n} \rangle$ can be computed graphically in terms of Feynman diagrams.

Let us compute the 4-pt function: four vertices can be Wick contracted into two pairs in three distinct ways. Each connected pair contributes a factor of $1/a$ to the Gaussian integral in (A.2). The corresponding Feynman diagram, given below, is a sum of three distinct diagrams, each corresponding to a unique Wick contraction, and contributing a factor of $1/a^2$ from the two pairs.

$$\begin{array}{c} \begin{array}{ccc} \begin{array}{c} \bullet \\ | \\ \bullet \end{array} & \begin{array}{c} \bullet \\ | \\ \bullet \end{array} & + \\ \left(\frac{1}{a} \cdot \frac{1}{a}\right) & + & \left(\frac{1}{a} \cdot \frac{1}{a}\right) \end{array} \quad \begin{array}{ccc} \begin{array}{c} \bullet \text{---} \bullet \\ \bullet \text{---} \bullet \end{array} & + & \begin{array}{c} \bullet \text{---} \bullet \\ \diagup \quad \diagdown \\ \bullet \text{---} \bullet \end{array} \end{array} = \frac{3}{a^2}.$$

The total of three diagrams, $3/a^2$, matches with (A.2) for $n = 2$.

More generally, a Gaussian integral including a source term, described as the one below,

$$\int_{-\infty}^{+\infty} dx \exp\left(-\frac{1}{2}ax^2 + Jx\right), \quad (\text{A.3})$$

can be evaluated by completing the square in the exponent:

$-ax^2/2 + Jx = -(a/2)(x^2 - 2Jx/a) = -(a/2)(x - J/a)^2 + J^2/2a$, and shifting the variable to $x \rightarrow y = x + J/a$, giving

$$\begin{aligned} \int_{-\infty}^{+\infty} dx \exp\left(-\frac{1}{2}ax^2 + Jx\right) &= \int_{-\infty}^{+\infty} dy \exp\left(-\frac{a}{2}y^2 + J^2/2a\right) \\ &= \left(\frac{2\pi}{a}\right)^{\frac{1}{2}} \exp(J^2/2a). \end{aligned} \quad (\text{A.4})$$

The $2n$ -pt function $\langle x^{2n} \rangle$ can be alternatively calculated by acting with the derivative $\delta/\delta J$ on (A.3) $2n$ times, then setting the source $J = 0$ to retrieve the Gaussian integral.

We can generalize (A.4) to a multivariate Gaussian integral by promoting a to a real symmetric $N \times N$ matrix A_{ij} and variable x to a $(N \times 1)$ dimensional vector x_i , given below

$$\int_{-\infty}^{+\infty} \dots \int_{-\infty}^{+\infty} \int_{-\infty}^{+\infty} dx_1 dx_2 \dots dx_N \exp\left(-\frac{1}{2}x \cdot A \cdot x + J \cdot x\right) = \left(\frac{(2\pi)^N}{\det|A|}\right)^{\frac{1}{2}} \exp\left(\frac{1}{2}JA^{-1}J\right). \quad (\text{A.5})$$

Here $x \cdot A \cdot x = x_i A_{ij} x_j$ and $J \cdot x = J_i x_i$. This can be exactly computed by an orthogonal basis transformation O and a diagonal matrix D , to give $A = O^{-1}DO$ and $y_i = O_{ij}x_j$ in the N -dimensional Euclidean space, to result in

$$\begin{aligned}
\int_{-\infty}^{+\infty} \cdots \int_{-\infty}^{+\infty} \int_{-\infty}^{+\infty} dy_1 dy_2 \cdots dy_N \exp \left(-\frac{1}{2} y D y + (OJ)y \right) &= \prod_{i=1}^N dy_i \exp \left(-\frac{1}{2} D_{ii} y_i^2 + (OJ)_i y_i \right) \\
&= \left(\frac{(2\pi)^N}{\det[A]} \right)^{\frac{1}{2}} \exp \left(\frac{1}{2} (OJ) D^{-1} (OJ) \right) \\
&= \left(\frac{(2\pi)^N}{\det[A]} \right)^{\frac{1}{2}} \exp \left(J (O^{-1} D^{-1} O) J \right) \\
&= \left(\frac{(2\pi)^N}{\det[A]} \right)^{\frac{1}{2}} \exp \left(\frac{1}{2} J A^{-1} J \right). \quad (\text{A.6})
\end{aligned}$$

The general expression of the n -pt function can be obtained by applying Wick contraction to (A.6), to give

$$\langle x_1 x_2 \cdots x_{n-1} x_n \rangle = \frac{\int_{-\infty}^{+\infty} \cdots \int_{-\infty}^{+\infty} \int_{-\infty}^{+\infty} dx_1 dx_2 \cdots dx_N \exp \left(-\frac{1}{2} x A x \right) x_1 x_2 \cdots x_{n-1} x_n}{\int_{-\infty}^{+\infty} \cdots \int_{-\infty}^{+\infty} \int_{-\infty}^{+\infty} dx_1 dx_2 \cdots dx_N \exp \left(-\frac{1}{2} x A x \right)} \quad (\text{A.7})$$

$$= \sum_{\text{Wick pairs}} \langle x_a x_b \rangle \cdots \langle x_c x_d \rangle = \sum_{\text{Wick pairs}} (A^{-1})_{ab} \cdots (A^{-1})_{cd}. \quad (\text{A.8})$$

For $n = 1$ and $n = 2$ these simplify into

$$\langle x_i \rangle = \frac{\int_{-\infty}^{+\infty} \cdots \int_{-\infty}^{+\infty} \int_{-\infty}^{+\infty} dx_1 dx_2 \cdots dx_N \exp \left(-\frac{1}{2} x A x \right) x_i}{\int_{-\infty}^{+\infty} \cdots \int_{-\infty}^{+\infty} \int_{-\infty}^{+\infty} dx_1 dx_2 \cdots dx_N \exp \left(-\frac{1}{2} x A x \right)} = 0, \quad (\text{A.9})$$

$$\langle x_i x_j \rangle = \frac{\int_{-\infty}^{+\infty} \cdots \int_{-\infty}^{+\infty} \int_{-\infty}^{+\infty} dx_1 dx_2 \cdots dx_N \exp \left(-\frac{1}{2} x A x \right) x_i x_j}{\int_{-\infty}^{+\infty} \cdots \int_{-\infty}^{+\infty} \int_{-\infty}^{+\infty} dx_1 dx_2 \cdots dx_N \exp \left(-\frac{1}{2} x A x \right)} = A_{ij}^{-1}. \quad (\text{A.10})$$

A.2. Continuous number of variables

When the variables describing a GPs are promoted to be continuous, the entire process can be defined in terms of a partition function, given by

$$\begin{aligned}
Z_{\text{GP}} &= \frac{1}{Z_{\text{GP},0}} \int d\mathbf{f} e^{-\frac{1}{2} \int d^d x d^d y f(x) \Xi(x,y) f(y) - \frac{1}{2} \int d^d x J(x) f(x) - \frac{1}{2} \int d^d y J(y) f(y)} \\
&= \frac{1}{Z_{\text{GP},0}} \int d\mathbf{f} e^{-(S_{\text{GP}} + \Delta S)}, \quad (\text{A.11})
\end{aligned}$$

where

$$\begin{aligned}
S_{\text{GP}} &= \frac{1}{2} \int d^d x d^d y f(x) \Xi(x,y) f(y) \\
\Delta S &= \frac{1}{2} \int d^d x J(x) f(x) + \frac{1}{2} \int d^d y J(y) f(y)
\end{aligned}$$

and $Z_{\text{GP},0} := Z_{\text{GP}}[J = 0] = \int d\mathbf{f} e^{-S_{\text{GP}}}$ is the normalization constant.

$\Xi(x,y)$, a real symmetric 2-tensor, is the continuous version of the inverse of the covariance matrix. We can evaluate (A.11) by a basis transformation such that $\Xi(x,y)$ is diagonal. However, here we choose a more direct evaluation of Z_{GP} by noting that it can be expressed as the following

$$\begin{aligned}
\int d\mathbf{f} e^{-(S_{\text{GP}} + \Delta S)} &= e^{\frac{1}{2} \int d^d x d^d y J(x) K(x,y) J(y)} \\
&\times \int d\mathbf{f} e^{-\frac{1}{2} \int d^d x d^d y \left(f(x) + \int d^d w J(w) K(w,x) \right) \Xi(x,y) \left(f(y) + \int d^d z J(z) K(y,z) \right)}. \quad (\text{A.12})
\end{aligned}$$

The terms in the last exponential of (A.12) can be expanded to obtain

$$\begin{aligned}
-\frac{1}{2} \int d^d x d^d y d^d w J(w) K(w,x) \Xi(x,y) f(y) &= -\frac{1}{2} \int d^d y d^d w J(w) \delta(w-y) f(y) \\
&= -\frac{1}{2} \int d^d y J(y) f(y), \quad (\text{A.13})
\end{aligned}$$

and a similar identity for $J(x)f(x)$. The remaining term in the last exponential of (A.12) is simplified to be

$$-\frac{1}{2} \int d^d x d^d y d^d w d^d z J(w) K(w, x) \Xi(x, y) K(y, z) J(z) \quad (\text{A.14})$$

$$= -\frac{1}{2} \int d^d x d^d y J(x) K(x, y) J(y). \quad (\text{A.15})$$

The last identity arises from the $\delta^{(d)}(w - y)$ resulting from x -integral evaluation, followed by renaming integration variables to x and y . Using these, the integral over output space on in (A.12) can be simplified. Further, by diagonalization $Z_{\text{GP},0} = [2\pi / \det(\Xi)]^{1/2}$. Putting it all together, we have the integrated form of the partition function

$$Z_{\text{GP}} = \exp \left(\frac{1}{2} \int d^d x d^d y J(x) K(x, y) J(y) \right), \quad (\text{A.16})$$

where $K(x, y)$ is the functional/operator inverse of $\Xi(x, y)$, i.e. $\int dy K(x, y) \Xi(y, z) = \delta(x - z)$.

The n -pt function of the GP over continuous variables is given by

$$G^{(n)}(x_1, \dots, x_n) = \frac{\int df f(x_1) \dots f(x_n) e^{-(S_{\text{GP}} + \Delta S)}}{Z_{\text{GP},0}}. \quad (\text{A.17})$$

It may be computed in a canonical way by taking functional J -derivatives,

$$\begin{aligned} G^{(n)}(x_1, \dots, x_n) &= \left[\left(-\frac{\delta}{\delta J(x_1)} \right) \dots \left(-\frac{\delta}{\delta J(x_n)} \right) \frac{\int df e^{-(S_{\text{GP}} + \Delta S)}}{Z_0} \right] \Big|_{J=0} \\ &= \left[\left(-\frac{\delta}{\delta J(x_1)} \right) \dots \left(-\frac{\delta}{\delta J(x_n)} \right) Z_{\text{GP}} \right] \Big|_{J=0}, \end{aligned} \quad (\text{A.18})$$

which can be directly evaluated from (A.16).

For the sake of thoroughness we demonstrate the calculations of some of the n -pt functions. The 1-pt function is

$$G^{(1)}(x_1) = \mathbb{E}[f(x_1)] = -\frac{\delta}{\delta J(x_1)} Z_{\text{GP}} \Big|_{J=0} = 0, \quad (\text{A.19})$$

where the derivative results in a factor of J , which sets the 1-pt function to 0. The 2-pt function is given by

$$\begin{aligned} G^{(2)}(x_1, x_2) &= \mathbb{E}[f(x_1)f(x_2)] = \left[(-1)^2 \frac{\delta}{\delta J(x_1)} \frac{\delta}{\delta J(x_2)} \exp \left(\frac{1}{2} \int d^d x d^d y J(x) K(x, y) J(y) \right) \right] \Big|_{J=0} \\ &= \frac{\delta}{\delta J(x_1)} \left[e^{\int d^d x d^d y J(x) K(x, y) J(y)} \int d^d x d^d y \left(\frac{1}{2} \delta(x_2 - x) K(x, y) J(y) \right. \right. \\ &\quad \left. \left. + \frac{1}{2} \delta(x_2 - y) J(x) K(x, y) \right) \right] \Big|_{J=0} \\ &= \frac{1}{2} \int d^d y \delta(x_1 - y) K(x_2, y) + \frac{1}{2} \int d^d x \delta(x_1 - x) K(x, x_2) \\ &= \frac{1}{2} K(x_2, x_1) + \frac{1}{2} K(x_1, x_2) = K(x_1, x_2). \end{aligned} \quad (\text{A.20})$$

The last line follows from the symmetry of the covariance $K(x_1, x_2)$.

The general expression of the n -pt function can be obtained by a similar calculation; it is given by

$$\begin{aligned}
G^{(n)}(x_1, \dots, x_n) &= \mathbb{E}[f(x_1) \dots f(x_n)] = \left[(-)^n \frac{\delta}{\delta J(x_1)} \dots \frac{\delta}{\delta J(x_n)} Z_{\text{GP}} \right] \Big|_{J=0} \\
&= \sum_{\text{Wick pairs}} \mathbb{E}[f(x_a)f(x_b)] \dots \mathbb{E}[f(x_c)f(x_d)] \\
&= \sum_{\text{Wick pairs}} K(x_a, x_b) \dots K(x_c, x_d), \text{ if } n \text{ even} \quad (\text{A.21})
\end{aligned}$$

$$= 0, \text{ if } n \text{ odd.} \quad (\text{A.22})$$

From (A.21) we deduce that the 3-pt function of a GP is identically zero. And the 4-pt function is given by

$$G^{(4)}(x_1, \dots, x_4) = K(x_1, x_2)K(x_3, x_4) + K(x_1, x_3)K(x_2, x_4) + K(x_1, x_4)K(x_2, x_3), \quad (\text{A.23})$$

which may be expressed in terms of Feynman diagrams, as done in (20).

A.3. Non-Gaussian integrals via perturbation theory

Small perturbations away from the GP can still be understood in terms of order-by-order perturbative corrections to the Gaussian integral. Let us assume that the small perturbations can be described in terms of correction terms $g_n f(x)^n$ to S_{GP} . The associated new partition function is

$$\begin{aligned}
Z[g_n, J] &= \frac{\int df e^{-\frac{1}{2} \int d^d x_1 d^d x_2 f(x_1) \Xi(x_1, x_2) f(x_2) - \frac{1}{2} \int d^d x_1 J(x_1) f(x_1) - \frac{1}{2} \int d^d x_2 J(x_2) f(x_2) - \int d^d x g_n f(x)^n}}{\int df e^{\frac{1}{2} \int d^d x_1 d^d x_2 f(x_1) \Xi(x_1, x_2) f(x_2) - \int d^d x g_n f(x)^n}} \\
&= \frac{\int df \sum_{m=0}^{\infty} \frac{(-1)^m}{m!} (g_n)^m \left[\int d^d x f(x)^n \right]^m e^{-\frac{1}{2} \int d^d x_1 d^d x_2 f(x_1) \Xi(x_1, x_2) f(x_2) - \frac{1}{2} \int d^d x_1 J(x_1) f(x_1) - \frac{1}{2} \int d^d x_2 J(x_2) f(x_2)}}{Z[g_n, J=0]} \\
&= \frac{\int df \sum_{m=0}^{\infty} \frac{(-1)^m}{m!} (g_n)^m \left[\int d^d x \left(-\frac{\delta}{\delta J(x)} \right)^n \right]^m e^{-\frac{1}{2} \int d^d x_1 d^d x_2 f(x_1) \Xi(x_1, x_2) f(x_2) - \frac{1}{2} \int d^d x_1 J(x_1) f(x_1) - \frac{1}{2} \int d^d x_2 J(x_2) f(x_2)}}{Z[g_n, J=0]} \\
&= \frac{\int df \sum_{m=0}^{\infty} \frac{(-1)^m}{m!} (g_n)^m \left[\int d^d x \left(-\frac{\delta}{\delta J(x)} \right)^n \right]^m e^{\frac{1}{2} \int d^d x_1 d^d x_2 J(x_1) K(x_1, x_2) J(x_2)}}{Z[g_n, J=0]} \\
&= \frac{\int df \sum_{s=0}^{\infty} \frac{1}{s!} \int d^d x_1 \dots \int d^d x_s J(x_1) \dots J(x_s) e^{-S_{\text{GP}} - \int d^d x g_n f(x)^n} f(x_1) \dots f(x_s)}{Z[g_n, J=0]} \\
&= \sum_{s=0}^{\infty} \frac{1}{s!} \int d^d x_1 \dots \int d^d x_s J(x_1) \dots J(x_s) G^{(s)}(x_1, \dots, x_s) \quad (\text{A.24})
\end{aligned}$$

where

$$\begin{aligned}
G^{(s)}(x_1, \dots, x_s) &= \frac{\int df e^{-S_{\text{GP}} - \int d^d x g_n f(x)^n} f(x_1) \dots f(x_s)}{Z[J=0, g_n]} \\
&= \left(\frac{\int df e^{-S_{\text{GP}} - \int d^d x g_n f(x)^n} f(x_1) \dots f(x_s)}{Z_0[J=0, g_n=0]} \right) \Bigg/ \left(\frac{Z[J=0, g_n]}{Z_0[J=0, g_n=0]} \right) \quad (\text{A.25})
\end{aligned}$$

The numerator and the denominator in (A.25) can be separately obtained using Wick contractions and Feynman diagrams; they both contain some diagrams where none of the internal vertices are connected to any of the external vertices. Such diagrams are called ‘vacuum bubbles’, and any diagram containing a vacuum bubble exactly cancels from the numerator and denominator upon series expansions, thus not contributing to the actual n -pt functions.

We take an example where the NGP is described by small perturbations away from the GP by $\Delta S = \int d^d x [g f(x)^3 + \lambda f(x)^4]$. The denominator of (A.25) is expanded below, in terms of Feynman diagrams, up to quadratic order terms in coupling constants g and λ .

$$\begin{aligned}
1 &= \lambda \left[3 \text{ (bubble)} \right] + \frac{g^2}{2!} \left[9 \text{ (two bubbles)} + 6 \text{ (bubble with internal line)} \right] + \frac{\lambda^2}{2!} \left[9 \text{ (two bubbles)} \right. \\
&\quad \left. + 72 \text{ (two bubbles with internal line)} + 24 \text{ (bubble with two internal lines)} \right].
\end{aligned}
\tag{A.26}$$

The three point vertices correspond to coupling constant g and occur at internal points labeled by w , and the four point vertices correspond to λ and occur at points labeled by y .

The numerator of the 1-pt function, up to same orders of correction terms, is given below:

$$\begin{aligned}
&-g \left[3 \text{ (bubble)} \right] + g\lambda \left[9 \text{ (bubble)} + 36 \text{ (bubble with internal line)} + 24 \text{ (bubble with two internal lines)} \right. \\
&\quad \left. + 36 \text{ (two bubbles)} \right].
\end{aligned}
\tag{A.27}$$

After vacuum bubbles cancel from both the numerator and denominator, the 1-pt function to quadratic orders in g and λ is

$$\begin{aligned}
G^{(1)}(x_1) &= -g \left[3 \text{ (bubble)} \right] + g\lambda \left[36 \text{ (bubble with internal line)} + 24 \text{ (bubble with two internal lines)} \right. \\
&\quad \left. + 36 \text{ (two bubbles)} \right].
\end{aligned}
\tag{A.28}$$

Similarly, the numerator of the 2-pt function is obtained to be

$$\begin{aligned}
&\text{ (two-point line)} = \lambda \left[3 \text{ (two bubbles)} + 12 \text{ (bubble with internal line)} \right] + \frac{g^2}{2!} \left[9 \text{ (two bubbles)} + 6 \text{ (bubble with internal line)} \right. \\
&\quad \left. + 18 \text{ (two-point line with bubble)} + 36 \text{ (two-point line with two bubbles)} + 36 \text{ (three-point vertex)} \right] \\
&\quad + \frac{\lambda^2}{2!} \left[9 \text{ (two bubbles)} + 72 \text{ (two bubbles with internal line)} + 72 \text{ (two bubbles with two internal lines)} + 192 \text{ (two-point line with two bubbles)} \right. \\
&\quad \left. + 288 \text{ (two-point line with three bubbles)} + 24 \text{ (bubble with two internal lines)} + 288 \text{ (two-point line with four bubbles)} \right].
\end{aligned}
\tag{A.29}$$

After canceling all vacuum bubbles, the exact 2-pt function is

$$\begin{aligned}
G^{(2)}(x_1, x_2) &= \text{ (two-point line)} - \lambda \left[12 \text{ (bubble with internal line)} \right] \\
&\quad + \frac{g^2}{2!} \left[18 \text{ (two-point line with bubble)} + 36 \text{ (two-point line with two bubbles)} + 36 \text{ (three-point vertex)} \right] \\
&\quad + \frac{\lambda^2}{2!} \left[192 \text{ (two-point line with two bubbles)} + 288 \text{ (two-point line with three bubbles)} + 288 \text{ (two-point line with four bubbles)} \right].
\end{aligned}
\tag{A.30}$$

Each of the higher order n -pt functions contains different topologically distinct Feynman diagrams, with various permutations of external vertices; each of these diagrams should be treated separately when external vertices are fixed. However, for illustration, we present such topologically distinct Feynman diagrams ignoring all external labels, and take care of the combinatorics of external vertices by multiplying with the total number of copies.

The numerator of the 3-pt function is given by the following diagrams:

$$\begin{aligned}
 & -g \left[9 \text{ (diagram: two horizontal lines, top has a loop labeled } w) + 6 \text{ (diagram: two horizontal lines, top has a vertex with two lines going up and one down)} \right] \\
 & + g\lambda \left[108 \text{ (diagram: two horizontal lines, top has a loop labeled } w \text{ and a vertex labeled } y) + 72 \text{ (diagram: two horizontal lines, top has a loop labeled } w \text{ and a vertex labeled } y) \right. \\
 & + 27 \text{ (diagram: two horizontal lines, top has a loop labeled } w \text{ and a vertex labeled } y) + 108 \text{ (diagram: two horizontal lines, top has a loop labeled } w \text{ and a vertex labeled } y) \\
 & + 108 \text{ (diagram: two horizontal lines, top has a loop labeled } w \text{ and a vertex labeled } y) + 72 \text{ (diagram: two horizontal lines, top has a loop labeled } w \text{ and a vertex labeled } y) \\
 & \left. + 216 \text{ (diagram: two horizontal lines, top has a loop labeled } w \text{ and a vertex labeled } y) + 216 \text{ (diagram: two horizontal lines, top has a loop labeled } w \text{ and a vertex labeled } y) \right. \\
 & \left. + 18 \text{ (diagram: two horizontal lines, top has a loop labeled } w \text{ and a vertex labeled } y) \right].
 \end{aligned}$$

The final expression for 3-pt function is

$$\begin{aligned}
 G^{(3)}(x_1, x_2, x_3) = & -g \left[9 \text{ (diagram: two horizontal lines, top has a loop labeled } w) + 6 \text{ (diagram: two horizontal lines, top has a vertex with two lines going up and one down)} \right] \\
 & + g\lambda \left[108 \text{ (diagram: two horizontal lines, top has a loop labeled } w \text{ and a vertex labeled } y) + 72 \text{ (diagram: two horizontal lines, top has a loop labeled } w \text{ and a vertex labeled } y) \right. \\
 & + 108 \text{ (diagram: two horizontal lines, top has a loop labeled } w \text{ and a vertex labeled } y) + 72 \text{ (diagram: two horizontal lines, top has a loop labeled } w \text{ and a vertex labeled } y) \\
 & \left. + 216 \text{ (diagram: two horizontal lines, top has a loop labeled } w \text{ and a vertex labeled } y) + 216 \text{ (diagram: two horizontal lines, top has a loop labeled } w \text{ and a vertex labeled } y) \right. \\
 & \left. + 108 \text{ (diagram: two horizontal lines, top has a loop labeled } w \text{ and a vertex labeled } y) \right]
 \end{aligned}$$

Following similar analysis the 4-pt function is given by

$$\begin{aligned}
 G^{(4)}(x_1, x_2, x_3, x_4) = & 3 \text{ (diagram: two horizontal lines) } - \lambda \left[72 \text{ (diagram: two horizontal lines, top has a loop labeled } y) + 24 \text{ (diagram: two horizontal lines, top has a loop labeled } y) \right] \\
 & + \frac{g^2}{2!} \left[108 \text{ (diagram: two horizontal lines, top has a loop labeled } w) + 216 \text{ (diagram: two horizontal lines, top has a loop labeled } w) \right. \\
 & + 216 \text{ (diagram: two horizontal lines, top has a loop labeled } w) + 144 \text{ (diagram: two horizontal lines, top has a loop labeled } w) + 216 \text{ (diagram: two horizontal lines, top has a loop labeled } w) \\
 & + \frac{\lambda^2}{2!} \left[1152 \text{ (diagram: two horizontal lines, top has a loop labeled } y) + 1728 \text{ (diagram: two horizontal lines, top has a loop labeled } y) \right. \\
 & + 1728 \text{ (diagram: two horizontal lines, top has a loop labeled } y) + 1728 \text{ (diagram: two horizontal lines, top has a loop labeled } y) \\
 & \left. + 2304 \text{ (diagram: two horizontal lines, top has a loop labeled } y) + 864 \text{ (diagram: two horizontal lines, top has a loop labeled } y) \right].
 \end{aligned} \tag{A.31}$$

Appendix B. 2-pt functions/kernels of example networks

A neural network with activation function $\phi(x)$ and one hidden layer has the following output function

$$f(x) = W_1 \phi(W_0 x + b_0) + b_1. \tag{B.1}$$

When the weights and biases W_0, W_1, b_0, b_1 are i.i.d. and drawn from a Gaussian distribution with mean 0 and standard deviations $\sigma_{W_0}, \sigma_{W_1}, \sigma_{b_0}, \sigma_{b_1}$ respectively, the kernel or 2-pt function is given by

$$\mathbb{E}[f(x)f(x')] = \sigma_{b_1}^2 + \sigma_{W_1}^2 V_\phi[\phi(W_0 x + b_0), \phi(W_0 x' + b_0)]. \tag{B.2}$$

The 2-pt function of the post-activation $V_\phi[\phi(W_0 x + b_0), \phi(W_0 x' + b_0)]$ can be evaluated by two methods: the first method is exact at any width, prescribed in [2]; and the second method is true in the GP

limit, described in [37]. We will refer to the two methods by superscripts ‘Williams’ and ‘Yang’ respectively. They are the following

$$V_{\phi}^{\text{Williams}}(x, x') = \frac{\int \phi(W_0 x + b_0) \phi(W_0 x' + b_0) e^{-\frac{1}{2} W_0^T \sigma_{W_0}^{-2} W_0 - \frac{1}{2} b_0^T \sigma_{b_0}^{-2} b_0} dW_0 db_0}{\int \exp\left(-\frac{1}{2} W_0^T \sigma_{W_0}^{-2} W_0 - \frac{1}{2} b_0^T \sigma_{b_0}^{-2} b_0\right) dW_0 db_0}, \quad (\text{B.3})$$

and

$$V_{\phi}^{\text{Yang}}(x, x') = \mathbb{E}_{f \sim \mathcal{N}(0, K)}[\phi(W_0 x + b_0), \phi(W_0 x' + b_0)], \quad (\text{B.4})$$

where K is the kernel or covariance function of the Gaussian distribution of f in the GP limit. For the three NN architectures discussed in this paper, kernels evaluated by both prescriptions are shown to agree in the limit of infinite width, i.e. GP.

B.1. Erf-net

We now turn to the case of Erf activation, which is given by

$$\phi(x) = \frac{2}{\sqrt{\pi}} \int_0^x \exp(-t^2) dt. \quad (\text{B.5})$$

At any width N , the associated kernel can be obtained by the method in [2]. This involves substituting (B.5) in (B.3), followed by computing the Gaussian integral and a transformation of variables. The kernel of Erf-net by this method is obtained to be

$$V_{\text{Erf-net}}^{\text{Williams}}[f(x)f(x')] = \sigma_{b_1}^2 + \sigma_{W_1}^2 N \frac{2}{\pi} \arcsin \left[\frac{2K(x, x')}{\sqrt{(1 + 2K(x, x)) (1 + 2K(x', x'))}} \right]. \quad (\text{B.6})$$

Normalization $\sigma_{W_1} = \frac{\sigma_{W_0}}{\sqrt{N}}$ is chosen to ensure width invariance of the kernel. The intermediate expressions, such as $K(x, x')$, are the kernels of the linear layer $W_0 x + b_0$, given below

$$K(x, x) = \sigma_{b_0}^2 + \sigma_{W_0}^2 x \cdot x, \quad K(x', x') = \sigma_{b_0}^2 + \sigma_{W_0}^2 x' \cdot x', \quad K(x, x') = \sigma_{b_0}^2 + \sigma_{W_0}^2 x \cdot x'. \quad (\text{B.7})$$

In the limit of infinite width, the method in [37] can be used. This involves substituting (B.5) in (B.4), defined in terms of PDF of output $f(x)$. Evaluating the Gaussian integral, followed by a change of variables, results in the same expressions as (B.6) for $V_{\text{Erf-net}}^{\text{Yang}}(x, x')$. This shows that the Erf-net kernel is exact at any width when $\sigma_{W_1} = \frac{\sigma_{W_0}}{\sqrt{N}}$, given by

$$\mathbb{E}_{\text{Erf-net}}[f(x)f(x')] = \sigma_{b_1}^2 + \sigma_{W_0}^2 \frac{2}{\pi} \arcsin \left[\frac{2(\sigma_{b_0}^2 + \sigma_{W_0}^2 x \cdot x')}{\sqrt{(1 + 2(\sigma_{b_0}^2 + \sigma_{W_0}^2 x \cdot x)) (1 + 2(\sigma_{b_0}^2 + \sigma_{W_0}^2 x' \cdot x'))}} \right]. \quad (\text{B.8})$$

B.2. ReLU-net

Next we study the case of ReLU activation, which is given by

$$\phi(x) = \max(0, x). \quad (\text{B.9})$$

At finite width N , (B.9) can be substituted into (B.3), followed by a rearrangement in terms of Heaviside function $\Theta(x) = \frac{1}{2}(1 + \text{sgn}(x))$, to obtain

$$V_{\text{ReLU-net}}^{\text{Williams}}(x, x') = \frac{\int \Theta(W_0 x + b_0) (W_0 x + b_0) \Theta(W_0 x' + b_0) (W_0 x' + b_0) e^{-\frac{1}{2} (W_0^T \sigma_{W_0}^{-2} W_0 + b_0^T \sigma_{b_0}^{-2} b_0)} dW_0 db_0}{\int \exp\left(-\frac{1}{2} W_0^T \sigma_{W_0}^{-2} W_0 - \frac{1}{2} b_0^T \sigma_{b_0}^{-2} b_0\right) dW_0 db_0}.$$

The arguments of the Heaviside function are chosen to lie in the first quadrant. After a basis transformation it results in the following

$$V_{\text{ReLU-net}}^{\text{Williams}}(x, x') = \frac{N(\sin \theta)^3}{2\pi} \sqrt{K(x, x)K(x', x')} \int da db a b \exp\left(-\frac{1}{2}|a|^2 - \frac{1}{2}|b|^2 - a \cdot b \cos \theta\right). \quad (\text{B.10})$$

Here $\cos \theta = \frac{K(x, x')}{\sqrt{K(x, x)K(x', x')}}}$ and intermediate kernels $K(x, x)$, $K(x, x')$ and $K(x', x')$ of the linear layer $W_0 x + b_0$ are defined in (B.7). A further change of variables $a = r \cos\left(\frac{\psi}{2} + \frac{\pi}{4}\right)$ and $b = r \sin\left(\frac{\psi}{2} + \frac{\pi}{4}\right)$, followed by integrating out the variable r , results in

$$V_{\text{ReLU-net}}^{\text{William}}(x, x') = \frac{N(\sin \theta)^3}{2\pi} \sqrt{K(x, x)K(x', x')} \int_0^{\pi/2} \frac{d\psi \cos \psi}{(1 - \cos \psi \cos \theta)^2}. \quad (\text{B.11})$$

Taking the derivative of the following trigonometric identity with respect to $\cos \theta$

$$\int_0^{\pi/2} \frac{d\psi}{1 - \cos \psi \cos \theta} = \frac{\pi - \theta}{\sin \theta}, \quad (\text{B.12})$$

and substituting it in (B.11), we obtain

$$V_{\text{ReLU-net}}^{\text{William}}(x, x') = \frac{N}{2\pi} \sqrt{K(x, x)K(x', x')} (\sin \theta + (\pi - \theta) \cos \theta). \quad (\text{B.13})$$

The final ReLU-net kernel, after setting $\sigma_{W_1} = \frac{\sigma_{W_0}}{\sqrt{N}}$, is given by

$$\begin{aligned} \mathbb{E}_{\text{ReLU-net}}[f(x)f(x')] &= \sigma_{b_1}^2 + \sigma_{W_0}^2 \frac{1}{2\pi} \sqrt{(\sigma_{b_0}^2 + \sigma_{W_0}^2 x \cdot x)(\sigma_{b_0}^2 + \sigma_{W_0}^2 x' \cdot x')} (\sin \theta + (\pi - \theta) \cos \theta) \\ \theta &= \arccos \left[\frac{\sigma_{b_0}^2 + \sigma_{W_0}^2 x \cdot x'}{\sqrt{(\sigma_{b_0}^2 + \sigma_{W_0}^2 x \cdot x)(\sigma_{b_0}^2 + \sigma_{W_0}^2 x' \cdot x')}} \right]. \end{aligned} \quad (\text{B.14})$$

In the infinite width limit, the 2-pt function of the hidden layer, given in terms of PDF of the output $f(x)$ following prescription in [37], can be expressed in terms of Heaviside function as well:

$$V_{\text{ReLU-net}}^{\text{Yang}}(x, x') = \frac{\int df \Theta(f(x)) \Theta(f(x')) f(x) f(x') e^{-\frac{1}{2} f(x) K^{-1}(x, x') f(x')}}{\int df e^{-\frac{1}{2} f(x) K^{-1}(x, x') f(x')}}. \quad (\text{B.15})$$

After a similar change of variables and basis transformations, this results in the same expression as (B.13) at infinite width. This shows that (B.14) is the exact kernel for ReLU-net at any width.

B.3. Gauss-net

We introduce a new activation function in order to obtain a translation invariant GP kernel. This architecture is obtained by having a normalization layer after an initial exponential activation, as the following

$$\begin{aligned} x &\rightarrow \exp(W_0 x + b_0) \rightarrow \frac{\exp(W_0 x + b_0)}{\sqrt{K_{\text{exp}}(x, x)}} \\ \Rightarrow f(x) &= W_1 \left(\frac{\exp(W_0 x + b_0)}{\sqrt{K_{\text{exp}}(x, x)}} \right) + b_1, \end{aligned} \quad (\text{B.16})$$

where $K_{\text{exp}}(x, x) = V_{\text{exp}}(x, x) = \exp[2(\sigma_b^2 + \sigma_{W_0}^2 x^2)]$ is the 2-pt function of the intermediate exponential activation layer given by $\phi'(x) = \exp(W_0 \cdot x + b_0)$.

The resulting activation is²²

$$\phi(x) = \frac{\exp(Wx + b)}{\sqrt{K_{\text{exp}}(x, x)}}. \quad (\text{B.17})$$

It is easy to check that the final kernel of Gauss-net architecture is given by

$$\mathbb{E}_{\text{Gauss-net}}[f(x)f(x')] = \sigma_{b_1}^2 + \sigma_{W_1}^2 N \exp \left[-\frac{\sigma_{W_0}^2 |x - x'|^2}{2} \right]. \quad (\text{B.18})$$

²² We thank Greg Yang for discussions of activations that yield translationally invariant kernels.

At width 1, the kernel of the exponential activation layer can be obtained by substituting $\phi'(x) = \exp(W_0 \cdot x + b_0)$ in (B.3), followed by computing the Gaussian integral, to obtain

$$V_{\text{exp}}^{\text{William}}(x, x') = \exp\left(\frac{1}{2}(K(x, x) + 2K(x, x') + K(x', x'))\right), \quad (\text{B.19})$$

where $K(x, x)$, $K(x, x')$ and $K(x', x')$ are the intermediate kernels for linear layer $W_0 x + b_0$, as defined in (B.7). Substituting (B.19) in (B.3) for activation (B.16) results in the following.

$$\begin{aligned} V_{\text{Gauss-net}}^{\text{William}}(x, x') &= \frac{N V_{\text{exp}}^{\text{William}}(x, x')}{\sqrt{V_{\text{exp}}^{\text{William}}(x, x) V_{\text{exp}}^{\text{William}}(x', x')}} \\ &= N \exp\left[-\frac{\sigma_{W_0}^2 |x - x'|^2}{2}\right]. \end{aligned} \quad (\text{B.20})$$

In the infinite width limit, the kernel or 2-pt function of the exponential activation layer is obtained using the PDF of output of this layer, following [37], as

$$\begin{aligned} V_{\text{exp}}^{\text{Yang}}(x, x') &= \frac{\int df e^{f(x)} e^{f(x')} e^{-\frac{1}{2}f(x) K^{-1}(x, x') f(x')}}{\int df e^{-\frac{1}{2}f(x) K^{-1}(x, x') f(x')}} \\ &= \frac{\int df e^{-\frac{1}{2}f(x) K^{-1}(x, x') f(x') + \int dy J(y) f(y)}}{\int df e^{-\frac{1}{2}f(x) K^{-1}(x, x') f(x')}} \end{aligned} \quad (\text{B.21})$$

with $J(y) = [\delta(y - x) + \delta(y - x')]$. Field theory methods, described in the previous section, can be used to simplify this and obtain

$$\begin{aligned} V_{\text{exp}}^{\text{Yang}}(x, x') &= \exp\left[\frac{1}{2}(\delta(w - x) + \delta(w - x'))K(w, z)(\delta(z - x) + \delta(z - x'))\right] \\ &= \exp\left(\frac{1}{2}(K(x, x) + 2K(x, x') + K(x', x'))\right). \end{aligned} \quad (\text{B.22})$$

Setting $\sigma_{W_1} = \frac{\sigma_{W_0}}{\sqrt{N}}$, the final expression of Gauss-net kernel is given by

$$\mathbb{E}_{\text{Gauss-net}}[f(x)f(x')] = \sigma_{b_1}^2 + \sigma_{W_0}^2 \exp\left[-\frac{\sigma_{W_0}^2 |x - x'|^2}{2}\right], \quad (\text{B.23})$$

which is translation invariant.

ORCID iDs

James Halverson  <https://orcid.org/0000-0003-0535-2622>

Anindita Maiti  <https://orcid.org/0000-0002-4712-6626>

Keegan Stoner  <https://orcid.org/0000-0002-1708-2773>

References

- [1] Neal R M 1995 Bayesian learning for neural networks *PhD Thesis* University of Toronto
- [2] Williams C K I 1997 Computing with infinite networks *Advances in Neural Information Processing Systems* pp 295–301
- [3] Lee J, Bahri Y, Novak R, Schoenholz S S, Pennington J and Sohl-Dickstein J 2017 Deep neural networks as Gaussian processes (arXiv:1711.00165)
- [4] Matthews A G G, Rowland M, Hron J, Turner R E and Ghahramani Z 2018 Gaussian process behaviour in wide deep neural networks (arXiv:1804.11271)
- [5] Novak R, Xiao L, Lee J, Bahri Y, Abolafia D A, Pennington J and Sohl-Dickstein J 2018 Bayesian convolutional neural networks with many channels are Gaussian processes (arXiv:1810.05148)
- [6] Garriga-Alonso A, Aitchison L and Rasmussen C E 2019 Deep convolutional networks as shallow Gaussian processes (arXiv:1808.05587)
- [7] Yang G 2019 Scaling limits of wide neural networks with weight sharing: Gaussian process behavior, gradient independence, and neural tangent kernel derivation (arXiv:1902.04760)
- [8] Yang G 2019 Tensor programs I: wide feedforward or recurrent neural networks of any architecture are Gaussian processes (arXiv:1910.12478)
- [9] Yang G 2020 Tensor programs II: neural tangent kernel for any architecture (arXiv:2006.14548)

- [10] He K, Zhang X, Ren S and Sun J 2016 Deep residual learning for image recognition *Proc. Conf. on Computer Vision and Pattern Recognition (CVPR)*
- [11] Huang G, Liu Z, van der Maaten L and Weinberger K Q 2016 Densely connected convolutional networks (arXiv:1608.06993)
- [12] Fukushima K 1975 Cognitron: a self-organizing multilayered neural network *Biol. Cybern.* **20** 121–36
- [13] Fukushima K 1980 Neocognitron: a self-organizing neural network model for a mechanism of pattern recognition unaffected by shift in position *Biol. Cybern.* **36** 193–202
- [14] Rumelhart D E, Hinton G E and Williams R J 1985 Learning internal representations by error propagation *Technical Report* (San Diego, La Jolla: California Univ., Inst. for Cognitive Science)
- [15] LeCun Y, Bottou Leon, Bengio Y and Haffner P 1998 Gradient-based learning applied to document recognition *Proc. IEEE* **86** 2278–324
- [16] LeCun Y, Haffner P, Bottou Leon and Bengio Y 1999 Object recognition with gradient-based learning *Shape, Contour and Grouping in Computer Vision* (Berlin: Springer) pp 319–45
- [17] Bruna J, Zaremba W, Szlam A and Yann L 2013 Spectral networks and locally connected networks on graphs (arXiv:1312.6203)
- [18] Henaff M, Bruna J and Yann L 2015 Deep convolutional networks on graph-structured data (arXiv:1506.05163)
- [19] Duvenaud D K, Maclaurin D, Iparraguirre J, Bombarell R, Hirzel T, Aspuru-Guzik A and Adams R P 2015 Convolutional networks on graphs for learning molecular fingerprints *Advances in Neural Information Processing Systems* 28 ed C Cortes, N D Lawrence, D D Lee, M Sugiyama and R Garnett (Red Hook, NY: Curran Associates, Inc.) pp 2224–32
- [20] Yujia Li, Tarlow D, Brockschmidt M and Zemel R 2015 Gated graph sequence neural networks (arXiv:1511.05493)
- [21] Defferrard M, Bresson X and Vandergheynst P 2016 Convolutional neural networks on graphs with fast localized spectral filtering *Advances in Neural Information Processing Systems* pp 3844–52
- [22] Kipf T N and Welling M 2016 Semi-supervised classification with graph convolutional networks (arXiv:1609.02907)
- [23] Ioffe S and Szegedy C 2015 Batch normalization: accelerating deep network training by reducing internal covariate shift (arXiv:1502.03167)
- [24] Ba J L, Kiros J R and Hinton G E 2016 Layer normalization (arXiv:1607.06450)
- [25] Bahdanau D, Cho K and Bengio Y 2014 Neural machine translation by jointly learning to align and translate (arXiv:1409.0473)
- [26] Vaswani A, Shazeer N, Parmar N, Uszkoreit J, Jones L, Gomez A N, Kaiser Lukasz and Polosukhin I 2017 Attention is all you need *Advances in Neural Information Processing Systems* pp 5998–6008
- [27] Lee J, Lechao Xiao S S, Schoenholz Y B, Novak R, Sohl-Dickstein J and Pennington J 2019 Wide neural networks of any depth evolve as linear models under gradient descent (arXiv:1902.06720)
- [28] Jacot A, Gabriel F and Hongler Clement 2018 Neural tangent kernel: convergence and generalization in neural networks *NeurIPS* (arXiv:1806.07572)
- [29] Antognini J M 2019 Finite size corrections for neural network Gaussian processes (arXiv:1908.10030)
- [30] Naveh G, Ben-David O, Sompolinsky H and Ringel Z 2020 Predicting the outputs of finite networks trained with noisy gradients (arXiv:2004.01190)
- [31] Yaida S 2019 Non-Gaussian processes and neural networks at finite widths (arXiv:1910.00019)
- [32] Cohen O, Malka O and Ringel Z 2020 Learning curves for deep neural networks: a Gaussian field theory perspective (arXiv:1906.05301)
- [33] Dyer E and Gur-Ari G 2020 Asymptotics of wide networks from Feynman diagrams (arXiv:1909.11304)
- [34] Yang G 2020 Tensor programs III: neural matrix laws (arXiv:2009.10685)
- [35] Yang G and Hu E J 2020 Feature learning in infinite-width neural networks (arXiv:2011.14522)
- [36] Khoury J and Weltman A 2004 Chameleon cosmology *Phys. Rev. D* **69** 044026
- [37] Yang G and Salman H 2019 A fine-grained spectral perspective on neural networks (arXiv:1907.10599)
- [38] Cho Y and Saul L K 2009 Kernel methods for deep learning *Advances in Neural Information Processing Systems* pp 342–50
- [39] Schwartz M D 2014 *Quantum Field Theory and the Standard Model* (Cambridge: Cambridge University Press)
- [40] Fermi E 1933 Tentativo di una teoria dell'emissione dei raggi 'beta' *Ric. Sci.* **4** 491–5
- [41] Zee A 2003 *Quantum Field Theory in a Nutshell* vol 11 (Princeton, NJ: Princeton University Press)